DETERMINATION OF OPTIMAL BIOREACTOR OPERATIONAL STRATEGY AND UNSTRUCTURED MACROKINETIC MODEL FOR RECOMBINANT HUMAN GROWTH HORMONE PRODUCTION ON ETHANOL BY A NOVEL *PICHIA PASTORIS* $P_{ADH2\text{-}Cat8\text{-}L2}$ BASED SYSTEM

A THESIS SUBMITTED TO
THE GRADUATE SCHOOL OF NATURAL AND APPLIED SCIENCES
OF
MIDDLE EAST TECHNICAL UNIVERSITY

BY

OMAR WEHBE AL MASRI

IN PARTIAL FULFILLMENT OF THE REQUIREMENTS
FOR
THE DEGREE OF MASTER OF SCIENCE
IN
CHEMICAL ENGINEERING

NOVEMBER 2019

Approval of the thesis:

DETERMINATION OF OPTIMAL BIOREACTOR OPERATIONAL STRATEGY AND UNSTRUCTURED MACROKINETIC MODEL FOR RECOMBINANT HUMAN GROWTH HORMONE PRODUCTION ON ETHANOL BY A NOVEL *PICHIA PASTORIS* $P_{ADH2\text{-}Cat8\text{-}L2}$ BASED SYSTEM

submitted by **Omar Wehbe Al Masri** in partial fulfillment of the requirements for the degree of **Master of Science in Chemical Engineering Department, Middle East Technical University** by,

Prof. Dr. Halil Kalıpçılar
Dean, Graduate School of **Natural and Applied Sciences** _____

Prof. Dr. Pınar Çalık
Head of Department, Chemical Engineering _____

Prof.Dr. Pınar Çalık
Supervisor, **Chemical Engineering, METU** _____

Examining Committee Members:

Prof. Dr. Tunçer H. Özdamar
Chemical Engineering, Ankara University _____

Prof.Dr. Pınar Çalık
Chemical Engineering, METU _____

Assoc.Prof. Dr. Erhan Bat
Chemical Engineering, METU _____

Assist.Prof. Dr. Harun Koku
Chemical Engineering, METU _____

Assoc. Prof. Dr. Eda Çelik Akdur
Chemical Engineering, Hacettepe University _____

Date: 29.11.2019

I hereby declare that all information in this document has been obtained and presented in accordance with academic rules and ethical conduct. I also declare that, as required by these rules and conduct, I have fully cited and referenced all material and results that are not original to this work.

Name, Surname: Omar Wehbe Al Masri

Signature:

ABSTRACT

DETERMINATION OF OPTIMAL BIOREACTOR OPERATIONAL STRATEGY AND UNSTRUCTURED MACROKINETIC MODEL FOR RECOMBINANT HUMAN GROWTH HORMONE PRODUCTION ON ETHANOL BY A NOVEL *PICHIA PASTORIS* $P_{ADH2\text{-}Cat8\text{-}L2}$ BASED SYSTEM

Wehbe Al Masri, Omar
Master of Science, Chemical Engineering
Supervisor: Prof.Dr. Pınar Çalık

November 2019, 117 pages

In recombinant protein (r-protein) production, the host *Pichia pastoris* (*Komagataella phaffii*) is used with the methanol-inducible *alcohol oxidase 1* promoter (P_{AOX1}), one of the strongest naturally occurring promoters, due to its tight regulation and exceptional strength. For the pharmaceutical and food sectors, since the use of methanol as a substrate in r-protein productions may complicate separation processes, and required documentations, methanol-free production by green bio-processes is encouraged but challenging. In this context, using the non-toxic carbon and energy source ethanol under our newly developed *alcohol dehydrogenase 2* (*ADH2*) hybrid promotor $P_{ADH2\text{-}Cat8\text{-}L2}$, ethanol feeding strategies were developed for rhGH production by *P. pastoris*. Prior to pilot-scale experiments, the effects of ethanol on the growth of *P. pastoris* were investigated in laboratory-scale batch-bioreactors at T=30°C and N=200 min^{-1} (rpm). An increase in ethanol concentration lead to an increase in the final cell concentration, however, at $C_{EtOH} > 3$ g L^{-1}, the substrate inhibited the growth marked by a decrease in specific cell growth rates and the longer cultivation time required to reach the same cell densities. This inhibition behavior was also mathematically modelled where the Haldane model was able to clearly depict the

inhibitory effect of ethanol at high concentrations with a critical substrate concentration of 1.97 g L^{-1} and a maximum specific growth rate of 0.194 h^{-1}. The effects of two different continuous feed stream (CFS) operational strategies on the specific growth rate, specific ethanol uptake rate and specific rhGH production rate were investigated as follows: CFS designed with three pre-determined specific growth rate (μ) values of 0.020, 0.035 and 0.050 h^{-1}, and ethanol-stat CFS designed with three constant C_{EtOH} values of 0.5, 1.0, and 1.5 g L^{-1} in the cultivation medium. In the ethanol-stat fed-batch bioreactors, approximately 1.6-fold higher maximum cell concentration and 2.1-fold higher maximum rhGH concentration (91 mg L^{-1}) were obtained compared to those obtained by the fed-batch bioreactors designed with pre-determined μ values. In addition, 2-fold higher maximum volumetric productivity was obtained by the ethanol-stat fed-batch bioreactors. The ethanol-stat strategy of $C_{EtOH,set}$=0.5 g L^{-1} was the most favorable operational strategy due to it having the highest rhGH titer, along with high volumetric productivity and protein on biomass yield ($Y_{p/x}$). In addition, high ethanol concentrations inhibited the specific growth rate, the specific ethanol uptake rate and the protein production rate, where the inhibition pattern was mathematically described according to the Haldane model. The relationship between the specific ethanol uptake rate and the specific growth rate was described by the linear Pirt model, whereas the relationship between the specific protein production rate and the specific growth rate was not linear, and thus could not be described by the Luedeking-Piret model. Lastly, cell generation and rhGH production were simulated based on the Haldane models relating the specific growth rate and specific rhGH production rate to the residual ethanol concentration.

Keywords: *Pichia pastoris*, $P_{ADH2\text{-}Cat8\text{-}L2}$, unstructured models, ethanol inhibition, recombinant human growth hormone, fed-batch feeding strategies, bioprocess simulation

ÖZ

PİCHİA PASTORİS İLE $P_{ADH2\text{-}Cat8\text{-}L2}$ PROMOTOR ALTINDA REKOMBİNANT İNSAN BÜYÜME HORMONU ÜRETİMİ İÇİN ETANOL-TEMELLİ BİYOREAKTÖR İŞLETİM STRATEJİSİ GELİŞTİRİLMESİ VE MODELLENMESİ

Wehbe Al Masri, Omar
Yüksek Lisans, Kimya Mühendisliği
Tez Danışmanı: Prof.Dr. Pınar Çalık

Kasım 2019, 117 sayfa

Rekombinant protein üretiminde konak *Pichia pastoris*'te (*Komagataella phaffii*) methanol-ile-indüklenen *alkol oxidaz 1* promotoru (P_{AOX1}) sıkı-regülasyonlarıyla ve olağanüstü gücüyle bilenen en-güçlü doğal promotorlardandır; P_{AOX1} kontrolunda toksik-alkol metanolun fermentasyonuyla yüksek verimle rekombinant protein (r-protein) üretimi yapılır. İlaç-ve-gıda sektörleri için r-protein üretiminde metanolun kullanılması, ayırma işlemlerini, ve insan-sağlığına-sakıncasızlığını belgelemede dökümantasyonu güçleştirdiğinden, yeşil-(green)-karbon kaynaklarıyla üretim için güçlü-yeni promotor için biyoproses geliştirilmesi gerekmektedir. Bu kapsamda, karbon ve enerji kaynağı etanol ile araştırma grubumuzda yeni geliştirilen *alkol dehidrojenaz 2* (ADH2) hibrit promotor $P_{ADH2\text{-}Cat8\text{-}L2}$ altında *P. pastoris*'te rekombinant insan büyüme hormonu üretimi için etanol besleme stratejisi geliştirilmiştir. Etanol derişiminin *P. pastoris*'in çoğalmasına etkisi V = 50 mL hacımlı mikrobiyolojik hava filtreli laboratuvar-ölçek orbital-çalkalamalı kesikli biyoreaktörlerde T=30°C ve N=200 dk^{-1} sabit karıştırma hızlarında araştırılmıştır. Etanol derişiminin artmasıyla hücre derişimini artırmış, ancak $C_{EtOH} > 3$ g L^{-1}'de - etanol, spesifik çoğalma hızını azaltarak çoğalmayı inhibe etmiştir. Etanol derişiminin *P. pastoris* çoğalması üzerine etkisi Haldane modeline uymuş; 1.97 g L^{-1} kritik

substrat derişimi ve 0.194 h^{-1} maksimum spesifik çoğalma hızı olarak belirlenmiştir. Yarı-kesikli işletimde, iki farklı araştırma programıyla iki farklı sürekli besleme stratejisinin etkisi araştırılmış; proses süresince spesifik çoğalma hızı, spesifik etanol tüketim hızı ve spesifik rhGH üretim hızı araştırılmıştır. 1.Araştırma Programında önceden belirlenmiş üç spesifik çoğalma hızında, μ= 0.020, 0.035 ve 0.050 st^{-1} ve 2.Araştırma Programında sabit etanol derişiminde (Etanol-stat) C_{EtOH} = 0.5, 1.0 ve 1.5 g L^{-1} deneyler yapılmıştır. Etanol derişiminin sabit tutulduğu işletimlerde, önceden belirlenmiş spesifik çoğalma hızında işletimlerinden daha yüksek hücre elde edilmiştir. Benzer şekilde, etanol derişiminin sabit tutulduğu işletimlerde, 2-kat yüksek hacimsel rhGH üretimi elde edilmiştir. Ek olarak, spesifik çoğalma hızı, spesifik etanol tüketim hızı ve rhGH üretim hızı, Haldane modeline uymuştur. Spesifik etanol tüketim hızı ile spesifik çoğalma hızı arasındaki ilişki, Pirt modeli ile tanımlanırken, spesifik protein üretim hızı ile spesifik çoğalma arasındaki ilişki doğrusal olmadığı için Luedeking-Piret modeli ile tanımlanmıştır. Son olarak, hücre oluşumu, rhGH üretimi, reaktördeki etanol derişimi, spesifik çoğalma hızı, ve spesifik protein üretim hızı Haldane modeli kullanılarak simüle edildi.

Anahtar Kelimeler: *Pichia pastoris*, $P_{ADH2\text{-}Cat8\text{-}L2}$, yapılandırılmamış modeller, etanol inhibisyonu, rekombinant insan büyüme hormonu, beslenme stratejileri, biyoproses simülasyonu

To my beloved family,

ACKNOWLEDGEMENTS

First and foremost, I would like to greatly thank my advisor Prof. Dr. Pınar Çalık whose continuous support, guidance and faith in me have allowed me to accomplish this work. Granting me the chance to conduct research in her lab has forever shaped my future and paved my career path in the direction of biotechnology.

I would also like to thank Dr. Erhan Bat, Dr. Salih Özçubukçu, Dr. Aytül Saylam, and Dr. Müslüm İlgu for their guidance and contribution to my previous research topic.

In addition, I would like to extend my gratitude towards my lab mates, Sibel Öztürk, Yiğit Akgün, Özge Kalender, Abdullah Keskin, İrem Demir, and İdil Dayangaç for their support, patience and mentorship, for being there with me in my numerous long, sleepless nights at the lab, for helping me stay focused and on track and, overall, for their friendship. I would especially like to thank Dr. Burcu Gündüz Ergün for teaching me everything she knows about bioreactors, for her excellent guidance throughout my master's studies, for allowing me to perform the ELISA experiments at the Ministry of Food and Agriculture and most importantly for her kind friendship. Also, my great appreciation goes towards Erdem Boy who was always there to help with the ethanol sensor he devised, who has allowed me to use the numerous facilities at the central lab of METU and whose conversations were always pleasant.

Moreover, I would like to thank the young and talented Oğuz Ulaş Yaman for his mathematical excellence and his assistance with the experiments that have allowed this work to take its current form. Also, I would like to thank our former lab mates Dr. Özge Ata, Damla Hüccetoğulları and Onur Ersoy for what they added to my knowledge.

Additionally, I would like to greatly thank Toprak Cağlar for assisting me with the gas chromatography experiments and teaching me everything she knows about the device.

Furthermore, I would like to whole-heartedly thank İrfan Gökçe Özer for always being there for me, especially during the busiest and most stressful term of my life, for his great companionship, for the knowledge he continuously adds to me and for helping me grow and evolve.

Emily Rutkowski, my angel best friend, you have forever helped me liberate myself from the chains of my own mind and continue to honor me for having you in my life. I wish nothing but to reunite with you soon and for this friendship to last forever.

Imad Mandi and Usman Kayode Abdulrasaq, you have accompanied me since my first year in Turkey and have opened your hearts and minds to me, for this I am forever grateful.

Dila Dönmez, our friendship in Turkey was short-lived, but I appreciated and cherished every bit of it, and I wish you every success on your academic path in the states with Ata. I would also like to thank every single person who has left a footprint on my mind and soul throughout my journey in Turkey.

Last but not least, I want to thank my number one support system, my family and especially mother dearest, for their continuous support and unconditional love that they have harbored towards me.

The Scientific and Technical Research Council of Turkey (TUBITAK) and BAP are greatly acknowledged for supporting my work under the project numbers 116Z215 and YLT-304-2018-3682, respectively.

TABLE OF CONTENTS

ABSTRACT v

ÖZ vii

ACKNOWLEDGEMENTS x

TABLE OF CONTENTS xii

LIST OF TABLES xvii

LIST OF FIGURES xviii

LIST OF ABBREVIATIONS xx

LIST OF SYMBOLS xxiii

CHAPTERS

1. INTRODUCTION 1

2. Literature Survey 5

2.1. Model Protein: Human Growth Hormone (hGH) 5

2.2. *Pichia pastoris* 6

2.2.1. Promoters of *P. pastoris* 6

2.2.1.1. P_{AOX} 6

2.2.1.2. P_{GAP} 7

2.2.1.3. P_{ADH2} 7

2.2.1.4. $P_{ADH2\text{-}Cat8\text{-}L2}$ 8

2.3. Bioreactor Experimental Design 9

2.3.1. Mass Conservation Equations 9

2.3.2. Fed-Batch Bioreactor Mathematical Model 11

2.3.3. Hybrid Fed-Batch Bioreactor Operation Design 12

2.3.4. Yield Coefficients 12
2.3.5. Volumetric Productivity 13
2.4. Fed-Batch Bioreactor Feeding Strategies 14
2.4.1. Continuous Feed Stream Design with Pre-Determined Specific Growth Rate and Other Parameters 14
2.4.2. Continuous Feed Stream Design with Constant C_S (Substrate-stat) 14
2.4.3. Co-Substrate Feeding (Mixed feeding) 16
2.4.4. Dissolved Oxygen-stat (DO-stat) 22
2.4.5. Oxygen-Limited Fed-Batch 24
2.5. Kinetic Models 26
2.5.1. Structured Models 26
2.5.1.1. Compartment Models 27
2.5.1.2. Cybernetic Models 29
2.5.2. Unstructured Models 30
2.5.2.1. Monod Model 31
2.5.2.2. Haldane Model 31
2.5.2.3. Andrews Model 32
2.5.2.4. Aiba Model 33
2.5.2.5. Moser Model 33
2.5.3. Pirt Model 33
2.5.4. Luedeking-Piret Model 34
2.5.5. Comparison of Macrokinetic Models 39
3. Materials & Methods 43
3.1. Strains 43

3.2. Inoculum Preparation 43
3.3. Air-filtered Shake Flask Bioreactors for Growth Curve Determination 43
3.4. Fed-batch Bioreactor Cultivation Medium and Operation Conditions 44
3.4.1. CFS Designed with Pre-Determined Specific Growth Rate and Other Parameters 45
3.4.1.1. Theoretical determination of $Y_{x/s}$ 45
3.4.2. CFS Designed with Constant C_{EtOH} (Ethanol-stat) 46
3.5. Determination of Ethanol Concentration 47
3.6. Determination of Cell Concentration 47
3.7. rhGH Quantification 47
3.8. Sodium dodecyl sulfate polyacrylamide gel electrophoresis (SDS-PAGE) ... 49
3.9. Mathematical Models 49
3.9.1. Specific Rates 49
3.9.2. Mean Specific Rates 50
3.9.3. Unstructured Kinetic Models 51
3.10. Mean Relative Error 52
3.11. Bioreactor Model Simulation 53
4. Results & discussion 57
4.1. Air-Filtered Shake Flask Bioreactor Experiments 57
4.1.1. Growth Curve Determination 58
4.1.2. Growth Inhibition Models 60
4.2. Fed-Batch Bioreactor Experiments 61
4.2.1. Cell Concentrations 62
4.2.2. Ethanol Concentrations 63

4.2.3. rhGH Concentrations 64
4.2.4. Specific Growth Rates 66
4.2.5. Specific Ethanol Uptake Rates 68
4.2.6. Specific rhGH Production Rates 69
4.2.7. Comparison of Fed-Batch Feeding Strategies 70
4.3. Kinetic Models 72
4.3.1. Specific Growth Rate Model 72
4.3.2. Specific Ethanol Uptake Rate Model 73
4.3.3. Specific rhGH Production Rate Model 75
4.3.4. Pirt and Luedeking-Piret Linear Models 76
4.4. Model Simulation and Validation 78
5. Conclusions 83
REFERENCES 87
APPENDICES
A. GC Calibration Curve for Ethanol Concentration 95
B. ELISA Calibration Curve 97
C. Gas Chromatography Negative Control Experiment 99
D. Haldane and Monod MATLAB® Code for Air-Filtered Shake Flask Bioreactor Experiments 101
E. Specific Growth Rate, Ethanol Uptake Rate and Protein Production Rate Calculations Using MATLAB® 103
F. Haldane and Monod Codes for CFS Bioreactor Experiments Using MATLAB® 107
G. Pirt and Luedeking-Piret Models for CFS Bioreactor Experiments Using MATLAB® 109

H. Codes of C_xV and C_pV Simulations for CFS Bioreactor Experiments Using MATLAB® 111

LIST OF TABLES

TABLES

Table 2.1. Results of Barrigón et al.'s 2013 study……16

Table 3.1. Gas chromatography device specifications and run parameters 47

Table 4.1. Parameter values for the Haldane and Monod models of the air-filtered shake flask bioreactor experiments. 60

Table 4.2. Comparison of process variables, yields and productivities for CFS fed-batch bioreactors designed with pre-determined μ and ethanol-stat. 71

Table 4.3. Model Parameters for the correlation between specific growth rate and residual ethanol concentration……....73

Table 4.4. Model parameters for correlation between specific ethanol uptake rate and residual ethanol concentration.……...74

Table 4.5. Model parameters for correlation between specific rhGH production rate and residual ethanol concentration.……..…..75

Table 4.6. Statistical data for the unstructured kinetic models relating μ, q_{EtOH} and q_p to C_{EtOH} ……...76

Table 4.7. Kinetic parameters and statistical data of the linear models.…..78

Table 4.8. Performance of the proposed model for the simulation of the global state variable C_xV throughout the cultivation time.…….…....80

Table 4.9. Performance of the proposed model for the simulation of the global state variable C_pV throughout the cultivation time……...…...81

TABLE C. Change of ethanol concentrations after t=8 h of incubation without cells 99

LIST OF FIGURES

FIGURES

Figure 2.1. The 3D structure of human growth hormone with disulphide bridges ……...……...5

Figure 3.1. The simulation algorithm for determining the evolution of cell generation throughout the cultivation time in the fed-batch bioreactor experiments..... 54

Figure 3.2. The simulation algorithm for determining the evolution of rhGH production throughout the cultivation time in the fed-batch bioreactor experiments. 55

Figure 4.1. Growth curve of $P_{ADH2\text{-}Cat8\text{-}L2}$ strain on different initial concentrations of ethanol..... 58

Figure 4.2. Variation in ethanol concentration with the cultivation time for the air-filtered shake flask bioreactor experiments ……59

Figure 4.3. Haldane model for the growth of $P_{ADH2\text{-}Cat8\text{-}L2}$ on different concentrations of ethanol ……...61

Figure 4.4. Variation of cell concentrations with the cultivation time in the CFS fed-batch bioreactor experiments……...…...63

Figure 4.5. Variation of ethanol concentrations with the cultivation time in the CFS fed-batch bioreactor experiments……....…..64

Figure 4.6. Variation of rhGH concentrations with the cultivation time in the CFS fed-batch bioreactor experiments. ……...65

Figure 4.7. SDS-PAGE results of the fed-batch bioreactors designed with pre-determined μ ……..……...66

Figure 4.8. Variation of specific growth rates with the cultivation time in the CFS fed-batch bioreactor experiments. …..……....67

Figure 4.9. Variation of specific ethanol uptake rates with the cultivation time in CFS fed-batch bioreactor experiments……...…..…...68

Figure 4.10. Variation of specific rhGH production rates with the cultivation time in the CFS fed-batch bioreactor experiments. …….……..70

Figure 4.11. Haldane and Monod models for the relationship between specific growth rates versus ethanol concentrations ……73

Figure 4.12. Haldane and Monod models for the relationship between specific ethanol uptake rates versus ethanol concentrations. 74

Figure 4.13. Haldane and Monod models for the relationship between specific rhGH production rates versus ethanol concentrations.....75

Figure 4.14. Pirt model for specific ethanol uptake rate versus specific growth rate. 77

Figure 4.15. Luedeking-Piret model for specific rhGH production rate versus specific growth rate 77

Figure 4.16. Evolution of cell generation, C_xV throughout the cultivation time for the CFS fed-batch bioreactors.....79

Figure 4.17. Evolution of rhGH production, C_pV throughout the cultivation time for the CFS fed-batch bioreactors.....82

Figure A. Calibration curve of ethanol concentration in GC.....95

Figure B. Calibration curve using hGH standards for ELISA readings.....97

LIST OF ABBREVIATIONS

ABBREVIATIONS

ADH	Alcohol dehydrogenase
AOX	Alcohol oxidase
ATP	Adenosine triphosphate
BMGY	Buffered glycerol complex
BSM	Basal salt medium
CFS	Continuous feed stream
CoA	Co-enzyme A
DCW	Dry cell weight
DO	Dissolved oxygen
eGFP	Enhanced green fluorescent protein
EIP	Ethanol induction phase
ETP	Ethanol transition phase
EtOH	Ethanol
FDA	Food and Drug Administration
GAP	Glyceraldehyde-3-phosphate dehydrogenase
GBP	Glycerol batch phase
GC	Gas chromatography
GI	Glucose isomerase

Gox	Glucose oxidase
HFBB	Hybrid fed-batch bioreactor
hGH	Human growth hormone
hIFN-γ	Human interferon gamma
hSA	Human serum albumin
max	maximum
MeOH	Methanol
min	minimum
MRE	Mean relative error
Mut^{+}	Methanol utilizing
Mut^{S}	Methanol utilizing slow
Mut^{-}	Non-methanol utilizing
NTC	Nourseothricin
OD	Optical density
PTM1	Trace salts
$P_{ADH2\text{-}Cat8\text{-}L2}$	Engineered promoter variant of ADH
PI	Proportional-integral
PID	Proportional-integral-derivative
pIFN-α	porcine interferon-α
rHuEPO	Recombinant human erythropoietin
rhSA	Recombinant human serum albumin

ROL	Rhizopus oryzae lipase
RQ	Respiratory quotient
SDS-PAGE	Sodium dodecyl sulfate-polyacrylamide gel electrophoresis
t-PA	Tissue plasminogen activator
TLFB	Temperature limited fed-batch
UP	Ultra-pure
WCW	Wet cell weight
YE	Yeast extract
YPD	Yeast extract, Peptone, Dextrose

LIST OF SYMBOLS

SYMBOLS

C	Concentration in the medium	g L^{-1}
K_s	Saturation constant	g L^{-1}
K_i	Inhibition constant	g L^{-1}
m	Maintenance coefficient	g g^{-1} h^{-1} or mg g^{-1} h^{-1}
OTR	Oxygen transfer rate	s^{-1}
OUR	Oxygen uptake rate	mmol m^{-3} s^{-1}
Q	Feed inlet rate	L h^{-1}
q_s	Specific substrate uptake rate	g g^{-1} h^{-1}
q_p	Specific protein production rate	mg g^{-1} h^{-1}
r_x	Cell formation rate	g L^{-1} h^{-1}
t	Cultivation time	h
V	Volume of the bioreactor	L
V_p	Volumetric productivity	mg L^{-1} h^{-1}
Y	Yield	g g^{-1} or mg g^{-1}

Greek Letters

ρ	Density	g L^{-1}
μ	specific growth rate	h^{-1}
α	growth-associated coefficient	mg g^{-1}

β	non-growth associated coefficient	mg g^{-1} h^{-1}

Subscripts

crit	Critical concentration
d	Refers to degradation
exp	Experimental
i	Refers to initial condition
p	Refers to protein
pro	Refers to protease
r	Refers to recombinant protein
s	Refers to ethanol or substrate
th	Theoretical
x	Refers to cell

CHAPTER 1

INTRODUCTION

Biotechnology is a field that applies science and engineering to process materials by biological organisms, systems and processes in order to industrially provide goods and services. Three key stages are typically present when a commercial product is being produced via industrial biotechnology processes: 1) upstream processing that involves preparing the microorganism(s) and the media required to sustain their growth and obtain the desired product, 2) fermentation that involves cultivating the microorganism in an industrial bioreactor to synthesize the desired product, e.g. antibodies, proteins, enzymes, and 3) downstream processing that involves the separation and purification of the desired product from the cultivation medium. Since the development of recombinant DNA technology in the 1970's, the ability to manipulate living things has grown exponentially due to the advances in DNA sequencing, DNA synthesis, PCR, monoclonal antibodies, genomics, proteomics and metabolomics (Glick, Pasternak, and Patten, 2002).

Methylotrophic yeast species are eukaryotes capable of acquiring all their carbon and energy needs for growth and cellular maintenance from methanol. Using methanol as the only carbon and energy source strongly induces the proliferation of key enzymes which are involved in methanol metabolism and are found in the peroxisomes. However, these peroxisomes are proteolytically degraded when the methylotrophic yeasts are transferred to a medium containing a different carbon source, such as ethanol (Yurimoto, Oku and Sakai, 2011). Also, these yeast species can utilize acetate, glycerol, and ethanol (Inan and Meagher, 2001:Karaoglan, M, Karaoglan, F.E. and Inan, 2016). Moreover, methylotrophic yeasts are mainly known for their strong ability to host and effectively express heterologous proteins with the genus *Pichia* being the most famous of them all. *S. cerevisiae* was used for the expression of

recombinant proteins due to the great amount of knowledge acquired about this yeast species owing to the completion of its genomic sequencing in 1996. It is also considered safe by the FDA and has been used to produce more than 50% of the world demand of insulin where some strains can even produce hepatitis B vaccines. However, *S. cerevisiae* has some major drawbacks such as hyperglycosylation of heterologous proteins that alter their function, retention of proteins in the periplasmic space which consequently increases purification cost and time, and over secretion of ethanol which is toxic to the cells (Crabtree effect) at high cell densities (Glick et al., 2019).

As production by green-clean biotechnological processes with high yield and productivity is the ultimate industrial target in order to compete with methanol-based production under P_{AOX1}, discovery of strong promoters, and especially design and construction of strong engineered-novel promoter variants (NEPVs) and systems to be active in methanol-free-media (ethanol, glucose, etc.), are required. Design and construction of NEPVs of *P. pastoris alcohol dehydrogenase 2* (*ADH2*) promoter for r-protein production has been investigated; compared to that with P_{ADH2}, *P. pastoris* cells constructed with the NEPV $P_{ADH2\text{-}Cat8\text{-}L2}$ (Ergün et al., 2019) having hybrid-promoter architecture designed by locating a single synthetic-binding-motif for Cat8 binding, enhanced r-protein synthesis 4.8-fold on ethanol, which indicates the importance of Cat synthetic binding-site to increase promoter strength (Ergün et al., 2019).

In this context, the effect of ethanol on the growth of a *P. pastoris* strain extracellularly expressing rhGH under the control of the NEPV $P_{ADH2\text{-}Cat8\text{-}L2}$ was determined in air-filtered shake flask bioreactors using eight initial ethanol concentrations between 1-16 g L^{-1}. Then, the effect of ethanol on the growth , ethanol consumption and rhGH production of the same strain were investigated by conducting two CFS fed-batch design strategies: ***(i)*** fed-batch bioreactors designed with three pre-determined μ values (0.020, 0.035, and 0.050 h^{-1}) and ***(ii)*** ethanol-stat fed-batch bioreactors designed with three constant C_{EtOH} values (0.5, 1.0, and 1.5 g L^{-1}) in the medium.

Unstructured kinetic models, Haldane and Monod, were used to mathematically describe the inhibition that high ethanol concentrations exert on μ, q_{EtOH} and q_p. q_{EtOH} and q_p were also modelled based on Pirt's maintenance energy model and Luedeking-Piret model for product formation, respectively. Using the Haldane models relating μ and q_p to C_{EtOH}, along with cell and protein mass conservation equations, cell generation and rhGH production were simulated throughout the cultivation time.

CHAPTER 2

LITERATURE SURVEY

2.1. Model Protein: Human Growth Hormone (hGH)

Human growth hormone (Figure 2.1) is a 191-amino acid, 22-kDa non-glycosylated polypeptide secreted by somatotropes in the pituitary gland. It plays a role in the stimulation of insulin gene expression, insulin biosynthesis and secretion, and cell proliferation (Møller, and Jørgensen, 2009). Also, hGH can stimulate linear growth (height), tissue growth, carbohydrate, protein, mineral and lipid metabolism. Recombinant human growth hormone (rhGH) is used to treat short stature among kids due to idiopathic growth hormone deficiency, Noonan syndrome, Turner syndrome, Prader-Willi syndrome, chronic renal insufficiency, short stature homeobox-containing gene deficiency and children small for gestational age. In the US, eight r-hGH drugs are approved by the FDA and marketed under the following names: Humatrope (*E. coli*), Tev-Tropin (*E. coli*), Genotropin (*E. coli*), Nutropin (*E. coli*), Nutropin AQ, Saizen (murine cell line, C127), Norditropin (*E. coli*) and Omnitrope (*E. coli*).

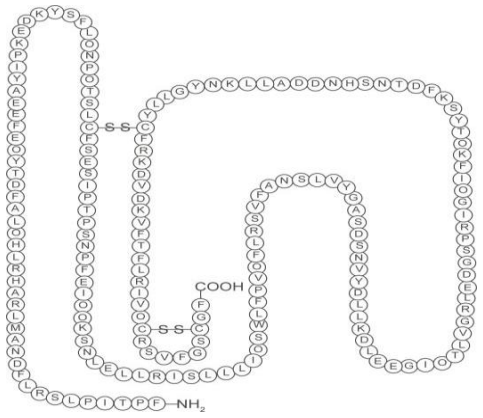

Figure 2.1. The 3D structure of human growth hormone with disulphide bridges (Graham et al., 2008).

2.2. *Pichia pastoris*

P. pastoris is a methylotrophic yeast whose innate cellular machinery has gained a lot of interest for the expression of foreign proteins on a milligram to gram basis (Macauley-Patrick et al., 2005). The advantages of using this type of yeast cells involves: ease of genetic manipulation, e.g. high-frequency DNA transformation and gene targeting, the ability to grow to high densities on minimal and inexpensive media (Cereghino et al., 2002; Heyland et al. 2010) and the ability to perform post-translational eukaryotic modifications such as glycosylation and disulfide bond formation without the inherent problem of hyperglycosylation found in *Saccharomyces cerevisiae* (Macauley-Patrick et al., 2005). Also, the low number of native secreted proteins and the absence of endotoxins facilitates the purification of recombinant proteins secreted to the extracellular medium (Romanos, 1995).

2.2.1. Promoters of *P. pastoris*

2.2.1.1. P_{AOX}

The ability of *P. pastoris* to utilize methanol lies within its strongly inducible promoter *alcohol oxidase* (P_{AOX1}) that induces the production of an enzyme known as alcohol oxidase, which is responsible for catalyzing the oxidation of methanol to form hydrogen peroxide and formaldehyde.

Regarding methanol utilization (Mut), three wild-type phenotype strains have been identified as follows: Mut^+, a high oxygen-consuming strain which is capable of fully utilizing methanol and is mainly used in recombinant protein production; Mut^s, an intermediate oxygen-consuming strain which lacks the peroxisomal alcohol oxidase AOX1 and thus utilizes methanol much slower than Mut^+ strains; and lastly Mut^-, a low oxygen-consuming strain which lacks both AOX1 and AOX2 and consequently lacks the ability to utilize methanol. When Mut^s strains are used, methanol accumulation in the bioreactor cultivations does not accelerate the growth rate of the cells unlike cultivations involving Mut^+ strains (Theron et al., 2018).

However, one of the limitations of this expression system lies in the carbon and energy source, i.e. methanol as its toxic and flammable nature gives rise to storage and handling difficulties and preclude its usage in the production of medical and food-grade products (Shen et al., 2016). Moreover, the by-product of methanol metabolism, hydrogen peroxide, gives rise to oxidative stress that can inadvertently degrade the desired recombinant proteins (Hilt and Wolf, 1992). Therefore, this has called for a search for methanol-free systems capable of expressing therapeutic proteins without the need for methanol to induce the naturally occurring *AOX1* promoter.

2.2.1.2. $\mathbf{P_{GAP}}$

Glyceraldehyde-3-phosphate dehydrogenase promoter (P_{GAP}) (Waterham et al., 1997) is a strong constitutive promoter that can be induced by glucose or glycerol as the carbon and energy source, consequently replacing the need for methanol altogether. Its main advantage lies in the fact that it does not require another carbon source to induce protein production, which makes it highly favorable for usage in continuous cultures. For the pharmaceutical sector, fermentation processes based on P_{GAP} in the presence of glucose-based defined media are more advantageous than the ones based on P_{AOX1}, since the use of methanol can complicate separation processes and required documentations (Vogl et al., 2013).

2.2.1.3. $\mathbf{P_{ADH2}}$

Alcohol dehydrogenase promoter (P_{ADH2}) was identified by Cregg and Tolstorukov (2012) as a strong ethanol-inducible promoter by conducting air-filtered shake flask bioreactor experiments and comparing the activity of the reporter protein β-lactamase under the expression of P_{ADH2} on ethanol to that of P_{GAP} on glucose. Ethanol is converted into acetaldehyde by ADH and then transformed into acetate by acetaldehyde dehydrogenase and lastly into acetyl-CoA by the help of acetyl-CoA synthase (Ren et al., 2003).

Karaoğlan et al. (2016) compared the production of *Aspergillus niger* xylanase (XylB) under the control of P_{ADH2} (termed as P_{ADH3} in the study), P_{GAP} and P_{AOX1} with ethanol,

glucose and methanol used as the carbon sources, respectively. The enzyme activity of xylanase was the highest for P_{ADH3} (3725 U/mL) which was 6.4- and 1.8-fold higher than that of P_{GAP} and P_{AOX1} cultures, respectively. Also, the specific productivity of P_{ADH2} was 1.2- and 6-fold higher than that of P_{AOX1} and P_{GAP} cultures, respectively. This indicates that r-protein production under P_{ADH2} and in the presence of ethanol is more efficient and favorable than P_{AOX1} and P_{GAP} r-protein-based productions.

2.2.1.4. $P_{ADH2\text{-}Cat8\text{-}L2}$

In order to make use of and enhance the ethanol utilization pathway of *P. pastoris*, Ergün et al. (2019) engineered a novel promoter variant of the ethanol inducible P_{ADH2} via engineering transcription factor binding sites and termed it $P_{ADH2\text{-}Cat8\text{-}L2}$. Air-filtered shake flask bioreactor experiments were conducted with 2% (v/v) ethanol added batch-wise to determine its effect on the production of enhanced green fluorescent protein (eGFP) under the expression of the novel $P_{ADH2\text{-}Cat8\text{-}L2}$ and wild-type P_{ADH2}. 4.8-fold higher eGFP levels were achieved by $P_{ADH2\text{-}Cat8\text{-}L2}$ when the cells were induced by ethanol. It was observed that wild type X33, and strains under the control of P_{AOX1}, P_{GAP}, P_{ADH2} and $P_{ADH2\text{-}Cat8\text{-}L2}$ reached very similar cell concentrations under the same substrate concentrations regardless whether ethanol or methanol were used as the carbon and energy source. Nevertheless, increasing ethanol and methanol concentrations exerted an inhibition effect on the growth after 2% (v/v) ethanol and methanol, especially at 5% where the inhibition effect was ~2.5- and 1.5-fold for when ethanol and methanol were used respectively. Moreover, the P_{AOX1}-controlled eGFP normalized expression level under 2% (v/v) methanol was 1.6-fold higher than P_{ADH2} under 2% (v/v) ethanol, whereas it was 7.1-fold less when 2% (v/v) ethanol was used when compared to P_{ADH2} under 2% (v/v) ethanol. On the contrast, the $P_{ADH2\text{-}Cat8\text{-}L2}$-controlled eGFP expression level under 2% (v/v) ethanol was 4.5-fold higher than P_{ADH2} under 2% (v/v) ethanol and only 1.3-fold higher under 2% (v/v) methanol. This clearly indicates that ethanol is a better inducer for $P_{ADH2\text{-}Cat8\text{-}L2}$ while methanol induces P_{AOX1} more efficiently. Lastly, another model protein, recombinant human serum albumin (rhSA), was used to compare the production rates of P_{ADH2} and $P_{ADH2\text{-}}$

Cat8-L2 strains in the presence of ethanol in air-filtered shake flask bioreactor experiments where $P_{ADH2\text{-}Cat8\text{-}L2}$ produced 4.4-fold more protein than the native promoter, serving as an indicator to the robustness of the engineered variant.

2.3. Bioreactor Experimental Design

Çalık et al. (2016) defined the cultivation time to be a bioreactor performance indicator between initial and final cultivation conditions that is both magnitude dependent and proportionally related to variations in C_s in the cultivation medium where q_s, μ, q_p and the production rate of by-products influence its value. In order to increase production and productivity in continuous feed stream strategies with pre-determined specific growth rates, the transition time period, i.e., time required to switch from batch phase to the recombinant protein induction phase, and specific growth rate selected ought to be optimized for maximum performance. First, μ is determined from batch cultivations and then the optimum transition time is investigated by starting with a transition time of 0 h and a substrate flow rate calculated by the determined μ. After that, increments of transition time are tested individually and the new substrate flow rates are recalculated until an optimum transition time is determined based on the r-protein production. Once the transition time has been optimized, different fed-batch runs utilizing the same determined optimum transition time are conducted but with increments of the μ found in the batch experiments where the volumetric flow rate of substrate is recalculated based on the different μ values tested until an optimal r-protein production is achieved. The mass conservation equations and the mathematical model for fed-batch bioreactor operations with continuous feed stream design are presented in subsections (2.4.1) and (2.4.2) according to Çalık et al. (2016).

2.3.1. Mass Conservation Equations

The general mass balance conservation equation for the species (cells, substrates, proteins) involved in fed-batch bioreactor operations can be represented as follows:

$$input - output + generation = accumulation \qquad (2.1)$$

After inoculation, cultivation proceeds without cell feed and small sample volumes are withdrawn as to minimize the perturbation effects on cell formation yielding the following cell mass conservation equation:

$$r_x V = \frac{d(C_x V)}{dt} \tag{2.2}$$

where t is the cultivation time, C_x is the cell concentration and V is the cultivation medium volume.

The cell formation rate, r_x, is defined by the following first-order kinetic equation:

$$r_x = \mu C_x \tag{2.3}$$

$\frac{dV}{dt}$ is the volume increase caused by continuous feeding and is represented by Q(t) which is the time-varying inlet stream flow rate.

Assuming constant cultivation medium density, equations (2.2) and (2.3) with the definition of Q(t) yield the following equation for μ:

$$\mu = \frac{1}{(C_X)}\frac{dC_x}{dt} + \frac{Q(t)}{V} \tag{2.4}$$

Performing a mass balance on the continuously fed substrate(s) yields the following equation:

$$Q(t)C°_s + r_s V = \frac{d(C_s V)}{dt} \tag{2.5}$$

where $C_s°$ is the substrate concentration in the inlet feed and

$$-r_s = q_s C_x \tag{2.6}$$

where q_s is the specific substrate uptake rate.

Substituting equation (2.6) into (2.5) yields the following relation for q_s:

$$q_s = -\frac{1}{C_x}\left(\frac{dC_s}{dt} + \frac{C_s}{V}Q(t) - \frac{Q(t)}{V}C°_s\right) \tag{2.7}$$

Performing a mass balance on the product(s) formed yields the following equation:

$$r_p V = \frac{d(C_p V)}{dt} \tag{2.8}$$

where r_p is the product formation rate defined as

$$r_p = q_p C_x \tag{2.9}$$

where q_p is the product formation rate.

Substituting equation (2.9) into (2.8) yields:

$$q_p = \frac{1}{C_x}\left(\frac{dC_p}{dt} + \frac{Q(t)}{V} C_p\right) \tag{2.10}$$

2.3.2. Fed-Batch Bioreactor Mathematical Model

Combining equations (2.2) and (2.3), the mathematical model for the cell yields:

$$\frac{d(C_x V)}{dt} - \mu C_x V = 0 \tag{2.11}$$

Rearranging equation (2.7) for the substrate(s) fed into the bioreactor yields:

$$\frac{dC_s}{dt} + \frac{Q(t)}{V} C_s + q_s C_x = \frac{Q(t)}{V} C°_s \tag{2.12}$$

Rearranging equation (2.10) for the product(s) formed yields:

$$\frac{dC_p}{dt} + \frac{Q(t)}{V} C_p - q_p C_x = 0 \tag{2.13}$$

Assuming dC_s/dt to be zero in equation (2.5) yields:

$$Q(t) C°_s + r_s V = C_s \frac{dV}{dt} \tag{2.14}$$

Substituting equation (2.6) into (2.14) and using the definition of biomass yield on substrate $Y_{x/s}$ yields:

$$Q(t) C°_s - \frac{r_x}{Y_{x/s}} V = C_s \frac{dV}{dt} \tag{2.15}$$

Integrating equation (2.11) from t=0 to t=t and from $C_xV=C_{x0}V_0$ to $C_xV=C_xV$ gives:

$$\int_0^t \mu dt = \int_{c_{x0}V_0}^{CxV} \frac{1}{C_x V} d(C_x V) \quad (2.16)$$

Equation (2.16) yields:

$$C_x V = C_{x0} V_0 e^{\mu t} \quad (2.17)$$

Substituting equations (2.3) and (2.18) into equation (2.15) yields:

$$Q(t) = \frac{\mu V_0 C_{x0}}{Y_{x/s}(C^\circ_s - C_s)} \exp(\mu t) \quad (2.18)$$

Assuming $C^\circ_S >> C_s$ yields:

$$Q(t) = \frac{\mu V_0 C_{x0}}{Y_{x/s} C^\circ_s} \exp(\mu t) \quad (2.19)$$

where μ (h^{-1}) represents the pre-determined specific growth rate, V_0 (L) is the initial cultivation volume, C_{x0} (g L^{-1}) is the cell concentration at the beginning of the induction phase, C°_S (g L^{-1}) is the inlet feed substrate concentration, and $Y_{x/s}$ (g g^{-1}) is the biomass yield on substrate.

2.3.3. Hybrid Fed-Batch Bioreactor Operation Design

Çalık et al. (2018) designed a novel fed-batch strategy termed as hybrid fed-batch bioreactor (HFBB) operation that controls q_s by successively shifting from fed-batch to batch operations within integrated designed cultivation time periods in order to drive the metabolism of the cell towards the production of the desired r-protein. Basically, after the glycerol batch phase, fed-batch operation is initiated for 1.5 h followed by 0.5 h of batch operation then again by fed-batch operation and so forth until the end of cultivation. Higher C_x values and higher r-protein titers can be achieved with this strategy compared to traditional fed-batch feeding strategies, with no substrate accumulation problems in the cultivation medium.

2.3.4. Yield Coefficients

Yield coefficients are used to obtain a better understanding of how efficient a bioprocess in converting substrate into cell and desired products is. Three general

definitions of yields are mainly used as follows: $Y_{x/s}$, which is the mass of cell produced per mass of substrate consumed, $Y_{p/s}$, which is the mass of product produced per mass of substrate consumes; and lastly, $Y_{p/x}$, which is the mass of product produced per mass of cell produced. These parameters can be calculated instantaneously as such:

$$Y_{x/s} = \frac{r_x}{-r_s} = \frac{dC_x/dt}{-dC_s/dt} \tag{2.20}$$

$$Y_{p/s} = \frac{r_p}{-r_s} = \frac{dC_p/dt}{-dC_s/dt} \tag{2.21}$$

$$Y_{p/x} = \frac{r_p}{r_x} = \frac{dC_p/dt}{dC_x/dt} \tag{2.22}$$

Yield coefficients can also be calculated as overall parameters as such:

$$Y_{x/s} = \frac{\Delta x}{-\Delta s} \tag{2.23}$$

$$Y_{p/s} = \frac{\Delta p}{-\Delta s} \tag{2.24}$$

$$Y_{p/x} = \frac{\Delta p}{\Delta x} \tag{2.25}$$

2.3.5. Volumetric Productivity

Productivity in biological systems is the rate of producing the desired produced per two critical elements: time and capacity, both of which give an idea of the efficiency of the system in hand.

Overall volumetric productivity is defined as the mass of product produced per volume of cultivation medium per time required and has the following equation (Ponte et al., 2018):

$$V_p = \frac{\Delta(C_p V)}{V \Delta t} \tag{2.26}$$

2.4. Fed-Batch Bioreactor Feeding Strategies

Fed-batch bioreactor strategies involve the addition of one or more nutrients to the medium during cultivation in an attempt to prevent the accumulation of substrates that can be growth-inhibitory at high concentrations and to prevent catabolite repression that results from the increase of the concentration of ATP, which represses enzyme biosynthesis, by controlling the substrate feed rate (Villadsen et al., 2011). This mode of operation is superior to traditional batch operations (Yamanè and Shimizu, 1984) most importantly when changing the concentration of substrates affects the productivity or yield of the desired recombinant protein (Villadsen et al., 2011).

2.4.1. Continuous Feed Stream Design with Pre-Determined Specific Growth Rate and Other Parameters

This type of strategy aims at maintaining the specific growth rate (μ) constant by assuming a quasi-steady state system, which states that substrate concentration, C_s, and the specific growth rate, μ, are constant, and cell concentration varies but within a limited range (Zhang et al., 2000). The feeding rate profile is derived from the mass balances performed on biomass and substrate fed (equation 2.19), with the biomass yield on substrate $Y_{x/s}$ assumed constant and the residual substrate concentration in the cultivation medium assumed negligible, since substrate uptake is either directly or indirectly associated with cell growth (Liu et al., 2019). Also, this strategy provides a systematic way to study the effects of changing specific growth rates on cell growth and recombinant protein production; however, there is a risk of undesired substrate accumulation especially at higher specific growth rates (Liu et al., 2019).

2.4.2. Continuous Feed Stream Design with Constant C_S (Substrate-stat)

This type of feeding strategy, also known as substrate-stat, aims at maintaining the residual concentration of the substrate in the cultivation medium constant through a PI or PID feedback-loop control mechanism with a probe inserted directly into the cultivation medium to measure C_s or by measuring C_s in the exhaust gas and accordingly adjusting the substrate flow rate supplied via a peristaltic pump. This type

of continuous feeding strategy allows studying the effects of varying C_s on cell growth and r-protein production, while eliminating the risk of undesired substrate accumulation in the cultivation medium.

Barrigón et al. (2013) compared two different methanol feeding strategies, a continuous methanol feed stream design with pre-determined specific growth rates of 0.015, 0.020 and 0.045 h^{-1}, and methanol-stat with methanol set points of 1, 2, 3, 5 and 10 g L^{-1} to study their effects on the production of *Rhizopus oryzae* lipase (ROL) expressed in a Mut^+ *P. pastoris* under the control of P_{AOX1}. Concerning the first set of experiments, as the pre-determined specific growth rate increased, the enzyme activity, protein yield on biomass, $Y_{p/x}$, and volumetric productivity decreased, where they were 5-fold, 5.5-fold, and 3-fold higher for μ=0.015 h^{-1} than μ=0.045 h^{-1}, respectively, as depicted in Table 2.1. However, these values were only slightly less for μ= 0.020 h^{-1}. In addition, the mean specific protein production rate was the same for μ= 0.015 and 0.020 h^{-1} but 2.6-fold less for μ= 0.045 h^{-1}. Also, the substrate uptake rate and specific growth rates were maintained almost constant over the cultivation time indicating the functionality of the pre-determined exponential feeding equation. Concerning the methanol-stat strategies, similar results were obtained up to 2 g L^{-1} after which the enzyme activity, $Y_{p/x}$ and volumetric productivity increased 22-, 2.6- and 2.2-fold respectively for methanol set-point of 3 g L^{-1}. Also, the mean specific protein production rate increased 3-fold at 3 g L^{-1}, whereas it was 1.8-fold less for the 10 g L^{-1} culture. The mean specific growth rates were also similar for all the methanol-stat cultures except for the 10 g L^{-1} culture, where it was 1.8-fold less with a 1.3-fold lower volumetric productivity and longer cultivation time than the 3 g L^{-1} culture. All in all, the optimal methanol feeding strategy was the methanol-stat 3 g L^{-1} culture with 2- and 2.9-fold higher enzyme activity and volumetric productivity than the best pre-determined specific growth rate feeding strategy i.e., 0.015 h^{-1}, with high methanol concentrations exerting an inhibitory effect on growth and productivity.

Table 2.1. *Results of Barrigón et al.'s 2013 study*

		Pre-determined μ			Methanol-stat				
		0.015 h^{-1}	0.02 h^{-1}	0.045 h^{-1}	1 g L^{-1}	2 g L^{-1}	3 g L^{-1}	5 g L^{-1}	10 g L^{-1}
Lipolytic activity	U mL^{-1}	135	112	27	59	13	280	210	294
$Y_{P/X}$	U g^{-1}	2644	2130	479	1070	2004	5282	3905	5635
Volumetric productivity	U L^{-1} h^{-1}	1857	1700	623	1243	2437	5406	3964	4264
μ_{mean}	h^{-1}	0.014	0.022	0.043	0.042	0.043	0.046	0.046	0.025
$q_{s,mean}$	g g^{-1} h^{-1}	0.07	0.12	0.17	0.23	0.19	0.20	0.20	0.14
qp_{mean}	U g^{-1} h^{-1}	46	46	18	45	106	322	234	175

2.4.3. Co-Substrate Feeding (Mixed feeding)

This type of feeding strategy incorporates a non-repressing carbon source such as sorbitol, mannitol or glucose that is co-fed with the main substrate in order to increase productivity of continuous feed stream design strategies and decrease the cellular burden on the main substrate.

Çelik et al. (2009) utilized sorbitol as a non-repressing carbon source with methanol in a mixed feeding strategy to produce recombinant human erythropoietin (rHuEpo) under the expression of P_{AOX1} in a Mut^+ strain. At the end of the methanol transition phase, sorbitol was batch-wise added at t= 0 h of the induction phase in such a fashion to increase its concentration in the cultivation medium to 50 g L^{-1} and methanol was fed in a continuous feed stream strategy with a pre-determined specific growth rate of 0.02, 0.03 and 0.04 h^{-1} with the strategies termed as MS-0.02, MS-0.03, MS-0.04, respectively. Another fed-batch strategy was implemented with only methanol being fed as the sole carbon and energy source with a pre-determined specific growth rate of 0.03 h^{-1} and was termed M-0.03. Sorbitol concentration was determined based on air-filtered shake flask bioreactor experiments in which different concentrations of sorbitol (0-80 g L^{-1}) were tested with 50 g L^{-1} being the optimum for cell growth and protein production. The addition of sorbitol to the fed-batch cultivations eliminated the long lag phase of 9 h observed in the strategy without sorbitol (M-0.03), led to a

1.7-fold higher C_x for MS-0.03 at t= 24 h, decreased the cultivation time by 2.3-fold, and increased C_p by 1.7-fold at t= 18 h. Also, the presence of sorbitol decreased the production of proteases and eliminated the accumulation of lactic acid resulting from insufficient O_2 in the medium by decreasing oxygen uptake rate (OUR) 2-fold. The highest sorbitol uptake rate, q_s, and specific protein production rate, q_p, were found to be 0.107 g g^{-1} h^{-1} and 0.172 mg g^{-1} h^{-1} for MS-0.04, respectively. However, the highest protein to biomass yield $Y_{p/x}$ was 1.97 mg g^{-1} for M-0.03. The lowest C_p was for MS-0.02 whereas those of MS-0.03 and MS-0.04 were quite similar. The highest C_p was achieved by M-0.03 but at the expense of a 2.3-fold longer cultivation time.

Çalık et al. (2013) designed and compared eight different fed-batch feeding strategies with sorbitol involved as a co-substrate to produce rhGH under the control of P_{AOX1} in a Mut^+ strain. The eight strategies were as follows: M involving a continuous feed stream of methanol with a pre-determined specific growth rate of 0.03 h^{-1}; MS involving a continuous feed stream of methanol with a pre-determined specific growth rate of 0.03 h^{-1} with batch-wise sorbitol addition at t=0 h of induction to increase its concentration to 50 g L^{-1} in the cultivation medium; MSS involving a continuous feed stream of methanol with a pre-determined specific growth rate of 0.03 h^{-1} with batch-wise sorbitol addition at t= 0 and 9 h of induction to increase its concentration to 50 g L^{-1} in the cultivation medium; MSSS involving a continuous feed stream of methanol with a pre-determined specific growth rate of 0.03 h^{-1} with batch-wise sorbitol addition at t= 0, 14 and 31 h of induction to increase its concentration to 50 g L^{-1} in the cultivation medium; SSM1 involving a continuous feed stream of methanol with a pre-determined specific growth rate of 0.03 h^{-1} with batch-wise sorbitol addition at t=0 h of induction to increase its concentration to 50 g L^{-1} in the cultivation medium and maintain it at that value between t= 0-15 h by a continuous feed stream of sorbitol with a pre-determined specific growth rate of 0.025 h^{-1} which was calculated based on $q_{sorbitol}$ between t= 0-6 h of the MS strategy; SSM2 involving a continuous feed stream of methanol with a pre-determined specific growth rate of 0.03 h^{-1} with batch-wise sorbitol addition at t= 0 h of induction to increase its

concentration to 50 g L^{-1} in the cultivation medium and maintain it at that value between t= 0-15 h by a continuous feed stream of sorbitol with a pre-determined specific growth rate of 0.025 h^{-1} with the pH reduced from 5.5 to 5.0 after the 24th hour of induction; SSM3 involving a continuous feed stream of methanol with a pre-determined specific growth rate of 0.04 h^{-1} with batch-wise sorbitol addition at t= 0 h of induction to increase its concentration to 50 g L^{-1} in the cultivation medium and maintain it at that value between t= 0-15 h; SM involving a continuous feed stream of methanol and sorbitol mixed in water at a ratio of 1.37:6.21 with a pre-determined total specific growth rate of 0.03 h^{-1} from t= 0-30 h followed by a continuous feed stream of methanol with a pre-determined specific growth rate of 0.03 h^{-1} beyond t= 30 h. When the pulse-feeding strategies MS, MSS and MSSS were compared to the M strategy, the highest rhGH concentration belonged to MSS at 0.3 g L^{-1} which was 1.67-fold higher than when only methanol was used and slightly higher than the MS and MSSS strategies. The C_x of the MSS strategy was approximately 1.8-fold higher than that of the M strategy. Concerning the remaining strategies, the highest rhGH concentration was achieved by SSM1 at 0.64 g L^{-1} which was 2.1-fold higher than the MSS strategy and approximately 3.8-fold higher than that of the M strategy. However, very low rhGH concentrations were achieved by the SSM3 and SM strategies approximately 4.3- and 5.9-fold lower than that of SSM1 respectively. Moreover, 1.7-1.9-fold higher C_x values than MSS were obtained by these strategies. Also, it was noticed that C_p increased rapidly after the pH in the SSM2 strategy was decreased to 5.0 indicating the importance of the medium pH on protein production.

Eskitoros and Çalık (2014) designed and compared six different fed-batch strategies using sorbitol, mannitol and/or glycerol as co-substrates to produce recombinant human erythropoietin (r-HuEpo) under the control of P_{AOX1} in a Mut^+ strain. The six strategies were as follows: MS* involving a continuous feed stream of methanol with a pre-determined specific growth rate of 0.03 h^{-1} with batch-wise sorbitol addition at t=0 h of induction to increase its concentration to 50 g L^{-1} in the cultivation medium; SSM involving a continuous feed stream of methanol with a pre-determined specific

growth rate of 0.03 h^{-1} with batch-wise sorbitol addition at t= 0 h of induction to increase its concentration to 50 g L^{-1} and maintaining it at that level for the first 15 hours of cultivation by a continuous feed stream of sorbitol with a pre-determined specific growth rate of 0.025 h^{-1}; MMM involving a continuous feed stream of methanol with a pre-determined specific growth rate of 0.03 h^{-1} with batch-wise mannitol addition at t= 0 h of induction to increase its concentration to 50 g L^{-1} and maintaining it at that level for the first 9 hours of cultivation by a continuous feed stream of mannitol with a pre-determined specific growth rate of 0.11 h^{-1}; MLM involving a continuous feed stream of methanol with a pre-determined specific growth rate of 0.03 h^{-1} with batch-wise mannitol addition at t= 0 h of induction to increase its concentration to 3 g L^{-1} and maintaining it at that level for the first 10 hours of cultivation by a continuous feed stream of mannitol with a pre-determined specific growth rate of 0.005 h^{-1}; MPM involving a continuous feed stream of methanol with a pre-determined specific growth rate of 0.03 h^{-1} with batch-wise mannitol addition at t=0, 6 and 12 h of induction to increase its concentration to 50 g L^{-1}; MPMG involving a continuous feed stream of methanol with a pre-determined specific growth rate of 0.03 h^{-1} with batch-wise mannitol-glycerol addition at t= 0, 7, 14 and 24 h of induction to increase mannitol and glycerol concentrations to 50 and 8 g L^{-1}, respectively. The highest rHuEpo concentration was obtained as 645 mg L^{-1} for the MPM strategy, which was 2-, 4-, 2-, 4-, and 2-fold higher than the SSM, MS, MMM, MLM and MPMG strategies, respectively. Also, the highest protein to biomass and protein to substrate yields belonged to the MPM strategy at values of 16.66 and 3.74 mg g^{-1} respectively, with the highest specific protein production rate as well. It was also noticed that mannitol metabolism was faster than that of sorbitol and caused a decrease in cultivation time.

Ata et al. (2015) utilized codon optimization and different fed-batch feeding strategies involving various co-substrates and continuous methanol feed stream designs for the productions of glucose isomerase (GI) in a Mut^{+} strain. The seven different strategies are summarized as follows: S1* involving wild type GI, continuous feed stream of

methanol with a pre-determined specific growth rate of 0.03 h^{-1} with batch-wise sorbitol addition at t= 0 h of induction to increase its concentration to 50 g L^{-1} in the cultivation medium; S1 involving codon-optimized GI strain, continuous feed stream of methanol with a pre-determined specific growth rate of 0.03 h^{-1} with batch-wise sorbitol addition at t= 0 h of induction to increase its concentration to 50 g L^{-1} in the cultivation medium; S2 involving codon-optimized GI strain, continuous feed stream of methanol and peptone with the same individual pre-determined specific growth rate of 0.03 h^{-1}; S3 involving codon-optimized GI strain, continuous feed stream of methanol with a pre-determined specific growth rate of 0.03 h^{-1} with batch-wise mannitol addition at t= 0 h of induction to increase its concentration to 25 g L^{-1} in the cultivation medium which was chosen according to the 3-fold increase in GI activity in previously-conducted air-filtered shake flask bioreactor experiments; S4 involving codon-optimized GI strain, continuous feed stream of methanol and peptone with the same individual pre-determined specific growth rate of 0.03 h^{-1} with batch-wise mannitol addition at t= 0 h of induction to increase its concentration to 25 g L^{-1} in the cultivation medium; S5 involving codon-optimized GI strain, and continuous methanol feeding to maintain its concentration at 5 g L^{-1} in the cultivation medium (methanol-stat); S6 involving codon-optimized GI strain, and continuous methanol feeding to maintain its concentration at 5 g L^{-1} in the cultivation medium (methanol-stat) with batch-wise mannitol addition at t= 0 h of induction to increase its concentration to 25 g L^{-1}. The codon optimization (S1) lead to slower consumption of sorbitol in the medium where it was present for 12 hours longer than $S1^{*}$, and to a 2.4- and 2.7-fold higher GI activity and average specific activity, respectively. In addition, the highest enzyme activity among the exponential feeding strategies was obtained for S3 whereas the lowest was for S1 indicating the advantage of using mannitol over sorbitol. Furthermore, the highest enzyme activity was among the methanol-stat strategy S5 which was 17-, 13.3-, 7.8- and 4-fold higher than S4, S2, S3 and S6. It was observed that the addition of mannitol shortened the growth phase and accelerated the initiation of the stationary phase. Also, the use of mannitol did not increase the enzyme activity when comparing S5 to S6 with a 4.1-fold lower activity for strategy S6.

Güneş et al. (2016) compared five different substrate feeding strategies to produce recombinant human growth hormone rhGH under the expression of P_{AOX1} in a Mut^+ strain. In the first two strategies, a continuous feed stream strategy was utilized with methanol being fed at a pre-determined specific growth rate of 0.03 h^{-1} with mannitol being maintained at 50 g L^{-1} in the first six hours of induction and termed MM1, whereas in the second strategy, mannitol was fed at t= 0, 8 and 15 h of induction to increase its concentration to 50 g L^{-1} and termed as MM2. In the third and fourth strategies, methanol-stat was applied where its concentration was maintained at 5 g L^{-1}, with sorbitol being fed batch-wise at t= 0 h to increase its concentration to 50 g L^{-1} for MC1 strategy, whereas no sorbitol was fed in the strategy termed as MC2. In the last strategy, SSM1, methanol was fed exponentially with a pre-determined specific growth rate of 0.03 h^{-1} but with sorbitol being fed for the first 15 h of induction to maintain its concentration at 50 g L^{-1}. It was observed that the specific uptake rate of mannitol was higher than that of sorbitol and that the highest C_x was obtained for MM1 where mannitol was used as a co-substrate being 1.5-fold of SSM1 where sorbitol was used instead. However, 1.2-fold and 2.1-fold higher protein yield of total substrate $Y_{p/st}$ and protein yield on biomass $Y_{p/x}$ were obtained for SSM1 when compared to MM1. Mannitol thus resulted in higher C_x but lower C_p yield and decreased cultivation time by more than 1.4-fold. Significantly, applying a methanol-stat strategy increased rhGH concentration 2-5.2-fold compared to the exponential feeding strategies. Also, the use of sorbitol decreased the methanol demand of the cells 2-fold, increased $Y_{P/St}$ 1.6-fold, shortened cultivation time by 12 hours, and increased productivity in the methanol-stat strategies.

As a summary, co-substrate feeding incorporates a non-repressing carbon source such as sorbitol, mannitol or glucose that is co-fed with the main substrate to eliminate long lag phases (Çelik et al., 2009), decrease cultivation time (Çelik et al., 2009; Zhu et al., 2011; Eskitoros and Çalık, 2014; Güneş et al., 2016), increase r-protein production (Çelik et al., 2009; Çalık et al., 2013, Eskitoros and Çalık, 2014; Güneş et al., 2016) and decrease the production of proteases (Çelik et al., 2009).

2.4.4. Dissolved Oxygen-stat (DO-stat)

Maintenance of dissolved oxygen (DO) at appropriate levels is of utmost importance in *P. pastoris* cultivations, as high DO levels can greatly reduce cell viability and consequently decrease r-protein production (Chung, 2000). This type of feeding strategy incorporates an indirect feedback control mode to maintain DO constant by altering the substrate feed rate (Trinh et al., 2003); however, the residual substrate concentration and specific growth rate are not held constant, thus precluding the ability to study their effects. Nevertheless, this simple operating strategy has its disadvantages, where during the rapid exponential growth phase, oxygen demand is high, and hence the substrate concentrations become limiting as no more substrate is fed to increase the DO level (Potvin et al., 2012); consequently, cell starvation and a decrease in protein yield occur (Potvin et al., 2012). On the contrary, if high substrate levels are reached, growth inhibition occurs and the DO reaches high levels, consequently increasing the substrate feeding rates eventually poisoning the system and decreasing cell viability (Potvin et al., 2012).

Trinh et al. (2003) compared three different fed-batch strategies for the production of mouse endostatin under the expression of P_{AOX1} in a Mut^+ strain. In the first strategy, methanol-stat was applied where a continuous feed stream of methanol was supplied to maintain its concentration at 3 g L^{-1} in the cultivation medium. In the second strategy, DO-stat was applied where methanol was added to increase its concentration to 0.3% in the cultivation medium when 10% of the DO set point was exceeded. In the third strategy, a continuous methanol feed stream with a pre-determined specific growth rate of 0.020 h^{-1} was implemented. 2-fold higher C_x for the methanol- and DO-stat strategies was obtained. Also, a 1.2-fold higher total endostatin production (mg) was achieved by the methanol-stat strategy than DO-stat and exponential continuous feed stream strategy. 1.5- and 2.3-fold higher C_p (mg L^{-1}) and $Y_{p/x}$ were achieved by the exponential continuous feed stream strategy than DO- and methanol-stat strategies respectively. Also, less methanol was consumed by the exponential continuous feed stream strategy.

Güneş and Çalık (2016) utilized two different oxygen transfer strategies to produce recombinant glucose isomerase (r-GI) under the expression of P_{GAP}. In the first strategy, constant oxygen transfer rate (OTR) was implemented where the aeration rate was either 3 or 10 vvm and the impeller speed was set to 900 min^{-1}. In the second strategy, DO-stat was applied at either 5, 10, 15, 20 or 40%. Both strategies involved a continuous glucose feed stream design based on a pre-determined specific growth rate of 0.15 h^{-1}. The highest C_x was obtained at 44 g L^{-1} for DO-stat 20%. The increase in aeration rate lead to a decrease in final cell density while increasing DO levels lead to an increase in C_x. The highest volumetric and specific enzyme activities were obtained as 4440 U L^{-1} and 126 U g^{-1} for DO-stat 15% respectively. The lowest volumetric enzyme activity was obtained for 10 vvm aeration rate which was approximately 3.6-fold lower than DO-stat 15%. However, decreasing aeration rate to 3 vvm increased the volumetric enzyme activity 2.4-fold. The optimal DO-stat was found to be 15% DO-stat, whereas the enzyme activity decreased below and beyond 15% DO, with the DO-stat<20% strategies being preferred due to their higher volumetric enzyme activities. The highest OTR and OUR rates were also obtained by DO-stat 15% at 0.045 s^{-1} and 8.91 mmol m^{-3} s^{-1}, respectively. Glucose accumulation was observed after t= 9-12 h in all strategies.

Liu et al. (2016) implemented a step by step fed-batch feeding strategy optimization for the large-scale production of glycoside hydrolase LXYL-P1-2 in a Mut^+ strain. In the first step, two DO-stat modes of operation with initial C_x= 75 g L^{-1} were tested: 1) normal operating pressure of 0.05 MPa and enriched oxygen was supplemented to maintain DO at 5% and 2) air pressure was increased to 0.10 MPa without any addition of enriched oxygen. The increase in air pressure caused a 1.4-fold increase in volumetric enzyme activity and volumetric enzyme production, and a 1.3-fold higher biomass enzyme activity and biomass enzyme production, but with almost a 2-fold longer cultivation time. Accordingly, a biomass-stat strategy (C_x= 75 g L^{-1}) at increased air pressure and 5% DO was implemented at three different methanol feeding rates (0.025, 0.035 and 0.050 mL g^{-1} h^{-1}) in order to increase biomass enzyme

activity while maintaining high volumetric enzyme activity. The optimal methanol feeding rate was found to be 0.035 mL g^{-1} h^{-1} with 1.6-fold higher biomass enzyme activity and biomass enzyme production than the previous optimal strategy but with a 1.2-fold longer cultivation time. Also, the highest methanol feeding rate was not suitable for maintaining constant biomass as C_x increased to 95 g L^{-1}. Based on these results, the optimal biomass-stat strategy (0.035 mL g^{-1} h^{-1} methanol feeding rate) was used to study the effects of maintaining DO at 1% instead of 5%. A 1.2-fold increase in volumetric and biomass enzyme activity, and volumetric enzyme production was observed. Moreover, 3 additional initial biomass concentrations (50, 100 and 140 g L^{-1}) with 1% DO-stat, 0.10 MPa and 0.035 mL g^{-1} h^{-1} methanol feed rate were tested and compared to the previous optimal strategy (1% DO-stat and 0.035 mL g^{-1} h^{-1} methanol feed rate) in order to optimize the initial induction biomass. The best strategy was found to be the one with an initial biomass induction 100 g L^{-1} where a 1.1-fold increase in volumetric enzyme activity and production was observed with 16 hours shorter cultivation time. Finally, when scaling up from 10 to 1000 L following the optimal conditions, a 1.4-fold increase in volumetric enzyme production and activity, and 1.3-fold increase in biomass enzyme activity and production was observed with a 1.6-fold shorter cultivation time required to reach peak volumetric enzyme activity and production.

As a summary, the selection of appropriate DO concentrations is crucial for enhancing oxygen transfer and, consequently r-protein production, as concentrations below or above the optimum level can lead to reduced r-protein titers (Güneş and Çalık, 2016; Liu et al.,2016).

2.4.5. Oxygen-Limited Fed-Batch

In oxygen-limited fed-batch bioreactor operations, the limiting nutrient is oxygen opposed to the carbon source(s), where the residual substrate concentration is kept constant, however, the DO level can vary (Potvin et al., 2012). In this type of operation condition, due to oxygen limitation, the DO always plummets to 0%, which in turn

increases the driving force for O_2 transfer and the rate of substrate uptake (Potvin et al., 2012).

Charoenrat et al. (2005) compared the production of Thai Rosewood β-glucosidase under the control of P_{AOX1} between oxygen-limited and DO-stat fed-batch feeding strategies. In the oxygen limited fed-batch strategy, the concentration of methanol in the cultivation medium was maintained constant at 0.35 g L^{-1} which resulted in a rapid decrease in the DO level, whereas in the methanol-limited/DO-stat strategy, the DO level was maintained constant at 25% by controlling the volumetric methanol feed rate. Similar C_x values were obtained, however, a 35% increase in oxygen uptake rate (OUR) was obtained in the oxygen-limited fed-batch culture, 40% higher than that of the DO-stat strategy, which resulted in 40% higher methanol uptake rates and 1.2-fold higher β-glucosidase production for the oxygen-limited fed-batch culture.

Baumann et al. (2008) implemented a hypoxic fed-batch strategy utilizing continuous feed stream with the exponential feeding of the carbon and energy source glucose for the production of 3H6 Fab, and human and porcine trypsinogens under the control of P_{GAP}. From chemostat experiments operating on fully aerobic and hypoxic conditions, the specific production rate of 3H6 Fab increased 2.5-fold only under hypoxic conditions (8.39 and 5.87% O2 in inlet air). Accordingly, two fed-batch strategies were tested: 1) constant glucose feed of 161.7 g h-1 with 20% DO to create carbon limited conditions and 2) hypoxic fed-batch strategy where glucose was first exponentially fed with a pre-determined specific growth rate of 0.2 h^{-1} until DO reached 0% and the concentration of ethanol (resulting from the partially fermentative strategy) in the cultivation medium reached 1% v/v, after which a feedback control was utilized to maintain the concentration of ethanol in the medium at 1% v/v by either increasing or decreasing the glucose flow. Thus, the feed was solely based on the equilibrium between glucose feed rate and oxygen transfer rate. As a result, cultivation time was reduced 2.5-fold, 13% more 3H6 Fab titer was obtained, 29% lower final C_x was reached which facilitates downstream processing, and 2-fold higher q_p was achieved when hypoxic conditions were implemented. Similar results were also

obtained when different model proteins were used i.e., human and porcine trypsinogens, with 2.9-fold lower cultivation time, 11% higher protein titer, and 28% less final C_x when compared to the constant glucose feed strategy. Additionally, more than 1.9-fold higher mean specific growth rates, 4.5$\pm$1.7-fold higher mean protein production rates and ultimately 2.36$\pm$0.16-fold volumetric productivities were obtained when hypoxic conditions were implemented for the three investigated proteins. Furthermore, the increased oxygen transfer rate induced by the limited oxygen concentration and low DO set point, allowed for lower aeration rates i.e., lower stirrer speeds and air flow, which is advantageous for high cell density cultivations on large scale.

As a summary, OLFB has been reported to increase r-protein production (Charoenrat et al., 2005; Baumann et al., 2008) and shorten cultivation time (Baumann et al., 2008). The low oxygen requirements, and increased oxygen and substrate uptake rates make this process economically attractive as these conditions lead to an overall increase in the synthesis of the desired protein (Charoenrat et al., 2005; Baumann et al., 2008).

2.5. Kinetic Models

The kinetic models that describe the growth kinetics of cell cultures can be divided into two main branches: unstructured and structured models.

2.5.1. Structured Models

Structured kinetic models (Montesinos et al., 1995; Ren et al., 2003; Çelik et al., 2009) incorporate aspects of the cell physiology, metabolism and transport phenomena such as the concentration of intracellular and extracellular proteases and enzymes, transport of extracellular substrate(s) into the cell and its internal consumption, intracellular r-protein synthesis and the metabolic reactions and metabolites involved (mRNA composition, amino acid concentration, energy required for polymerization of protein etc.) (Feist et al., 2007; Sohn et al., 2010), and r-protein excretion to the extracellular medium.

2.5.1.1. Compartment Models

In these models, the cell is divided into a few macromolecular pools or compartments where cell components possessing similar functions are grouped together (Çelik et al., 2009). The protein synthesizing system is used as a key component in structured models due to its central role in cellular metabolism (Villadsen et al., 2011). This system consists of ribosomes, which are made up of 40% ribosomal protein and 60% ribosomal RNA, where the latter consists of more than 80% of stable RNA in the cell (Villadsen et al., 2011). The ribosomal level is easily detected by measuring the concentration of RNA is the cell (Villadsen et al., 2011). Hence, the good correlation between the protein synthesizing system and specific growth rate give a good representation of the activity state of the cell. The protein synthesis system is thus placed in the active compartment of the cell (Villadsen et al., 2011).

Çelik et al. (2009) proposed a structured kinetic model based on the fed-batch bioreactor experiments done to produce rHuEPO under the expression of AOX1 using sorbitol as a co-substrate. The cell was divided into three main compartments: 1) the recombinant protein rHuEPO compartment, 2) an enzymatic compartment consisting of alcohol oxidase, the enzyme produced by methanol-induced P_{AOX1} which was driving the expression of rHuEPO, and extracellular protease enzymes that degraded the recombinant protein, and 3) the rest of the cellular components including intracellular proteases. The intracellular accumulation rate of the protein was considered to be zero based on the assumption that the production rate of extracellular proteins is the same as their rate of transport to the extracellular medium. The mass conservation balances done on the cell, substrate, AOX, proteases, and rHuEPO are shown below in the same order:

$$\frac{dC_x}{dt} = C_x(\mu - \frac{Q(t)}{V}) \tag{2.27}$$

$$\frac{dC_s}{dt} = q_s C_x - \frac{Q(t)}{V} C_s \tag{2.28}$$

$$\frac{dC_{AOX}}{dt} = q_{AOX} C_x - \mu C_{AOX} \tag{2.29}$$

$$\frac{dC_{Pro}}{dt} = q_{Pro}C_x - \frac{Q(t)}{V}C_{Pro} \quad (2.30)$$

$$\frac{dC_p}{dt} = q_pC_x - \frac{Q(t)}{V}C_p - q_dC_x \quad (2.31)$$

Constant liquid phase density was assumed and that the change in volume was resulting only from the methanol fed into the reactor Q(t), i.e. dV/dt=Q(t). Also, the degradation term, q_d, was included for extracellular degradation of rHuEPO by the proteases. In addition, the intracellular and extracellular dilution terms were "-μC" and "-Q(t)C/v" respectively.

A Monod equation for the specific growth rate on sorbitol was proposed as follows:

$$\mu_s = \frac{\mu_{max}C_s}{K_s+C_s} \quad (2.32)$$

where μ_s was the specific growth on sorbitol, μ_{max} was the maximum specific growth rate, and K_s was the substrate saturation constant.

The total specific growth rate μ_t was given as follows:

$$\mu_t = \mu_M + \mu_s = \mu_M + \frac{\mu_{max}C_s}{K_s+C_s} \quad (2.33)$$

where μ_M was the pre-determined specific growth rate used for the methanol continuous feed stream, i.e., 0.02, 0.03 or 0.04 h^{-1}.

The specific sorbitol uptake rate followed Pirt's model as it was assumed that sorbitol was used for both growth and maintenance:

$$q_s = -(\frac{\mu_s}{Y_{x/s}} + m_s) \quad (2.34)$$

The specific AOX fermentation rate was related to the specific methanol consumption rate, q_M, since AOX production was induced by methanol:

$$q_{AOX} = k_{a1}q_M + k_{a2} \quad (2.35)$$

k_{a1} accounted for the impact of methanol on q_{AOX} and k_{a2} accounted for all other factors.

The specific production rate of protease was considered to be related to q_M since it was in the same enzymatic compartment as AOX as follows:

$$q_{pro} = k_{p1} q_M + k_{p2} \tag{2.36}$$

k_{p1} accounted for the impact of methanol on q_{pro} and k_{p2} accounted for all the other factors affecting protease production.

The specific protein production rate was related to C_{AOX} as follows:

$$q_p = k_p \frac{C_{AOX}}{C_x} \tag{2.37}$$

k_p showed the dependence of rHuEPO production on AOX production.

Lastly, the degradation of protein was related to the concentration of proteases present in the medium as follows:

$$q_d = k_{d1} \frac{C_{pro}}{C_x} + k_{d2} \tag{2.38}$$

k_{d1} showed the dependence of degradation on the protease concentration while k_{d2} accounted for all other factors.

The model was successfully simulated by simultaneously solving the set of ordinary differential equations (2.27-2.31) using MATLAB® and Runge-Kutta-Fehlberg method (RFK45). The simplex method, an iterative method for calculating the optimal solution to a given linear programming problem, was used for estimating the various parameters.

2.5.1.2. Cybernetic Models

Cybernetic models are dynamic metabolic models consisting of a set of ordinary differential equations that can explain the dynamic change of enzyme and metabolite concentrations both intra- and extracellularly (Young, 2015). Cybernetic control laws are dictated based on the assumption that cells have evolved to efficiently allocate resources towards metabolic pathways (Young, 2015). These models are used for the

prediction of the metabolic regulation effects on the dynamic behavior of biochemical reaction networks based on a quantitative mathematical framework, with various applications such as redesigning cellular hosts by metabolic engineering, and bioprocess control and optimization (Young, 2015). Unlike stoichiometric models, e.g., unstructured models, which necessitate the specification of the substrate uptake rate for flux calculations, cybernetic models, with their kinetic description of reaction rates, can predict the effects of genetic recombination on yields and productivities (Young, 2015). Also, cybernetic models are advantageous to use when diauxic growth is concerned, i.e. growth resulting from the utilization of two different substrates that serve the same purpose in the cell (Villadsen et al., 2011). Shortly, the preferred primary substrate, which usually provides the cells with more nutritional benefits based on the higher specific growth rates observed, is completely consumed and followed by an intermediate lag phase during with the cells switch their regulatory metabolic pathways to synthesizing enzymes capable of metabolizing the secondary substrate (Young, 2015).

2.5.2. Unstructured Models

Unstructured models are the extreme end of simple structured models that can predict the specific growth rate in a biochemical reaction defined by a single "Black Box" model stoichiometry as a function of one or more independent variables:

$$aC_s + bC_{O_2} \rightarrow C_x + dC_{CO_2} + eC_p \quad (2.39)$$

where a, b, d, e and g are stoichiometric coefficients that are equivalent to the overall biomass yields ($Y_{a/x}$, $Y_{b/x}$, $Y_{d/x}$, and $Y_{e/x}$); C_s, C_x and C_p represent the substrate consumed, biomass generated, and protein produced respectively. This equation represents a simplified model of the consumption of ethanol in *P. pastoris* to produce biomass and products. The specific rates of production or consumption of the substrates and products can be determined based on the empirical relation between μ and the independent variables. The rates of production or consumption of all the reactants are proportional to the key reaction rate except for the key reactant, i.e.

ethanol (Villadsen et al., 2011). The primary assumption of these unstructured kinetic models is that growth is limited by a single substrate.

2.5.2.1. Monod Model

The Monod model is the most widely used model to describe the relationship between the substrate and the specific growth rate. Simply, it states that in a steady state condition, the specific growth rate is linear when substrate concentration is small, however, for excess substrate concentrations, the specific growth rate becomes independent of the substrate itself. The cell composition is assumed to be constant since the cell concentration, C_x, is the only representative of cell which has a hugely complex composition (Monod, 1949; Villadsen et al., 2011):

$$\mu = \frac{\mu_{max} C_s}{K_s + C_s} \tag{2.32}$$

where μmax (h^{-1}) is the maximum specific growth rate reached on the specific substrate used and K_s is the saturation constant which is equal to the lowest substrate concentration at which μ is equal to half μ_{max} in the absence of any inhibition (Andrews, 1968).

Jahic et al. (2002) used the Monod model to describe the specific methanol uptake rate of a Mut^+ *P. pastoris* producing a fusion protein under the control of P_{AOX1} on methanol and incorporated it into a kinetic model based on the metabolic flux of carbon substrate and molecular oxygen consumption that could predict oxygen consumption and biomass growth. Maximum methanol uptake rate, q_{smax}, was determined to be 0.57 g L^{-1}, and K_s was determined to be 0.1 g L^{-1}.

2.5.2.2. Haldane Model

The Haldane model (Zhang et al.,2000; Barrigon et al., 2015) offers a slight, but rather important variation of the Monod model, where it does not accept the notion that after a high substrate concentration, the specific growth rate plateaus and becomes independent of the substrate. On the contrary, it offers a mathematical representation of how at high substrate concentrations, a growth inhibition and decrease is observed,

corroborated by an additional term called the inhibition constant, K_i. The inhibition constant is defined as the highest concentration of substrate at which the specific growth rate is half the maximum in the absence of inhibition. The mathematical representation of the model is as follows:

$$\mu = \frac{\mu_{max} C_S}{K_S + C_S + \frac{C_S^2}{K_i}} \tag{2.40}$$

At μmax, $C_{s,crit}$ represents the substrate concentration at which the specific growth rate is at its maximum point. $C_{s,crit}$ can be calculated as:

$$C_{s,crit} = \sqrt{K_S K_i} \tag{2.41}$$

Zhang et al. (2000) used the Haldane model to describe the specific growth rate of a Mut^+ *P. pastoris* producing the heavy-chain fragment C of botulinum neurotoxin serotype A under the control of P_{AOX1} on methanol using to fed-batch feeding strategies. The maximum specific growth rate, K_s and K_i derived from the model were 0.08 h^{-1}, 1.5 g L^{-1}, and 8.86 g L^{-1} respectively. $C_{s,crit}$ was determined as 3.65 g L^{-1} after which the specific growth rate started to decrease with increasing substrate concentration. In addition, the specific substrate uptake rate was modeled according to Pirt's model (equation 2.45) where $Y_{s/x}$ and m_s were determined as 0.84 g g^{-1} and 0.0071 g g^{-1} h^{-1} respectively.

2.5.2.3. Andrews Model

Andrews model offers a slight variation to the Haldane model as such (Andrews, 1968):

$$\mu = \frac{\mu_{max} C_S}{(K_S + C_S)\left(1 + \frac{C_S}{K_i}\right)} \tag{2.42}$$

This model can explain inhibition at high substrate concentrations, however, just like the Haldane model, after a certain range of K_i, this model starts behaving like Monod. In this model, more emphasis is placed on the inhibition exerted by the substrate

concentration represented by the additional $\frac{K_S C_S}{K_i}$ term, which is not found in the Haldane model.

2.5.2.4. Aiba Model

The Aiba model (Aiba et al., 1968) is a variation of the Haldane model that introduces an exponential term $\frac{C_S}{K_i}$ as follows:

$$\mu = \frac{\mu_{max} C_S}{(K_S + C_S)} \exp\left(-\frac{C_S}{K_i}\right) \tag{2.43}$$

2.5.2.5. Moser Model

Moser model (Prabhu and Venkata Dasu, 2017) is a variation of the Monod model where it offers power terms for the substrate concentration as follows:

$$\mu = \frac{\mu_{max} C_S^n}{K_S + C_S^n} \tag{2.44}$$

The power coefficient predicts the degree of substrate inhibition, however, $C_{s,crit}$ cannot be determined from this model.

2.5.3. Pirt Model

Pirt suggested a linear equation for the relationship between the specific substrate uptake rate, qs, and the specific growth rate, μ, (Pirt, 1965):

$$q_s = Y_{s/x}\mu + m_s \tag{2.45}$$

Where $Y_{s/x}$ represents the true conversion of substrate into cell which is the reciprocal of the term itself. The maintenance coefficient, m_s, represents the amount of substrate consumed to perform cellular processes that do not lead to an increase in C_x (Jahic et al., 2002). These processes can be summarized as follows (Villadsen, Nielsen, Lidén, 2011):

- Maintenance of electrical potential and gradients: To ensure homeostasis, the maintenance of electrical potentials and concentration gradients across the

cellular membrane is essential, e.g. a proton gradient. These processes demand an energy source which is provided by the substrate, however, the process itself does not give rise to any cell formation

- Futile Cycles: These represent pairs of reactions which lead to the net hydrolysis of ATP such as the conversion of fructose-6-phosphate (F6P) to fructose 1,6-bisphosphate, which is a reaction that utilizes ATP, followed by its consequent hydrolysis to F6P again, which is a reaction that does not lead to the formation of ATP. This futile cycle is usually prevented by the presence of an inhibitory substrate such as glucose which represses phosphatase
- Turnover of macromolecules: Several macromolecules such as mRNA undergo a continuous cycle of degradation and re-synthesis inside the cell which requires a great amount of Gibbs free energy.

Zhang et al. (2003) used the Pirt model to describe the linear relationship of the specific methanol uptake rate to the specific growth rate of a Mut^+ *P. pastoris* intracellularly producing the heavy-chain fragment C of botulinum neurotoxin serotype C under the control of P_{AOX1} on methanol using two fed-batch feeding strategies. The maximum specific growth rate on methanol and maximum specific methanol uptake rate were 0.02 h^{-1} and 0.028 g h^{-1} g^{-1} WCW, respectively. The true yield $Y_{s/x}$ was found as 0.766 g methanol g^{-1} WCW and the maintenance energy was 0.0128 g methanol h^{-1} g^{-1} WCW.

2.5.4. Luedeking-Piret Model

The Luedeking-Piret model is synonymous with the Pirt model and is used to describe the linear relationship between product formation and specific growth rate instead; it takes on the following general form (Luedeking and Piret, 1959):

$$\frac{dCp}{dt} = \alpha \frac{dCx}{dt} + \beta Cx \qquad (2.46)$$

where α represents the inverse of protein yield on biomass and β represents the maintenance coefficient, mp, which is the minimum amount of protein produced without any increase in biomass

Dividing both sides by Cx yields:

$$\frac{1}{Cx}\left(\frac{dCp}{dt}\right) = \frac{\alpha}{Cx}\left(\frac{dCx}{dt}\right) + \beta \tag{2.47}$$

Equation 2.47 is synonymous with the following equation:

$$q_p = \alpha\mu + \beta \tag{2.48}$$

where α and β are the growth-associated and non-growth associated coefficients of the Luedeking-Piret model respectively. Accordingly,

$$q_p = Y_{p/x}\mu + m_p \tag{2.49}$$

where $Y_{p/x}$ represents the inverse of protein yield on biomass and m_p represents the maintenance coefficient which is the minimum amount of protein produced without any increase in biomass.

Garnier and Gaillet (2015) proposed an analytical solution for the combination of Monod growth kinetics and Luedeking-Piret model in batch cultures using the following equations and assumptions:

$$\frac{dC_x}{dt} = \mu C_x \tag{2.50}$$

$$\frac{dC_s}{dt} = -q_s C_x \tag{2.51}$$

$$\frac{dC_p}{dt} = \alpha\frac{dC_x}{dt} + \beta C_x \tag{2.46}$$

$$\mu = \frac{\mu_{max} C_s}{K_s + C_s} \tag{2.32}$$

$$q_s = \frac{\mu}{Y_{x/s}} \tag{2.52}$$

$$Y_{x/s} = -\frac{dC_x}{dC_s} \tag{2.20}$$

Assuming constant biomass to substrate yield $Y_{x/s}$, negligible cell death and lag phase:

$$C_s = \frac{1}{Y_{x/s}}(C_{x,max} - C_x) \tag{2.53}$$

where $C_{x,max}$ is the maximum C_x at stationary phase calculated with $C_x = C_{x0}$ and $C_s = C_{s0}$.

Substituting equations (2.32), (2.50), and (2.53) yields:

$$\frac{d(C_x)}{dt} = \frac{\mu_{max}(C_{x,max} - C_x)}{K_s Y_{x/s} + (C_{x,max} - C_x)} C_x \tag{2.54}$$

Integrating between $C_x = C_{x0}$ at t= 0 and $C_x = C_x$ at t= t yields the following non-explicit relationship:

$$\left(\frac{K_s Y_{x/s} + C_{x,\max}}{C_{x,\max}}\right) \ln\left(\frac{C_x}{C_{x0}}\right) - \left(\frac{K_s Y_{x/s}}{C_{x,\max}}\right) \ln\left(\frac{C_{x,max} - C_x}{C_{x,max} - C_{x0}}\right) = \mu_{max} t \tag{2.55}$$

This equation is solved by performing a linear regression on biomass and time data with t being the variable linearly dependent on both $\ln\left(\frac{C_x}{C_{x0}}\right)$ and $\ln\left(\frac{C_{x,max} - C_x}{C_{x,max} - C_{x0}}\right)$ as such:

$$t = a_1 \ln\left(\frac{C_x}{C_{x0}}\right) + a_2 \ln\left(\frac{C_{x,max} - C_x}{C_{x,max} - C_{x0}}\right) \tag{2.56}$$

where $a_1 = \left(\frac{K_s Y_{x/s} + C_{x,\max}}{\mu_{max} C_{x,\max}}\right)$ and $a_2 = -\left(\frac{K_s Y_{x/s}}{\mu_{max} C_{x,\max}}\right)$

Then, μ_{max} and $K_s Y_{x/s}$ are calculated as:

$$\mu_{max} = \frac{1}{a_1 + a_2} \tag{2.57}$$

$$K_s Y_{x/s} = -\frac{a_2}{a_1 + a_2} C_{x,max} \tag{2.58}$$

$Y_{x/s}$ can be calculated from the slope of C_x vs C_s values.

For r-protein production, a partial integration of equation 2.46 gives:

$$C_p - C_{p0} = \alpha(C_x - C_{x0}) + \beta \int_0^t C_x dt \quad (2.59)$$

Temporarily assuming t to be the dependent variable in equation (2.55) and integrating it between $C_x = C_{x0}$ at t= 0 and $C_x = C_x$ at t= t yields:

$$\int_{C_{x0}}^{C_x} t dC_x = \frac{1}{\mu_{max}} [\{ C_x \ln\left(\frac{C_x}{C_{x0}}\right) - (C_x - C_{x0})\} +$$

$$\frac{K_s Y_{x/s}}{C_{x,\max}} \{(C_{x,max} - C_x)\ln(\frac{C_{x,max} - C_x}{C_{x,max} - C_{x0}}) + C_x \ln\left(\frac{C_x}{C_{x0}}\right)\}] \quad (2.60)$$

$$\int_0^t C_x dt = C_x t - \int_{C_x 0}^{C_x} t dC_x \quad (2.61)$$

Accordingly:

$$\int_0^t C_x dt = \frac{1}{\mu_{max}} [C_x - C_{x0} - K_s Y_{x/s} \ln\left(\frac{C_{x,max} - C_x}{C_{x,max} - C_{x0}}\right) \quad (2.62)$$

Substituting equation 2.62 into 2.59 yields:

$$C_p - C_{p0} = \left[\alpha + \frac{\beta}{\mu_{max}}\right](C_x - C_{x0}) - \frac{\beta K_s Y_{x/s}}{\mu_{max}} \ln\left(\frac{C_{x,max} - C_x}{C_{x,max} - C_{x0}}\right) \quad (2.63)$$

This equation is solved by performing a linear regression on biomass and product concentration data as such:

$$C_p - C_{p0} = b_1(C_x - C_{x0}) + b_2 \ln\left(\frac{C_{x,max} - C_x}{C_{x,max} - C_{x0}}\right) \quad (2.64)$$

where $b_1 = \alpha + \frac{\beta}{\mu_{max}}$ and $b_2 = -\frac{\beta K_s Y_{x/s}}{\mu_{max}}$

Then α and β are calculated as:

$$\alpha = b_1 + \frac{b_2}{K_s Y_{x/s}} \quad (2.65)$$

$$\beta = -b_2 \frac{\mu_{max}}{K_s Y_{x/s}} \quad (2.66)$$

The analytical solution for the combination of Haldane growth kinetics and Luedeking-Piret relation follows the same order with equation (2.40) used to describe the specific growth rate relation with substrate concentration.

Equation (2.55) becomes:

$$-\left(\frac{K_S Y_{x/s}}{C_{x,\max}}\right)\ln\left(\frac{C_{x,max}-C_x}{C_{x,max}-C_{x0}}\right)+\left(\frac{K_S Y_{x/s}}{C_{x,\max}}+\frac{C_{x,\max}}{K_i Y_{x/s}}+1\right)\ln\left(\frac{C_x}{C_{x0}}\right)-\frac{1}{K_i Y_{x/s}}C_x+\frac{1}{K_i Y_{x/s}}C_{x0}=\mu_{max}t \quad (2.67)$$

Equation (2.62) becomes:

$$\int_0^t C_x dt=\frac{1}{\mu_{max}}\left[-K_S Y_{x/s}\ln\left(\frac{C_{x,max}-C_x}{C_{x,max}-C_{x0}}\right)+\left(1+\frac{C_{x,max}}{K_i Y_{x/s}}\right)(C_x-C_{x0})-\frac{1}{2K_i Y_{x/s}}(C_x^2-C_{x0}^2)\right] \quad (2.68)$$

Equation (2.63) becomes:

$$C_p-C_{p0}=\left[\alpha+\frac{\beta}{\mu_{max}}\left(1+\frac{C_{x,max}}{K_i Y_{x/s}}\right)\right](C_x-C_{x0})-\frac{\beta K_S Y_{x/s}}{\mu_{max}}\ln\left(\frac{C_{x,max}-C_x}{C_{x,max}-C_{x0}}\right)-\frac{\beta}{2\mu_{max}K_i Y_{x/s}}(C_x^2-C_{x0}^2) \quad (2.69)$$

Kobayashi et al. (2000) used the Luedeking-Piret model to describe the protein production rate of *P. pastoris* producing human serum albumin under the control of P_{AOX1} on methanol. A continuous feed stream design where methanol was maintained constant at different concentrations ranging between 0.24 and 24 g L^{-1} was used. Growth inhibition was observed after approximately 1.5 g L^{-1}. From a specific growth rate of 0.002 h^{-1} to a μ value of 0.015 h^{-1}, a Luedeking-Piret behavior was observed with $Y_{p/x}$ and m_p being -14.2 mg g^{-1} and 0.28 mg g^{-1} h^{-1} respectively. The negative value of $Y_{p/x}$ indicated that the increase in specific growth rate caused a decrease in the amount of protein produced. After a μ value of 0.015 h^{-1}, q_p remained constant with a maintenance coefficient of 0.067 mg g^{-1} h^{-1}

Ren et al. (2003) used the Luedeking-Piret model to describe the protein production rate of *P. pastoris* producing human serum albumin under the control of P_{AOX1} on methanol. Moreover, a Monod model was proposed to describe the relationship between the specific methanol uptake rate and the specific growth rate. The kinetic

parameters $q_{s,max}$, $Y_{x/s}$, K_s, $Y_{p/x}$ and m_p were determined as 0.0012-0.0016 mol g^{-1} h^{-1}, 0.15 g g^{-1}, 0.3 g L^{-1}, 0.48-0.63 g g^{-1} and 0.0008 g g^{-1} h^{-1} respectively.

Maurer et al. (2006) used the Luedeking-Piret model to describe the protein production rate of a wild type X33 *P. pastoris* strain producing the Fab fragment of the anti-HIV antibody 2F5 under the control of P_{GAP} on glucose. A continuous feed stream design with specific growth rates decreasing from 0.05 to 0.005 h^{-1} was used for the model where the $Y_{p/x}$ and m_p values were determined as 0.2051 mg g^{-1} and 0.002 mg g^{-1} h^{-1} respectively.

2.5.5. Comparison of Macrokinetic Models

Barrigon et al. (2015) established an unstructured, macrokinetic model based on the results of their previous study (Barrigon et al., 2013) where they compared two different fed-batch operational strategies, continuous feed stream designed with different pre-determined specific growth rates and methanol-stat with different methanol set-points, for the production of ROL under the expression of P_{AOX1}. The relationship between the specific growth rate and residual methanol concentration was determined to be of Haldane nature rather than Monod with an $R^2_{Haldane}$ $=0.81>R^2_{Monod}=0.67$ and a μ_{max}, K_s, K_i and C_{Scrit} of 0.069 h^{-1}, 0.40 g L^{-1}, 8.85 g L^{-1}, and 1.9 g L^{-1}, respectively, clearly illustrating the inhibitory effect of methanol on the growth of *P. pastoris*. Similarly, the relationship between the specific ethanol uptake rate and residual methanol concentration was found to be of Haldane nature with $R^2_{Haldane}$ $=0.92>R^2_{Monod}=0.76$ and a q_{max}, K_s, K_i and C_{Scrit} of 0.034 g g^{-1} h^{-1}, 0.42 g L^{-1}, 7.57 g L^{-1}, and 1.7 g L^{-1}, respectively. Also, the relationship between the specific protein production rate and residual methanol concentration was found to be of Haldane nature with $R^2_{Haldane}$ $=0.80>R^2_{Monod}=0.64$ and a q_{max}, K_s, K_i and C_{Scrit} of 1844 U g^{-1} h^{-1}, 10.2 g L^{-1}, 1.0 g L^{-1}, and 3.2 g L^{-1}, respectively. Thus, high methanol concentrations also exert a negative, inhibitory effect on q_s and q_p. Moreover, the relationship between q_s and μ followed the linear Pirt maintenance energy model with an $R^2=0.92$, and $Y_{s/x}$= 4.21 g g^{-1} and m_s= 0.0142 g g^{-1} h^{-1}. However, the relationship

between q_p and μ branched into two models depending on the critical substrate concentration of biomass: if $C_s<C_{Scrit,x}$ then q_p was independent of μ and linear with $Y_{p/x}=0$; if $C_s>C_{Scrit,x}$, q_p was linearly dependent on μ and followed the Luedeking-Piret model with $Y_{p/x}$= 4367 U g^{-1} and m_p= 39.3 U g^{-1} h^{-1}. Based on these models, two models, A and B, were proposed to simulate the evolution of biomass and protein throughout the cultivation time. Model A proposed that the relationship between μ-C_S, q_s-C_S, and q_p-C_S was of Haldane nature. Model B proposed that the relationship between μ-C_s was again Haldane, but q_p-C_s and q_s-C_s followed the linear Luedeking-Piret and Pirt models, respectively. As a result, both models estimated the biomass profiles with a mean relative error (MRE) of 5%. However, the substrate simulations experienced large errors with both models, especially in the continuous feed stream design with pre-determined μ cultivations where the MRE's exceeded 100% due to low existing residual methanol concentrations in the cultivation medium. On the other hand, Model B provided better protein evolution profiles with MRE of 12%, much less than that of Model A where it was 24%, making it the superior model. The minimum MRE's for biomass evolution were lower for continuous feed stream design with pre-determined μ cultivations, whereas higher maximum MRE's for protein evolution were obtained by the methanol-stat strategies due to poorer fitting of the kinetic models evident at high C_s values.

Prabhu and Venkata Dasu (2017) investigated five different unstructured kinetic models: Andrew's, Aiba, Moser, Webb and Haldane to study the effect of increasing substrate concentration on the growth of *P. pastoris* producing human interferon gamma (hIFN-γ) under the expression of P_{AOX1}. Air-filtered shake flask bioreactor experiments were used for the determination of the kinetic parameters with gluconate or methanol added batch-wise at the beginning of the induction phase in the range of 10-100 g L^{-1} and 2-50 g L^{-1}, respectively. It was observed that the highest C_x values of approximately 10 g L^{-1} achieved were at 60 g L^{-1} and 10 g L^{-1} gluconate and methanol respectively. In addition, the specific growth rates in the presence of increasing initial substrate concentrations increased to a maximum of 0.020 and

0.019 h^{-1} for gluconate and methanol respecetively, where the maximums coincided with the substrate concentrations yielding the highest C_x values i.e., 60 g L^{-1} and 10 g L^{-1} for gluconate and methanol, respectively, afterwhich the specfic growth rates started decreasing indicating substrate inhibition on growth. Similarly, the r-protein concentration in the presence of the carbon and energy source methanol increased in the same strend as the specific growth rates reaching a maximum of 13 mg L^{-1} at 10 g L^{-1} initial methanol concentration and then continued decreasing with increasing methanol concentrations indicating inhibition of protein production. Concerning the unstructured inhibition models for the methanol cultivations, the highest R^2 was obtained by the Haldane model at 0.96, followed by the Webb model at 0.95 which was expected since at high K values ($1.19x10^8$ in this case) the Webb model is reduced to a Haldane model. The kinetic parameters for the Haldane model were: μ_{max}= 0.054 h^{-1}, K_s= 10.97 g L^{-1}, and K_i= 12.74 g L^{-1}; the kinetic models for the Webb model were similar with μ_{max}= 0.055 h^{-1}, K_s= 10.7 g L^{-1}, and K_i= 12.4 g L^{-1} due to the high K value. A sensitivity analysis where the kinetic parameters were varried $\pm$50% to study the effect on R^2 was also performed for the Haldane and Webb models of the methanol cultivations. The maximum specific growth rate showed the highest sensitivity, whereas K_s showed high sensitivity in the upper variations, i.e., at lower K_s values, while K_i showed greater sensitivity in the downside variations, i.e., at higher K_i values.

CHAPTER 3

MATERIALS & METHODS

3.1. Strains

Recombinant human growth hormone (r-hGH) expressed in *P. pastoris* under the control of a novel engineered promoter $P_{ADH2\text{-}Cat8\text{-}L2}$ (Ergün et al.,2019) strain was used for establishing the growth curves in the air-filtered shake flask bioreactors and for conducting the 5-L bioreactor experiments.

3.2. Inoculum Preparation

The $P_{ADH2\text{-}Cat8\text{-}L2}$ strain was streaked over agar plates containing. The plates contained 20 g L^{-1} agar and YPD medium consisting of 10 g L^{-1} yeast extract, 20 g L^{-1} peptone, 20 g L^{-1} dextrose, and 100 µg mL^{-1} NTC (Nourseothricin), and were incubated for 48 h at 30°C. Following incubation, the cells were inoculated into 250-mL air-filtered shake flask bioreactors containing 50 mL BMGY medium which consisted of: potassium buffer (11.3 g L^{-1} KH_2PO_4 and 3 g L^{-1} K_2HPO_4 adjusted to pH 6.0 using 5 M KOH), 10 g L^{-1} yeast extract, 20 g L^{-1} peptone, 10 g L^{-1} glycerol, 3.4 g L^{-1} yeast nitrogen base without amino acids, 10 g L^{-1} ammonium sulphate, 0.4 mg L^{-1} filter-sterilized biotin and 34 mg L^{-1} filter-sterilized chloramphenicol. The flasks were incubated at 30°C and 200 rpm for approximately 24 hours until an OD_{600} of 4-6 was achieved.The cells were then harvested by centrifugation at 4500 g and 4°C for 5 mins and re-suspended in either production medium for air-filtered shake flask bioreactor experiments or in basal salt medium (BSM) for the 5-L bioreactor experiments.

3.3. Air-filtered Shake Flask Bioreactors for Growth Curve Determination

Following pre-cultivation, the cells were inoculated into air-filtered shake flask bioreactor production medium consisting of potassium buffer, 14.9 g L^{-1}

$MgSO_4.7H_2O$, 1.2 g L^{-1} $CaSO_4.2H_2O$, 15.3 g L^{-1} ammonium sulphate, 34 mg L^{-1} chloramphenicol, 4.35 mL L^{-1} of filter-sterilized trace salts medium (PTM1), containing: 6 g L^{-1} $CuSO_4$, 80 mg L^{-1} KI, 3 g L^{-1} $MnSO_4$, 0.2 g L^{-1} Na_2MoO_4, 20 mg L^{-1} H_3BO_3, 0.5 g L^{-1} $CoCl_2$, 20 g L^{-1} $ZnCl_2$, 65 g L^{-1} $FeSO_4 \cdot 7H_2O$, 0.2 g L^{-1} biotin and 5 mL L^{-1} of 98% (w/w) H_2SO_4. Ethanol was added batchwise at the beginning of the production phase (t= 0 h) to adjust the initial concentration of ethanol in the production medium to 1, 2, 3, 4, 5, 7, 8, or 16 g L^{-1}. The initial OD_{600} was calibrated to ~0.50 (0.12 g L^{-1}). The flasks were incubated at 30°C and 200 rpm with OD_{600} being measured every 2 hours until the stationary phase was observed (20-62 h). All the experiments were performed in duplicates.

3.4. Fed-batch Bioreactor Cultivation Medium and Operation Conditions

After the pre-cultivation, the cells were inoculated into 2 L basal salt medium (BSM) consisting of: 1.2 g L^{-1} $CaSO_4.2H_2O$, 14.9 g L^{-1} $MgSO_4.7H_2O$, 4.1 g L^{-1} KOH, 18.2 g L^{-1} K_2SO_4, 40 g L^{-1} glycerol, 53.4 ml H_3PO_4 (85%), 5 mL L^{-1} PTM1, 0.4 mg L^{-1} biotin, 34 mg L^{-1} chloramphenicol and 2 mL antifoam (10% v/v) and introduced into a 5 L BIOSTAT® Cplus bioreactor (Sartorius Stedim Biotech, France).

The bioreactor cultivations consisted of three phases known as the glycerol batch phase (GBP), ethanol transition phase (ETP) and ethanol induction phase (EIP). In all of these phases, the cells were cultivated at 30°C, 700 rpm, and 15% dissolved oxygen (DO) maintained by a built-in PID controller that adjusts the air and O_2 flow rate ratios through a cascade system while keeping the total inlet gas flow at 2 vvm. A pH of 5.50 was maintained constant by the addition of 25% (v/v) NH_4OH.

In the GBP, the only carbon source was glycerol itself which was solely used by the cells to reach a high cell density without synthesizing r-hGH. The end of this phase was marked by a sharp DO peak indicating the total consumption of glycerol. ETP then commenced for 4 h during which the cells gradually acclimated to the carbon source ethanol, which was pumped in 18 min intervals into bioreactor by a peristaltic-

pump (Watson Marlow 120, ThermoFisher Scientific, MA, USA) at a flow rate of ~0.4 mL/min. Following that, EIP was initiated and lasted for 24 h with the continuous ethanol feed stream strategy implemented branching into two operational designs: continuous feed stream (CFS) with pre-determined specific growth rate or continuous feed stream (CFS) with residual ethanol concentration maintained constant and known as ethanol-stat. During this phase, 100% pure ethanol was supplemented with 5 mL L^{-1} PTM1 and 2 mL L^{-1} biotin (0.02% w/v) and was fed into the cultivation medium through an external pump.

3.4.1. CFS Designed with Pre-Determined Specific Growth Rate and Other Parameters

A continuous feed stream of ethanol was fed into the bioreactor in a fashion that would theoretically maintain the specific growth rate constant at 0.050, 0.035 or 0.020 h^{-1} by using equation (2.19)

$$Q(t) = \frac{\mu V_0 C_{x0}}{Y_{x/s} C^\circ_s} \exp(\mu t) \tag{2.19}$$

where Q(t) represented the ethanol feed rate in L h^{-1}, μ represented the pre-determined specific growth rates 0.050, 0.035 or 0.020 in h^{-1}, V_0 represented the initial cultivation volume 2 L, C_{x0} represented the cell concentration at the beginning of the EIP in g L^{-1}, C°_S represented the inlet ethanol feed substrate concentration which was 790 g L^{-1}, t represented the induction time in h, and $Y_{x/s}$ represented the biomass yield on substrate which was theoretically determined to be 0.67 g cell g^{-1} as explained in subsection 3.4.1.1.

3.4.1.1. Theoretical determination of $Y_{x/s}$

The black-box model for ethanol assimilation and biomass formation in *P. pastoris* was represented by the following equation:

$$C_2H_5OH + aO_2 + bNH_4 \rightarrow cCH_{1.66}N_{0.134}O_{0.6} + dCO_2 + eH_2O \tag{3.1}$$

Performing elemental mole balances yields:

Carbon balance: $2 = c + d$ (3.2)

Hydrogen balance: $6 + 4b = 1.66c + 2e$ (3.3)

Oxygen balance: $1 + 2a = 0.6c + 2d + e$ (3.4)

Nitrogen balance: $b = 0.134c$ (3.5)

$$RQ = \frac{mol\ CO2}{mol\ O2} = \frac{d}{a} = 0.43 \quad (3.6)$$

where RQ represented the respiratory quotient.

When equations (3.2-3.6) were solved simultaneously, the stoichiometric coefficients were obtained as follows: a= 1.79 mol, b= 0.165 mol, c= 1.23 mol, d=0.77 mol and e= 2.31 mol.

According to stoichiometry,

$n_{cell} = (1.23)(n_{C2H5OH}) = 1.23$ mol where n_{cell} represented the number of moles of the cell.

$m_{cell} = (n_{cell}).\ (M_{cell}) = (1.23\ mol)(25.136\ g\ mol^{-1}) = 30.9$ g where m_{cell} and M_{cell} represented the mass and molar mass of the cell, respectively.

$m_{EtOH} = (n_{EtOH})(M_{EtOH}) = (1\ mol)(46.07\ g\ mol^{-1}) = 46.07$ g where m_{EtOH} and M_{EtOH} represent the mass and molar mass of ethanol respectively.

$Y_{x/s} = \frac{\Delta C_x}{\Delta C_s} = \frac{30.9}{46.07} = 0.67$ g biomass g^{-1} ethanol.

3.4.2. CFS Designed with Constant C_{EtOH} (Ethanol-stat)

The residual ethanol concentration in the bioreactor medium was maintained constant at either 0.5, 1.0 or 1.5 g L^{-1} by an ethanol control unit (Metador, Enzim Biyoteknoloji Ltd, Ankara, Turkey) that indirectly measured the concentration of ethanol in the medium by analyzing the composition of the exhaust gas. Consequently, the flow rate of ethanol was adjusted by the PI algorithm of the control unit and delivered via a

peristaltic pump. The ethanol feeding flask was placed on a digital balance to gravimetrically monitor its utilization.

3.5. Determination of Ethanol Concentration

Residual ethanol concentration was determined by gas chromatography (GC) using Agilent (Wilmington, DE, USA) 6850 with the specifications and experimental conditions listed in Table (3.1).

Table 3.1. *Gas chromatography device specifications and run parameters.*

Column	30 m x 530 µm x 40 µm, Agilent 19095P-Q04E
Carrier gas	Helium at 19.62 psi constant pressure mode
Inlet split/splitless	EPC 180°C 10:1 split ratio and 120 mL min^{-1} split flow
Oven temperature	170°C maintained constant
Detector	TCD at 200°C at 5 Hz with 12 mL min^{-1} reference flow
Injection size	1 µL
Run time	3 min

3.6. Determination of Cell Concentration

Cell concentration was quantified as dry cell weight DCW (g L^{-1}) and determined by centrifuging 1 mL cultivation medium samples at 4500 g for 10 mins at 4°C, discarding the supernatant and drying the pellets at 105°C for 6 hours. The difference between the empty and dried microcentrifuge tubes represented the DCW.

OD_{600} values were read using MilliporeSigma Spectroquant Pharo 300 Spectrophotometer. OD_{600} readings were converted to cell concentrations using the following formula:

$$C_x = (OD_{600})(Dilution\ Factor)(0.24) \quad (3.7)$$

3.7. rhGH Quantification

rhGH was quantified using an ELISA hGH quantification kit in 96-well microplates according to the manufacturer's manual (Roche Diagnostics GmbH , Mannhelm, Germany) as follows:

- hGH standards were prepared in duplicates in 1:2 serial dilution steps starting from 400 pg mL^{-1} until 12.5 pg mL^{-1}
- 200 µL of each standard dilution were pipetted to the first two columns of the microplate with 200 µL POD substrates (blanks) pipetted to the first well of each column
- The bioreactor culture supernatant samples were diluted to the detection range of the hGH standard in POD substrate and 200 µL of each diluted sample was pipetted in parallel starting from the 3rd column of the microplate
- The microplate was covered and incubated for 1 h at 37°C
- The content of the microplate was removed thoroughly. Each well was rinsed 5 times with 250 µL washing buffer for 30s each and the washing buffer was removed after each rinse
- 200 µL of anti-hGH-DIG was pipetted into each well, the microplate was covered and incubated for 1 h at 37°C
- The content of the microplate was removed thoroughly. Each well was rinsed 5 times with 250 µL washing buffer for 30s each and the washing buffer was removed after each rinse
- 200 µL of anti-DIG-POD was pipetted into each well, the microplate was covered and incubated for 1 h at 37°C
- The content of the microplate was removed thoroughly. Each well was rinsed 5 times with 250 µL washing buffer for 30s each and the washing buffer was removed after each rinse
- 200 µL of POD substrate was pipetted into each well and incubated at room temperature until the color green was developed for photometric detection (10-30 min)
- The absorbance of the samples was measured at 405 nm using a microplate (ELISA) reader (Multiskan Sky Microplate Spectrophotometer, Thermo Scientific™, US).

3.8. Sodium dodecyl sulfate polyacrylamide gel electrophoresis (SDS-PAGE)

SDS-PAGE was used to semi-quantitatively compared the amount of rhGH produced in the CFS fed-batch strategies designed with pre-determined μ.

13 μL of supernatant or hGH standard, 5 μL of (x4) loading buffer and 2 μL of dithiothreitol were mixed together and 15 μL of the mixture was loaded into the wells of the gel. BIO-RAD Mini-PROTEAN tetra vertical electrophoresis cell was set to a constant voltage of 200 V and run for approximately 50 min. The gel was prepared according to the procedure of BIO-RAD TGX Stain-Free FastCast acrylamide solutions kit. Then, Coomassie Blue Staining was applied using Coomassie R250 staining solution as follows:

- 1 h Fixing with gentle agitation using the following fixer solution: 1.2 mL formaldehyde, 45 mL ethanol, 4.083 g sodium acetate trihydrate and UP water up to 150 mL
- 1 h Coomassie R250 Staining with gentle mixing using the following staining solution: 63 mg Coomassie R250, 19 mL methanol, 3.1 mL acetic acid and UP water up to 63 mL
- Gels were washed with the following de-stain solution until a clear background was obtained: 150 mL methanol, 25 mL acetic acid and UP water up to 500 mL
- Gels were stored in 30 mL of the following solution: 25 mL methanol, 35 mL acetic acid and UP water up to 500 mL.

3.9. Mathematical Models

3.9.1. Specific Rates

All the specific rates were calculated using MATLAB® R2019b (MathWorksInc.,MA) with the respective codes attached in the Appendix.

The specific growth rate, μ, was calculated based on equation (2.4):

$$\mu = \frac{1}{(C_x)}\frac{dC_x}{dt} + \frac{Q(t)}{V} \quad (2.4)$$

In the case of air-filtered shake flask bioreactor experiments, the volume change was assumed negligible and thus the specific growth rate was calculated during the exponential growth phase based on this modification of equation (2.11) to yield equation (3.8):

$$\frac{d(C_x)}{dt} = \mu C_x \quad (3.8)$$

Integrating from t= t_0 to t=t and C_x= $C_{x,0}$ to C_x=C_x yields:

$$\mu = \frac{\ln\left(\frac{C_x}{C_{x,0}}\right)}{(t-t_0)} \quad (3.9)$$

The specific ethanol uptake rate, q_{EtOH}, was calculated based on equation (2.7):

$$q_{EtOH} = -\frac{1}{C_x}\left(\frac{dC_{EtOH}}{dt} + \frac{C_{EtOH}}{V}Q(t) - \frac{Q(t)}{V}C^{\circ}{}_{EtOH}\right) \quad (2.7)$$

The specific rhGH production rate, q_p, was calculated based on equation (2.10):

$$q_p = \frac{1}{C_x}\left(\frac{dC_p}{dt} + \frac{Q(t)}{V}C_p\right) \quad (2.10)$$

3.9.2. Mean Specific Rates

The mean specific rates were calculated based on the equations suggested by Barrigón et al. (2013) using MATLAB® R2019b (MathWorksInc.,MA) with the respective codes attached in the Appendix.

For the mean specific growth rate, μ_{mean}:

$$\int_{(C_xV)i}^{(C_xV)f} d(C_xV) = \mu_{mean}\int_{t_i}^{t_f}(C_xV)dt \quad (3.10)$$

$$\mu_{mean} = \frac{\int_{(C_xV)i}^{(C_xV)f} d(C_xV)}{\int_{t_i}^{t_f}(C_xV)dt} \quad (3.11)$$

For the mean ethanol uptake rate, $q_{EtOH,mean}$:

$$C°_{EtOH}\int_{t_i}^{t_f} Q(t)dt - \int_{(C_{EtOH}V)i}^{(C_{EtOH}V)f} d(C_{EtOH}V) = q_{EtOH,mean}\int_{t_i}^{t_f}(C_xV)dt \quad (3.12)$$

$$q_{EtOH,mean} = \frac{C°_{EtOH}\int_{t_i}^{t_f} Q(t)dt - \int_{(C_{EtOH}V)i}^{(C_{EtOH}V)f} d(C_{EtOH}V)}{\int_{t_i}^{t_f}(C_xV)dt} \quad (3.13)$$

For the mean rhGH production rate, $q_{p,mean}$:

$$\int_{(C_pV)i}^{(C_pV)f} d\left(C_pV\right) = q_{p,mean}\int_{t_i}^{t_f}(C_xV)dt \quad (3.14)$$

$$q_{p,mean} = \frac{\int_{(C_pV)i}^{(C_pV)f} d\left(C_pV\right)}{\int_{t_i}^{t_f}(C_xV)dt} \quad (3.15)$$

3.9.3. Unstructured Kinetic Models

The Monod and Haldane models for growth inhibition were solved using the mean values based on equations (2.32) and (2.40), respectively, using nonlinear regression via MATLAB® (MathWorksInc.,MA) with the respective codes attached in the Appendix. Initial estimates of 0.1 h^{-1}, 0.1 g L^{-1} and 1 g L^{-1} were given for μ_{max}, K_s, and K_i respectively.

$$\mu = \frac{\mu_{max}C_{EtOH}}{K_s+C_{EtOH}} \quad (2.32)$$

$$\mu = \frac{\mu_{max}C_{EtOH}}{K_s+C_{EtOH}+\frac{C_{EtOH}^2}{K_i}} \quad (2.40)$$

For ethanol uptake rate inhibition, equations (3.16) and (3.17) were used with the mean values based on the Monod and Haldane models, respectively, and solved using nonlinear regression via MATLAB® (MathWorksInc.,MA) with the respective codes attached in the Appendix. Initial estimates of 0.1 g g^{-1} h^{-1}, 0.1 g L^{-1} and 1 g L^{-1} were given for $q_{EtOH,max}$, $K_{s,s}$, and $K_{i,s}$, respectively.

$$q_{EtOH} = \frac{q_{EtOH,max}C_{EtOH}}{K_{s,s}+C_{EtOH}} \quad (3.16)$$

$$q_{EtOH} = \frac{q_{EtOH,max} C_{EtOH}}{K_{s,s} + C_{EtOH} + \frac{C_{EtOH}^2}{K_{i,s}}} \quad (3.17)$$

where $q_{EtOH,max}$, $K_{s,s}$ and $K_{i,s}$ represent the maximum specific ethanol uptake rate, the saturation and inhibition constants for substrate, respectively.

For rhGH production rate inhibition, equations (3.18) and (3.19) were used with the mean values based on the Monod and Haldane models respectively and solved using nonlinear regression via MATLAB® (MathWorksInc.,MA) with the respective codes attached in the Appendix. Initial estimates of 0.1 mg g^{-1} h^{-1}, 0.1 g L^{-1} and 1 g L^{-1} were given for $q_{p,max}$, $K_{s,p}$ and $K_{i,p}$, respectively.

$$q_p = \frac{q_{p,max} C_{EtOH}}{K_{s,p} + C_{EtOH}} \quad (3.18)$$

$$q_p = \frac{q_{p,max} C_{EtOH}}{K_{s,p} + C_{EtOH} + \frac{C_{EtOH}^2}{K_{i,p}}} \quad (3.19)$$

where $q_{p,max}$, $K_{s,p}$ and $K_{i,p}$ represent the maximum rhGH production rate, the saturation and inhibition constants for r-protein, respectively.

The Pirt and Luedeking-Piret models were solved with the mean values based on equations (2.45) and (2.49), respectively, using linear regression via MATLAB® (MathWorksInc.,MA) with the respective codes attached in the Appendix.

$$q_{EtOH} = Y_{s/x}\mu + m_s \quad (2.45)$$

$$q_p = Y_{p/x}\mu + m_p \quad (2.49)$$

3.10. Mean Relative Error

The mean relative error (MRE) was used as a criterion to assess the performance and adequacy of the kinetic models. A mathematical representation of the term is presented as follows (Barrigón et al., 2015) :

$$MRE = \frac{1}{N}\sum_{i=1}^{n} \frac{|y_{exp,i} - y_{th,i}|}{y_{exp,i}} \quad (3.20)$$

where n is the number of data points for one experiment, $y_{exp,i}$ is the experimental i^{th} value, $y_{th,i}$ is the simulated or theoretical i^{th} value, and N is the number of experiments performed.

3.11. Bioreactor Model Simulation

For the determination of biomass evolution throughout the cultivation time, equation (2.17) based on the cell mass conservation was used:

$$C_x V = C_{x0} V_0 e^{\mu t} \tag{2.17}$$

If the feeding strategy used was CFS with pre-determined μ, μ_{mean} was simply inserted as the μ value in equation (2.17) and C_xV was determined. However, if the feeding strategy used was ethanol-stat, the mean residual ethanol concentration C_{EtOH} was inserted into the Haldane model with the determined kinetic parameters, equation (3.21), and the resulting μ value was inserted into equation (2.17) to determine C_xV. The algorithm is illustrated in Figure 3.1.

$$\mu = \frac{0.507 C_{EtOH}}{2.66 + C_{EtOH} + \frac{C_{EtOH}^2}{0.618}} \tag{3.21}$$

For the determination of protein evolution throughout the cultivation time, the Haldane model for protein production rate inhibition equation was used to determine q_p as follows:

$$q_p = \frac{0.0613 C_{EtOH}}{0.146 + C_{EtOH} + \frac{C_{EtOH}^2}{3.83}} \tag{3.22}$$

If the feeding strategy used was CFS with pre-determined μ, μ_{mean} was inserted as the μ value in the Haldane model for growth inhibition, equation (3.21), and C_{EtOH} was determined. Following that, C_{EtOH} was inserted into equation (3.22) to obtain q_p. However, if the feeding strategy used was ethanol-stat, $C_{EtOH,mean}$ was directly inserted as C_{EtOH} into the Haldane model for protein production rate inhibition, equation (3.22) to obtain q_p. Once q_p was obtained, it was inserted as $q_{p,mean}$ into equation (3.23) which is the expanded version of equation (3.14) to obtain C_pV. The time integral of C_xV

was based on the C_xV values resulting from the model itself, i.e., C_xV values of equation (2.17). The algorithm is illustrated in Figure (3.2).

$$\int_{(C_pV)i}^{(C_pV)f} d(C_pV) = q_{p,mean} \int_{t_i}^{t_f} (C_xV)dt \tag{3.14}$$

$$(C_pV)_f = (C_pV)_i + q_{p,mean} \int_{t_i}^{t_f} (C_xV)dt \tag{3.23}$$

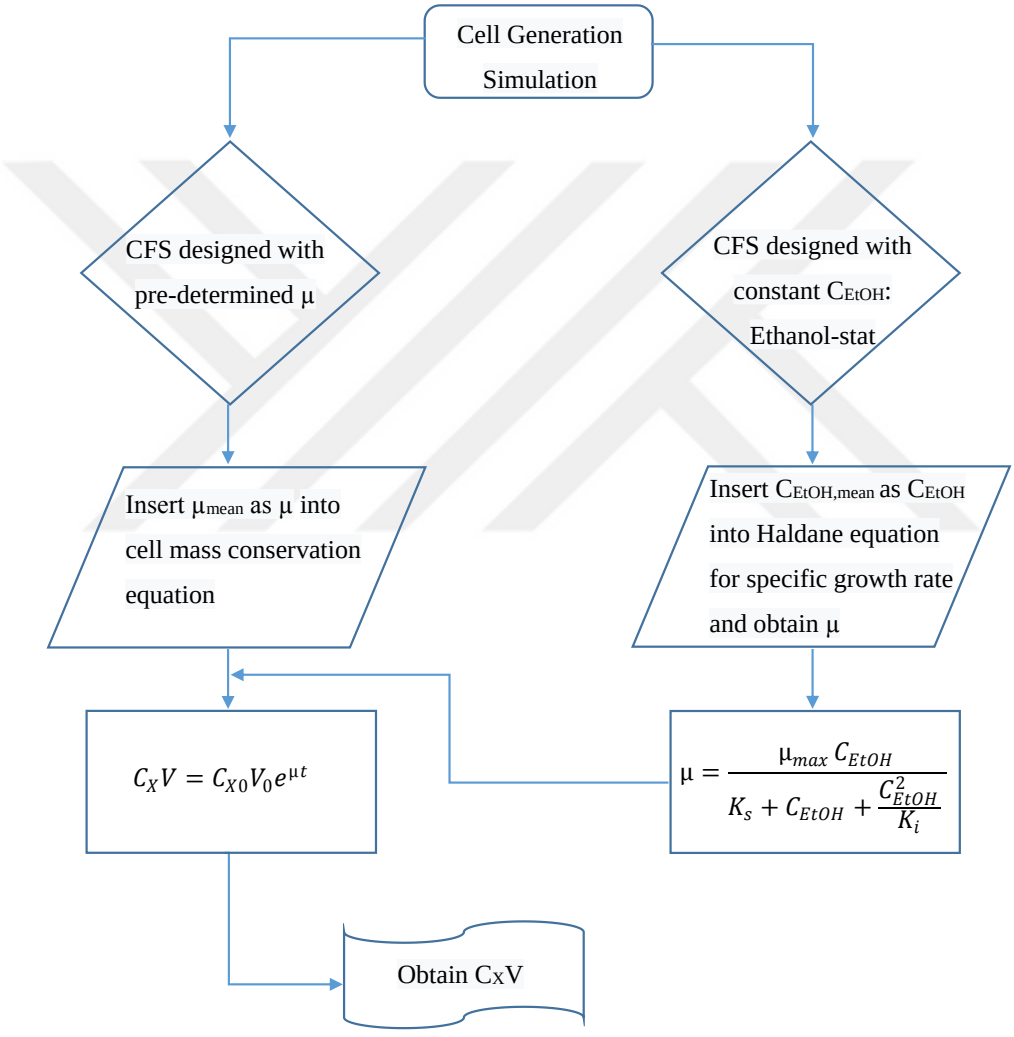

Figure 3.1. The simulation algorithm for determining the evolution of cell generation throughout the cultivation time in the fed-batch bioreactor experiments.

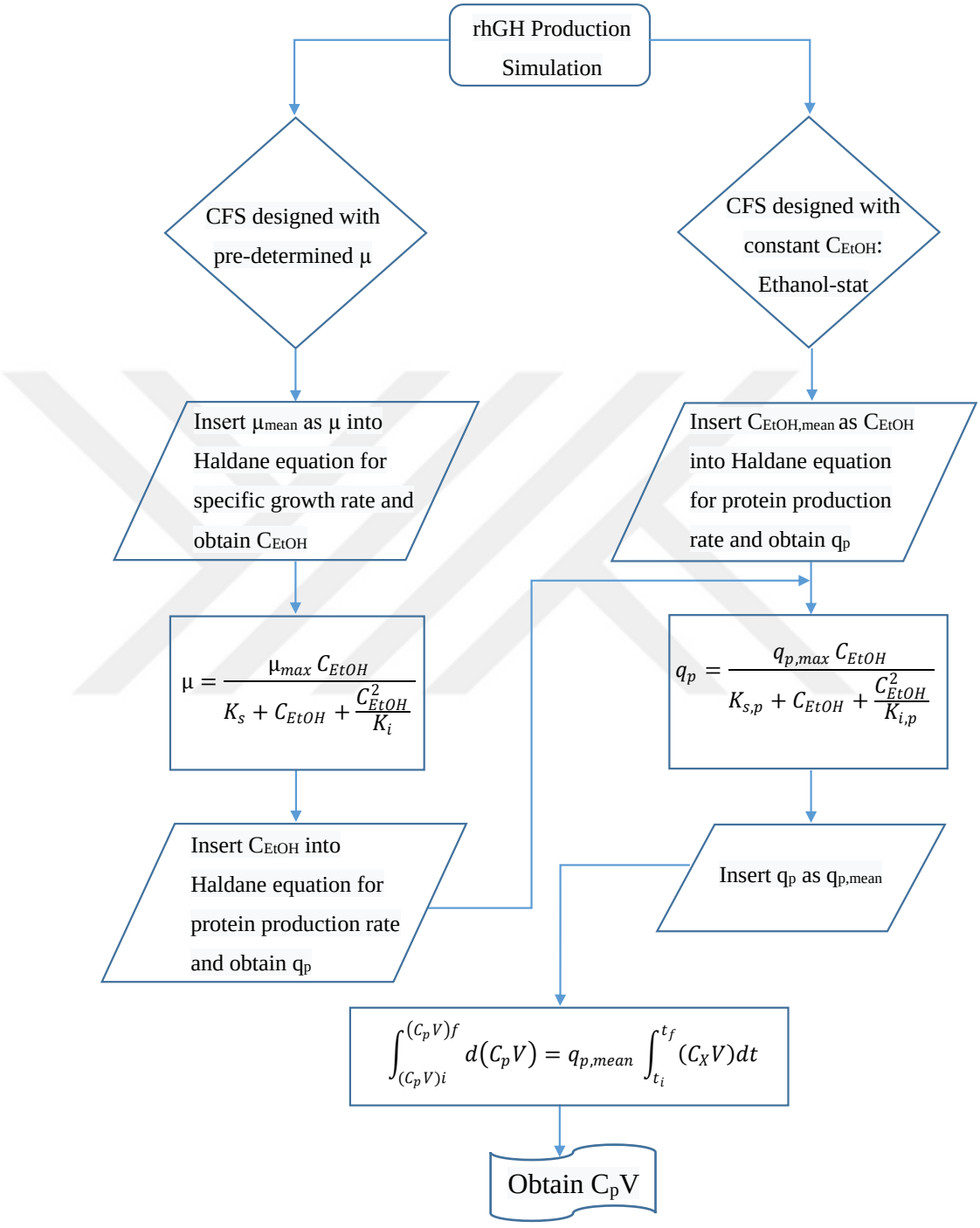

Figure 3.2. The simulation algorithm for determining the evolution of rhGH production throughout the cultivation time in the fed-batch bioreactor experiments.

The bioreactor simulation models were obtained using MATLAB® R2019b (MathWorksInc.,MA) with the respective codes attached in the Appendix.

CHAPTER 4

RESULTS & DISCUSSION

In this work, the effects of increasing concentrations of ethanol on the growth of a novel engineered promoter variant of P_{ADH2} called $P_{ADH2\text{-}Cat8\text{-}L2}$ were investigated by conducting air-filtered shake flask bioreactor experiments at eight different ethanol concentrations ranging between 1-16 g L^{-1}. Later on, the observed growth inhibition was modeled using the Haldane model for growth inhibition. Following that, in an attempt to find the best ethanol feeding strategy to obtain the highest rhGH concentration and productivities, two different CFS strategies were conducted: 1) CFS designed with three different pre-determined μ values (0.020, 0.035, and 0.050 h^{-1}), and 2) CFS designed with constant residual ethanol concentration (ethanol-stat; 0.5, 1.0, and 1.5 g L^{-1}). These strategies also allowed to study the effects of different pre-determined specific growth rates and residual ethanol concentrations on the specific growth rate, the specific ethanol uptake rate and the specific rhGH production rate. Based on the mean specific rates and the mean residual ethanol concentrations, unstructured kinetic models (Haldane and Monod) were established and compared to mathematically express the inhibition relationships between the specific rates and ethanol concentrations in the cultivation medium. Also, the relationship between the specific ethanol uptake rate and specific growth rate was represented by the linear Pirt model. Finally, the evolution of biomass and protein mass, C_xV and C_pV, throughout the cultivation time were modeled based on the unstructured kinetic models.

4.1. Air-Filtered Shake Flask Bioreactor Experiments

In order to characterize the growth of the $P_{ADH2\text{-}Cat8\text{-}L2}$ strain of *P. pastoris* on ethanol and in order to further understand the inhibitory effect of the substrate ethanol on the growth of this strain of *P. pastoris*, air-filtered shake flask bioreactor experiments

were conducted using eight different initial ethanol concentrations (1, 2, 3, 4, 5, 7, 8 and 16 g L^{-1}) fed batchwise at the beginning of the cultivation time of the induction phase, with an identical initial C_x value of 0.12 g L^{-1} for all cultures. Due to the long lag phase resulting from the adaptation time required after the inoculation of *P. pastoris* into a new defined medium with the new carbon and energy source, ethanol, the cell concentrations were started to be measured only after t= 8 h of induction to allow the cultures enough time to enter the exponential growth phase.

4.1.1. Growth Curve Determination

As the ethanol concentration increased, the cultivation time increased (Figure 4.1) due to the presence of more ethanol in the medium to support cell growth (Figure 4.2).

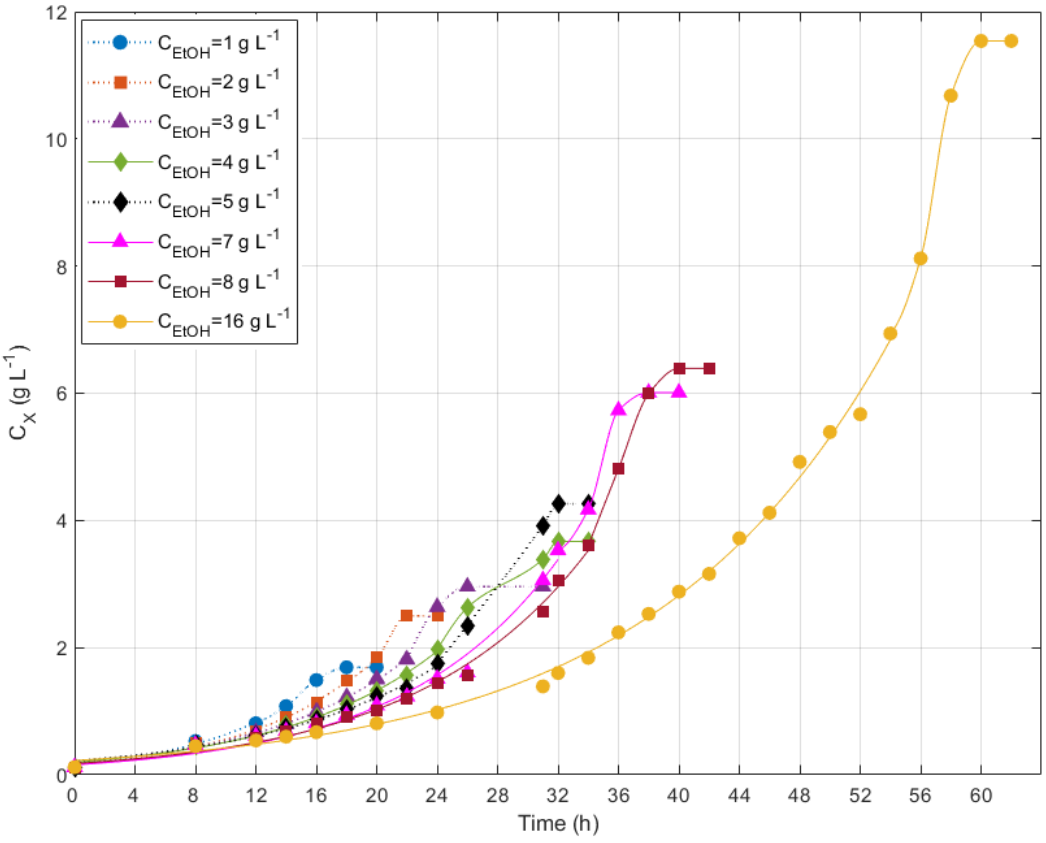

Figure 4.1. Growth curve of $P_{ADH2\text{-}Cat8\text{-}L2}$ strain on different initial concentrations of ethanol.

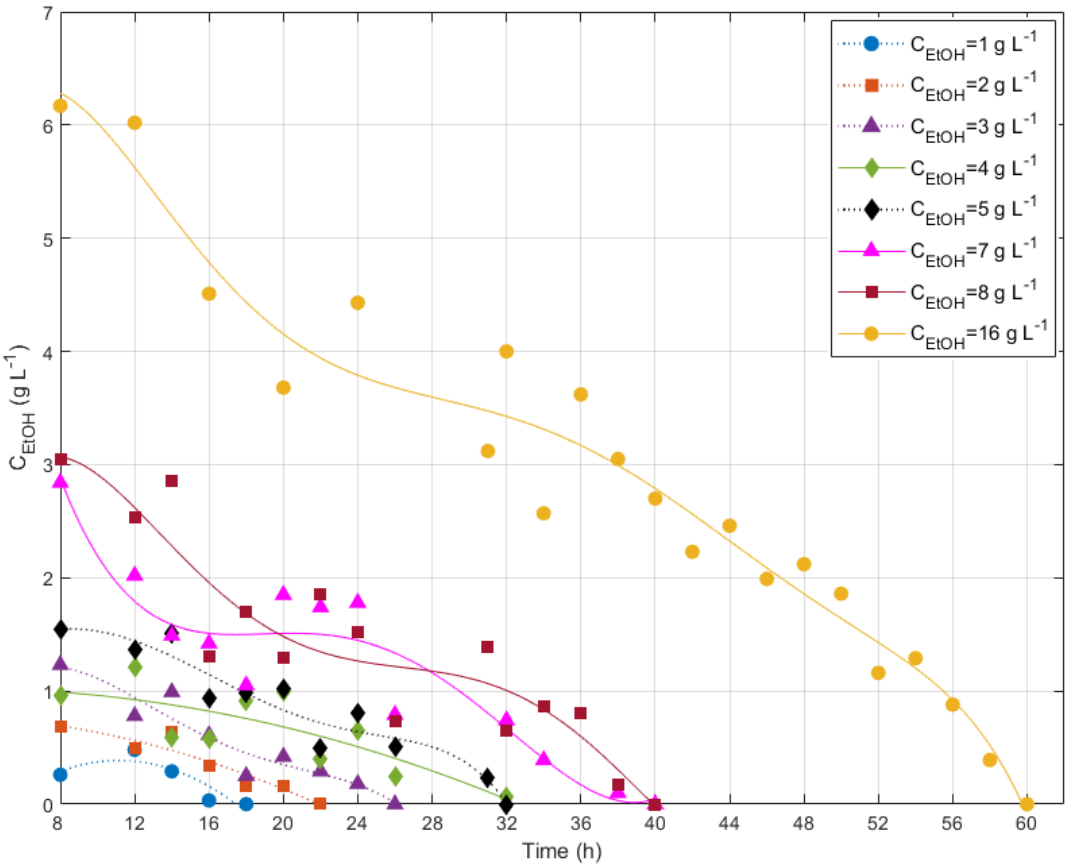

Figure 4.2. Variation in ethanol concentration with the cultivation time for the air-filtered shake flask bioreactor experiments.

The beginning of the stationary phase started after t= 16, 22, 24, 26, 32, 36, 38, and 58 h for the initial ethanol concentration cultures of 1, 2, 3, 4, 5, 7, 8, and 16 g L^{-1}, respectively. In addition, it was noticed that the ethanol concentrations decreased by more than 50% at t=8 h when the C_x values were started to be measured. Ethanol concentrations decreased more than 50% at t = 8 h, when the C_X values were started to be measured. In order to test whether the cells were utilizing ethanol, or the decrease was resulting from ethanol evaporation, a negative control experiment was conducted mimicking the same experimental conditions and ethanol concentrations without the cells where ethanol concentrations were measured at t = 0 h and t = 8 h (Appendix). An average 3.5% decrease in ethanol concentrations was observed at t = 8 h, with an absolute negligible C_{EtOH} change observed for the 2, 3, 8 and 16 g L^{-1} initial ethanol concentrations. This indicated that cellular ethanol uptake was taking place rather than

loss of ethanol because of evaporation. In addition, the cell concentrations seized to increase when ethanol concentration in the cultivation medium was depleted. With the increase in initial ethanol concentration, the final cell concentration increased; at 16 g L^{-1} initial ethanol concentration, C_X reached 11.5 g L^{-1}, which was 1.8-, 1.9-, 2.7-, 3.1-, 3.9-, 4.6-, and 6.8-fold higher than that of the 8, 7, 5, 4, 3, 2, and 1 g L^{-1} initial ethanol

4.1.2. Growth Inhibition Models

In order to mathematically describe the effects of different initial concentrations of ethanol on the specific growth rate of *P. pastoris*, two common growth inhibition models were used: Monod and Haldane. The Monod model dictates that after a certain substrate concentration, the specific growth rate becomes independent of C_{EtOH} and stabilizes, whereas the Haldane model dictates that increasing concentrations of substrate adversely affect the specific growth rate and lead to its decrease. The specific growth rates determined during the exponential growth phase data were used to obtain the growth inhibition model shown in Figure (4.3).

Table 4.1. *Parameter values for the Haldane and Monod models of the air-filtered shake flask bioreactor experiments.*

Parameter	Haldane	Monod
μ_{max} (h^{-1})	0.194	0.107
K_s (g L^{-1})	0.406	-0.237
K_i (g L^{-1})	9.56	-----
$C_{EtOH,crit}$ (g L^{-1})	1.97	-----
R^2	0.99	0.84

The substrate inhibition pattern followed the Haldane model rather than Monod (Figure 4.3) with increasing initial ethanol concentrations causing an increase in the specific growth rates to reach an experimental maximum of 0.14 h^{-1} beyond which the specific growth rates started decreasing. According to the model, a critical substrate concentration of 1.97 g L^{-1} and a theoretical maximum specific growth rate of 0.194 h^{-1} were obtained (Table 4.1). To the best of our knowledge, there are no studies

found on the specific growth rate for *P. pastoris* grown on ethanol in the literature. However, several studies have been conducted on the growth of *Saccharomyces cerevisiae* under ethanol, with μ_{max} reported as 0.13 h^{-1} by Paalme et al. (1997) being in proximity with our experimental value of 0.14 h^{-1}.

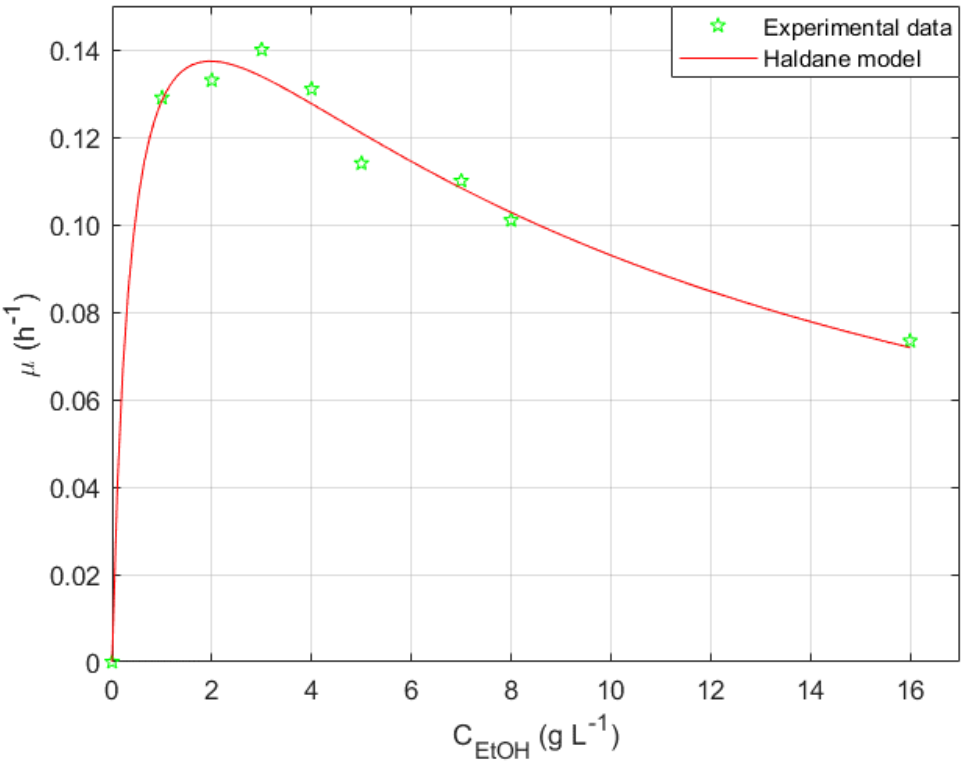

Figure 4.3. Haldane model for the growth of $_{PADH2\text{-}Cat8\text{-}L2}$ on different initial concentrations of ethanol.

4.2. Fed-Batch Bioreactor Experiments

In order to determine the superior ethanol feeding strategy for rhGH production under the expression of the novel engineered promoter $P_{ADH2\text{-}Cat8\text{-}L2}$, six fed-batch bioreactor experiments with two strategies were performed: three continuous feed stream fed-batch bioreactors designed with pre-determined specific growth rates of 0.020, 0.035 and 0.050 h^{-1}, and three continuous feed stream fed-batch bioreactors designed with constant ethanol concentrations in the bioreactor (ethanol-stat) of 0.5, 1.0 and 1.5 g L^{-1} were conducted to determine the effect of different C_{EtOH} on rhGH

production, cell growth and ethanol utilization. The pre-determined specific growth rates were determined based on the Haldane inhibition model's maximum specific growth rate of 0.194 h^{-1}, where the chosen values were kept at least 75% below it at 0.050, 0.035 and 0.020 h^{-1} to avoid the risk of ethanol accumulation in the cultivation medium. First, CFS with pre-determined μ of 0.050 h^{-1} was tested, however due to ethanol accumulation in the cultivation medium, a slightly lower pre-determined μ of 0.035 h^{-1} was chosen; no ethanol accumulation and higher rhGH production were observed. Accordingly, to test whether a slightly lower pre-determined μ value can result in higher rhGH titer, μ= 0.020 h^{-1} was tested however inappreciable C_x and rhGH titer were obtained indicating that the favorable pre-determined μ value was 0.035 h^{-1}.

4.2.1. Cell Concentrations

As the pre-determined specific growth rate increased (Figure 4.4), C_x increased to reach a maximum of 87 g L^{-1} at t= 24 h for μ_{set}= 0.050 h^{-1}, which was 1.2- and 1.7-fold higher than the maximum C_x values of μ_{set}= 0.035 and 0.020 h^{-1}, respectively. The C_x value of μ_{set}= 0.020 h^{-1} was significantly low at 52.1 g L^{-1} with an early stationary phase starting after t= 21 h, unlike the other bioreactors with higher pre-determined μ values whose exponential growth phases were observed until the end of cultivation time. This indicates that a pre-determined μ value of 0.020 h^{-1} does not suffice to maintain exponential growth in CFS fed-batch bioreactor strategies and achieve high cell densities due to the low amount of ethanol volumetric flow rate dictated by equation (2.19), resulting in the low amount of ethanol introduced for a short period of time to be rapidly directed towards cell maintenance rather than cell growth. On the other hand, the CFS fed-batch bioreactors designed with constant residual ethanol concentration (ethanol-stat) reached higher cell densities, with the highest belonging to $C_{EtOH,set}$= 0.5 and 1.0 g L^{-1} at 128 and 135 g L^{-1}, respectively, whereas $C_{EtOH,set}$= 1.5 g L^{-1} reached a significantly lower final C_x of 101 g L^{-1} which was 1.3-fold lower than that of the other ethanol-stat fed-batch bioreactors. Also, the stationary phase was observed after t=15 h for the ethanol-stat fed-batch bioreactors

with the highest and lowest C_{EtOH} of 1.5 and 0.5 g L^{-1}, respectively, whereas that of the intermediate C_{EtOH} fed-batch bioreactor was observed after t= 18 h. Moreover, the highest C_x value attained by the ethanol-stat bioreactors ($C_{EtOH,set}$= 1.0 g L^{-1}) was 1.6-fold higher than that obtained by the bioreactors designed with pre-determined μ (μ_{set}=0.050 h^{-1}), indicating that the continuous presence of ethanol as a carbon and energy source is essential to achieve high cell densities.

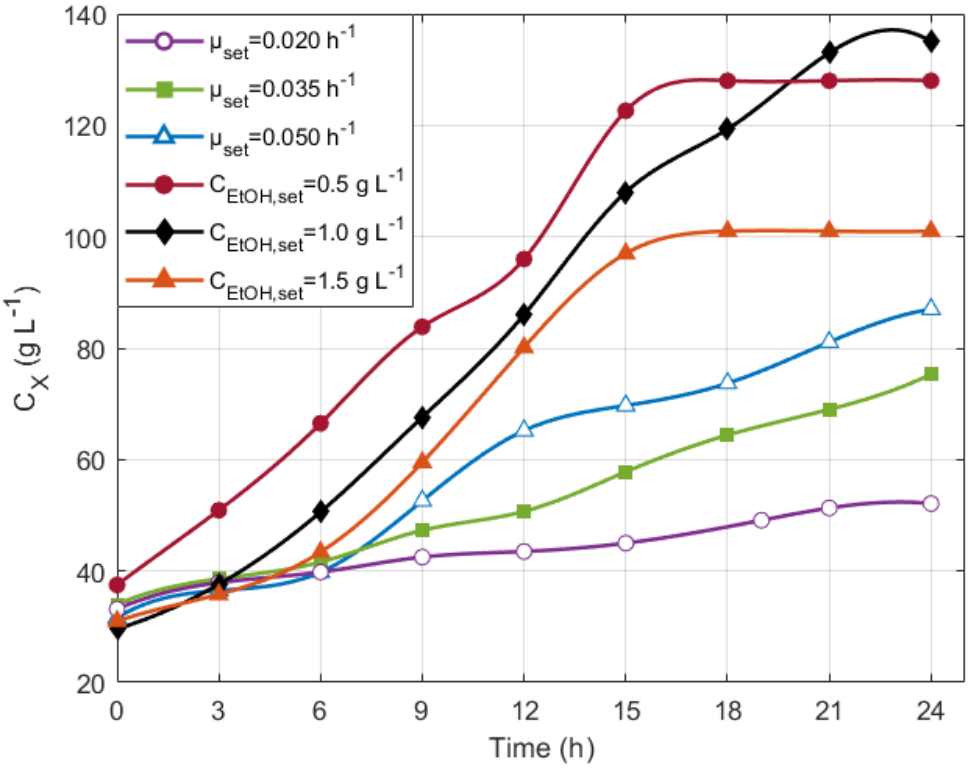

Figure 4.4. Variation of Cell concentrations with the cultivation time in the CFS fed-batch bioreactor experiments.

4.2.2. Ethanol Concentrations

The residual ethanol concentrations of μ_{set}= 0.035 and 0.020 h^{-1} became undetectable after t= 6 and 3 h (Figure 4.5), respectively, indicating the rapid utilization of ethanol. However, the ethanol concentration of μ_{set}= 0.050 h^{-1} reached a local maximum of 8 g L^{-1} at t=6 h and then decreased to approximately 2 g L^{-1} between t= 9 and 12 h and then continued to accumulate to reach 15 g L^{-1} at t= 21 h and remained constant

till the end of the cultivation time. This indicates that a μ value of 0.050 h^{-1} allowed for a high volumetric ethanol flow rate that was excessive for the cells to utilize, which resulted in the accumulation of ethanol in the cultivation medium. The ethanol concentrations in the CFS fed-batch bioreactors designed with ethanol-stat fluctuated around their set-points with mean values of 0.64, 0.96 and 1.6 g L^{-1} for $C_{EtOH,set}$= 0.5, 1 and 1.5 g L^{-1}, respectively.

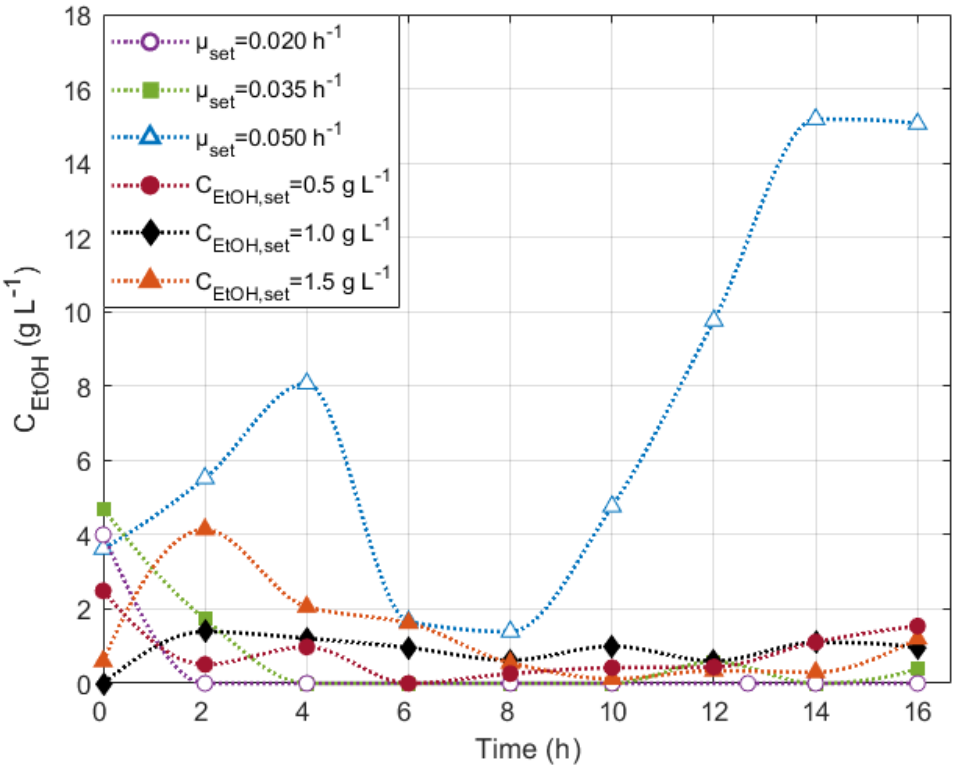

Figure 4.5. Variation of ethanol concentrations with the cultivation time in the CFS fed-batch bioreactor experiments.

4.2.3. rhGH Concentrations

μ_{set}= 0.035 h^{-1} had a maximum rhGH concentration of 43.6 mg L^{-1} at t= 21 h (Figure 4.6), which was 1.5-fold higher than that of μ_{set}= 0.050 h^{-1}. Concerning the fed-batch bioreactor with the lowest pre-determined μ of 0.020 h^{-1}, an SDS-PAGE experiment was conducted (Figure 4.7) to semi-quantitatively compare the rhGH concentrations of the CFS fed-batch bioreactors designed with pre-determined μ. The bioreactor with

the lowest pre-determined μ had a very low, indiscernible rhGH band when compared to the other bioreactors. This further proves that the low pre-determined μ of 0.020 h^{-1} did not support high cell density growth nor r-protein production with the ethanol being directed towards cell maintenance. Therefore, the optimal pre-determined μ value for maximum rhGH production was 0.035 h^{-1} whereupon a higher μ value decreased the r-protein production and a lower μ value yielded inappreciable cell density and negligible rhGH concentration. It was also noticed that there was no significant increase in C_p for the bioreactor with the pre-determined μ of 0.050 h^{-1}after t= 12 h which coincided with the time after which ethanol accumulation was observed (Figure 4.5) indicating that elevated ethanol concentrations had an inhibitory effect on rhGH production.

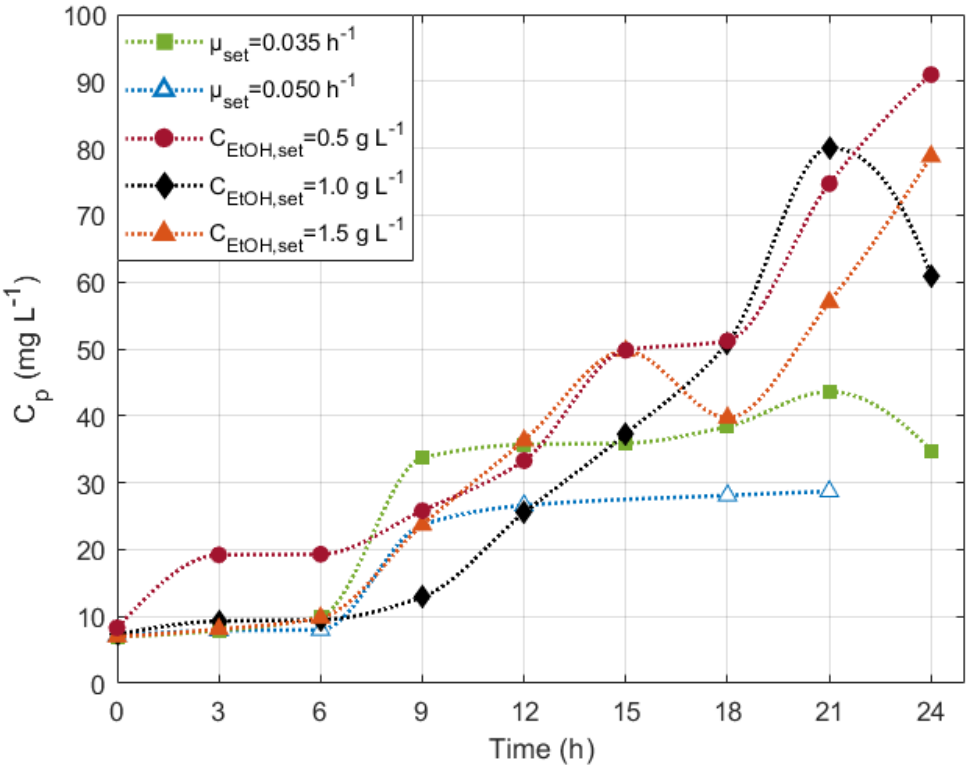

Figure 4.6. Variation of rhGH concentrations with the cultivation time in the CFS fed-batch bioreactor experiments.

On the other hand, the CFS fed-batch bioreactors designed with ethanol-stat had significantly higher rhGH production levels than the bioreactors with pre-determined

μ. The highest rhGH concentration was attained by $C_{EtOH,set}$= 0.5 g L^{-1} at 91 mg L^{-1} followed by $C_{EtOH,set}$= 1.0 and 1.5 g L^{-1} at 80.1 and 78.8 mg L^{-1}, respectively. $C_{EtOH,set}$=0.5 g L^{-1} had a 2.1-fold higher maximum rhGH concentration than that of μ_{set}= 0.035 h^{-1}. This indicates that the continuous presence of ethanol is essential for cells to reach high cell densities and rhGH concentrations expressed by the ethanol-inducible $P_{ADH2\text{-}Cat8\text{-}L2}$.

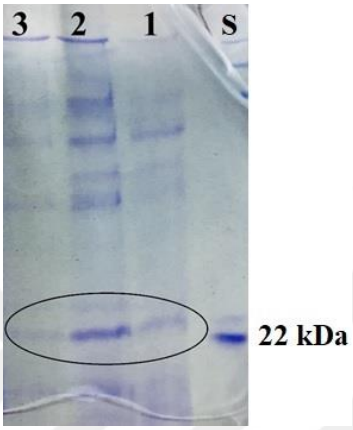

Figure 4.7. SDS-PAGE results of the fed-batch bioreactors designed with pre-determined μ where S, 1, 2 and 3 represent the lanes for the standard (50 mg L^{-1} rhGH), μ_{set} values 0.050, 0.035, and 0.020 h^{-1}, respectively.

The decrease in rhGH concentration observed after t=21 h for $C_{EtOH,set}$= 1.0 g L^{-1} and μ_{set}= 0.035 h^{-1} was potentially due to an accumulation of extracellular proteases that degraded rhGH, where the rate of protease production exceeded the rate of rhGH production (Çelik et al., 2009).

4.2.4. Specific Growth Rates

The specific growth rates of μ_{set}= 0.035 h^{-1} and 0.020 h^{-1} started from the same value of approximately 0.043 h^{-1} and fluctuated around their mean values of 0.035 and 0.017 h^{-1} throughout the cultivation time (Figure 4.8), respectively. The proximity of the specific growth rate mean values to their respective pre-determined μ values indicates that the parameters chosen to calculate the volumetric flow rate of ethanol Q(t) in equation (2.19), specifically the biomass on substrate yield, $Y_{x/s}$, was an accurate theoretical estimation. However, the specific growth rates of μ_{set}= 0.050 h^{-1} increased

to a maximum of 0.087 h^{-1} at t= 9 h and then decreased to 0.029 h^{-1} at t= 15 h^{-1} and fluctuated between 0.027 and 0.040 h^{-1} until the end of the cultivation time; this observation coincides with the time when ethanol started accumulating after t= 12 h indicating that high residual ethanol concentrations inhibit the specific growth rate and that the chosen pre-determined specific growth rate (0.050 h^{-1}) yielded high Q(t) values, causing a rapid increase in C_{EtOH} in the cultivation medium faster than the cells' ethanol utilization capacity.

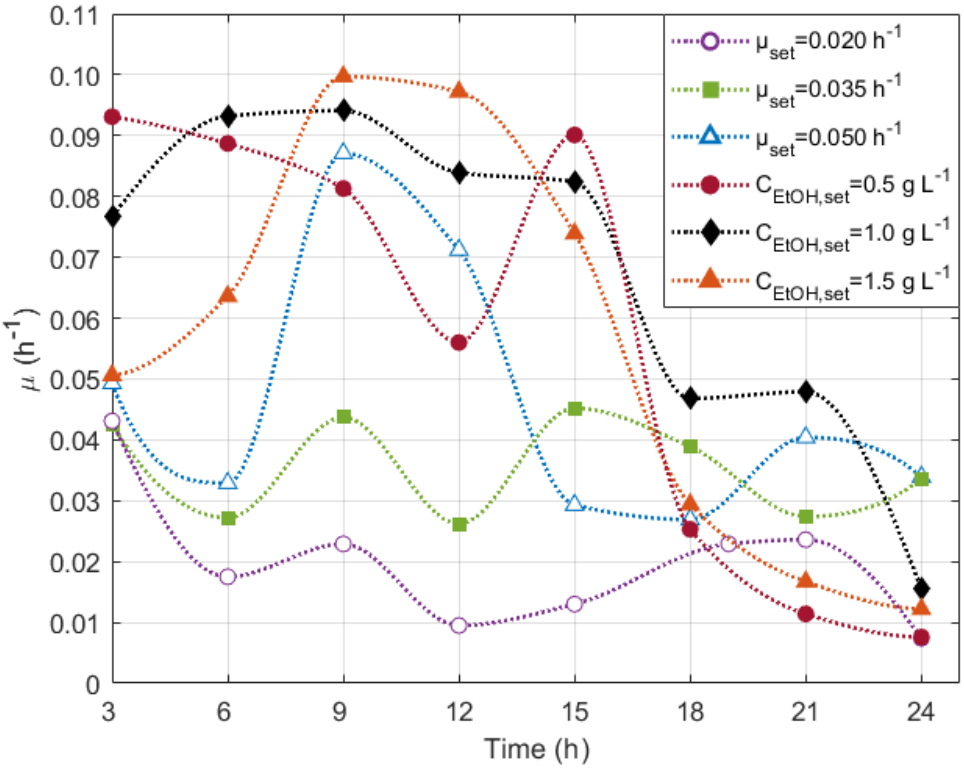

Figure 4.8. Variation of specific growth rates with the cultivation time in the CFS fed-batch bioreactor experiments.

The specific growth rates of $C_{EtOH,set}$= 0.5, 1.0 and 1.5 g L^{-1} generated higher maximum specific growth rates than the pre-determined specific growth rate strategies with an average value of 0.095 h^{-1} . The specific growth rates of the ethanol-stat bioreactors remained relatively high until t= 15 h after which the C_x increase became slower and started plateauing, indicating the beginning or approach of the stationary phase and thus explaining the observed decrease in the specific growth

rates. This decrease was more pronounced after t= 15 h for $C_{EtOH,set}$= 0.5 and 1.5 g L^{-1} due to the onset of the stationary phase, while the specific growth rate of $C_{EtOH,set}$= 1.0 g L^{-1} remained constant between t= 18 and 21 h, after which it continued to decrease again.

4.2.5. Specific Ethanol Uptake Rates

The specific ethanol uptake rates of μ_{set}= 0.035 and 0.020 h^{-1} started from high values of approximately 0.084 and 0.066 g g^{-1} h^{-1} at t=3 h (Figure 4.9), respectively, and then decreased to approximately 0.060 and 0.030 g g^{-1} h^{-1} at t=9 and 6 h, respectively, after which q_{EtOH} stabilized and varied slightly until the end of cultivation time; this coincided with the time the ethanol concentrations started becoming negligible in the cultivation medium of these bioreactors (Figure 4.5).

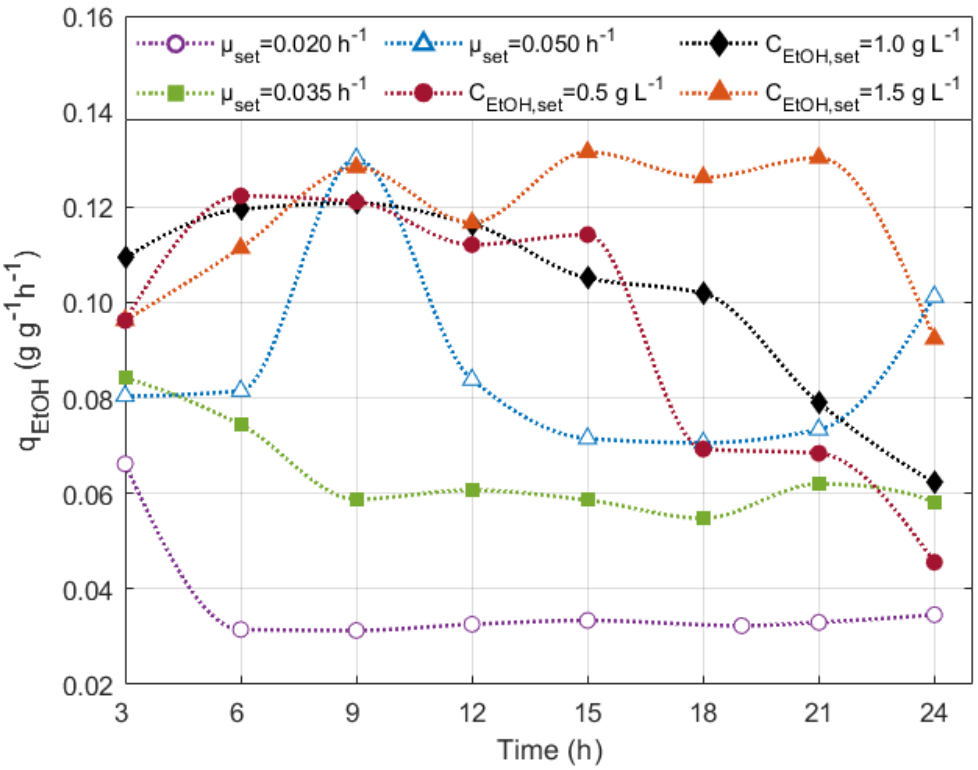

Figure 4.9. Variation of specific ethanol uptake rates with the cultivation time in CFS fed-batch bioreactor experiments.

However, the ethanol uptake rate of μ_{set}= 0.050 h^{-1} started from approximately the same value as that of bioreactor with pre-determined μ of 0.035 h^{-1}, but then increased after t= 6 h to reach a maximum of 0.13 g g^{-1} h^{-1} at t= 9h, after which it decreased and stabilized around 0.070 g g^{-1} h^{-1} until t= 21 h coinciding with the time when ethanol accumulation started occurring. Then q_{EtOH} increased again to reach 0.1 g g^{-1} h^{-1} at the end of the cultivation time.

The specific ethanol uptake rates for the ethanol-stat fed-batch bioreactors were relatively higher during cultivation where they fluctuated around 0.12 g g^{-1} h^{-1} in the first 12-15 hours of cultivation. q_{EtOH} decreased after t= 15 h for $C_{EtOH,set}$= 0.5 g L^{-1} which coincided with the time the stationary phase was observed and μ started decreasing. Similarly, q_{EtOH} for $C_{EtOH,set}$= 1.0 g L^{-1} started decreasing around the same time when μ started decreasing as well. However, for the highest set C_{EtOH} bioreactor of 1.5 g L^{-1} the ethanol uptake rate continued fluctuating around 0.13 g g^{-1} h^{-1} after t= 15 h and until t= 21 h after which it exhibited a sharp decrease.

4.2.6. Specific rhGH Production Rates

The specific rhGH production rates of μ_{set}= 0.035 and 0.050 h^{-1} and that of $C_{EtOH,set}$= 1.5 g L^{-1} exhibited maximums of 0.169, 0.102 and 0.0817 mg g^{-1} h^{-1} at t= 9 h (Figure 4.10), respectively. Sharp decreases in q_p at t= 24 h for $C_{EtOH,set}$=1.0 g L^{-1} and μ_{set}=0.035 h^{-1} should have resulted from an accumulation of extracellular proteases that degraded rhGH, where the rate of protease production exceeded the rate of rhGH production (Çelik et al., 2009). Generally, the q_p values of the ethanol-stat fed-batch bioreactors fluctuated at higher values than the specific rhGH production rates of the fed-batch bioreactors designed with pre-determined μ.

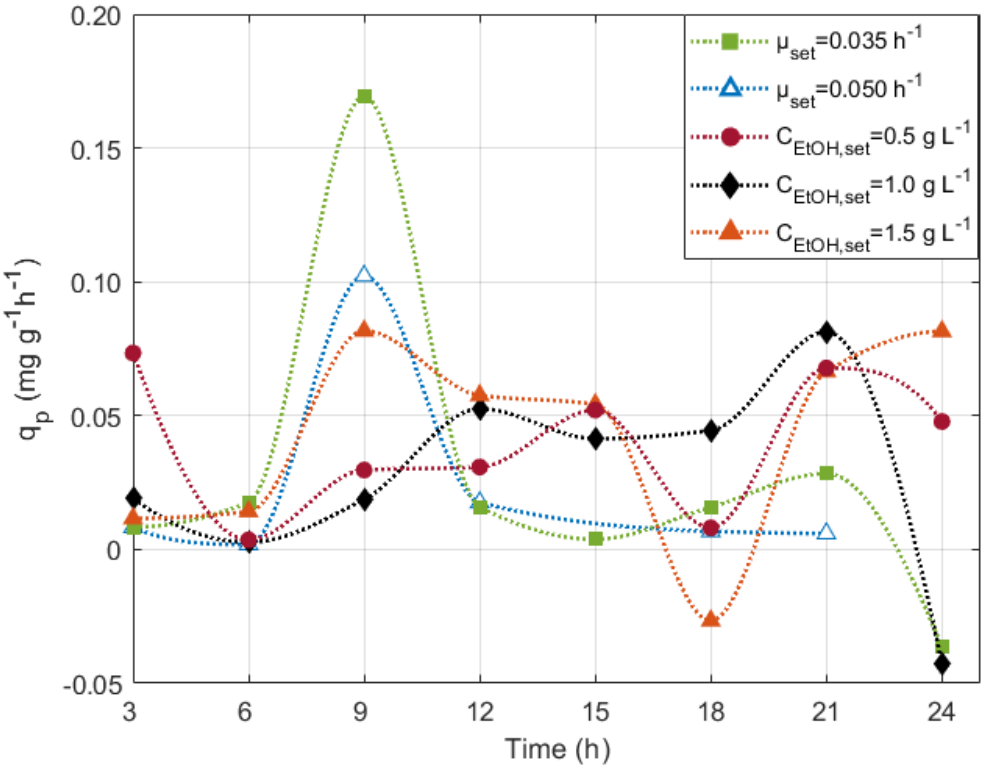

Figure 4.10. Variation of specific rhGH production rates with the cultivation time in the CFS fed-batch bioreactor experiments.

4.2.7. Comparison of Fed-Batch Feeding Strategies

The highest biomass on ethanol yield, $Y_{x/s}$, for the CFS fed-batch bioreactors designed with pre-determined μ was 0.61 g g^{-1} for μ_{set}= 0.035 h^{-1}, which was 1.2- and 1.4-fold higher than that of μ_{set}= 0.050 and 0.020 h^{-1}, respectively, but 1.2-fold lower than those of the ethanol-stat CFS fed-batch bioreactors that had an average 0.71 g g^{-1} $Y_{x/s}$. The protein on ethanol yield, $Y_{p/EtOH}$, was 0.68 mg g^{-1} for μ_{set}= 0.035 h^{-1}, which was 2.8-fold higher than that of μ_{set}= 0.050 h^{-1}. $Y_{p/EtOH}$ values for the ethanol-stat CFS fed-batch bioreactors were similar to each other, with an average value of 0.46 mg g^{-1}. The protein on biomass yield, $Y_{p/x}$, of the bioreactor with μ_{set}= 0.035 h^{-1} was 1.13 mg g^{-1} which was 2.5-fold higher than that of bioreactor with μ_{set}= 0.050 h^{-1}. The highest $Y_{p/x}$ of the ethanol-stat bioreactors belonged to the one with $C_{EtOH,set}$= 1.5 g L^{-1} at 0.97 mg g^{-1} which was 1.2- and 1.4-fold higher than that of the bioreactors with $C_{EtOH,set}$= 0.5 and 1.0 g L^{-1}, respectively, and 1.2-fold lower than that of

μ_{set}= 0.035 h^{-1}.The maximum volumetric productivity of the bioreactor with pre-determined μ of 0.035 h^{-1} was 2 mg L^{-1} h^{-1} which is 1.7-fold higher than that of the bioreactor with pre-determined μ of 0.050 h^{-1} (Table 4.2). On the other hand, the highest volumetric productivity was obtained by the ethanol-stat bioreactor of $C_{EtOH,set}$= 1.0 g L^{-1} at 4.08 mg L^{-1} h^{-1} which was around 1.2-fold higher than that of the other ethanol-stat bioreactors and 2-fold higher than that of μ_{set}=0.035 h^{-1} bioreactor. The high volumetric productivities coupled with high rhGH titers makes the ethanol-stat strategies more advantageous from an industrial-scale perspective. Moreover, the fed-batch bioreactor with the ethanol-stat strategy of $C_{EtOH,set}$= 0.5 g L^{-1} is the best operational strategy with the highest rhGH concentration, along with high volumetric productivity and protein on biomass yield. Hence, the continuous presence of ethanol at non-inhibitory concentrations in the cultivation medium is essential for *P. pastoris* to reach high cell densities and to increase rhGH production.

Table 4.2. *Comparison of process variables, yields and productivities for CFS fed-batch bioreactors designed with pre-determined μ and ethanol-stat.*

Strategy		CFS with pre-determined μ			CFS with ethanol-stat		
		μ_{set} (h^{-1})			$C_{EtOH,set}$ (g L^{-1})		
		0.020	0.035	0.050	0.5	1.0	1.5
C_p,max	mg L^{-1}	---	43.6	28.7	91	80.1	78.8
$Y_{p/x,max}$	mg g^{-1}	---	1.13	0.45	0.83	0.69	0.97
$Y_{p/EtOH}$	mg g^{-1}	---	0.68	0.24	0.47	0.49	0.41
$Y_{x/EtOH}$	g g^{-1}	0.43	0.61	0.53	0.72	0.71	0.71
Maximum volumetric productivity	mg L^{-1} h^{-1}	---	2	1.20	3.55	4.08	3.48
μ_{mean}	h^{-1}	0.017	0.035	0.047	0.093	0.088	0.096
$q_{EtOH,mean}$	g g^{-1} h^{-1}	0.032	0.061	0.082	0.11	0.11	0.12
$q_{p,mean}$	mg g^{-1} h^{-1}	---	0.039	0.021	0.036	0.047	0.045

4.3. Kinetic Models

In order to model the growth of *P. pastoris* on ethanol and acquire a tool that can be used to study rhGH production under the control of the novel $P_{ADH2\text{-}Cat8\text{-}L2}$, and hence allow the simulation of various cultivation conditions under continuous feed stream design concept, the relationships between the specific rates and residual ethanol concentrations were mathematically modeled using unstructured kinetic models. The models are based on the mean specific rates and mean residual ethanol concentrations which were calculated on the following basis: 1) the initial time was chosen when the C_x values were in close proximity to one another, i.e., the initial time for the bioreactors of μ_{set}= 0.020, 0.035 and 0.050 h^{-1}, and $C_{EtOH,set}$= 1.0 and 1.5 g L^{-1} was chosen as t=3 h whereas that of $C_{EtOH,set}$= 0.5 g L^{-1} was chosen as t=0 h so that all the C_x values are within an average of 37 g L^{-1}; 2) the end of cultivation for the bioreactors with pre-determined μ was chosen as t=21 h; 3) the end of cultivation for the ethanol-stat bioreactors was chosen before the stationary phase was observed, i.e., the final time for the bioreactors of $C_{EtOH,set}$= 0.5, 1.0 and 1.5 g L^{-1} was chosen as t= 15, 18 and 15 h, respectively; 4) the mean q_p values for the ethanol-stat bioreactors were determined based on the 3rd degree polynomial fitting of the C_p data in an effort to normalize the data and eliminate the experimentally observed decreases in q_p values before the end of cultivation.

4.3.1. Specific Growth Rate Model

As C_{EtOH} increased, the mean specific growth rate increased to reach a maximum of 0.096 h^{-1} at C_{EtOH}= 1.6 g L^{-1}, followed by a 2-fold decrease with increasing C_{EtOH} (Figure 4.11), indicating that the Haldane model would be a better representation of growth inhibition than the Monod model. This was indeed corroborated by the high coefficient of determination ($R^2_{Haldane}$= 0.98) and low mean relative error (RE_{mean}= 0.085) of the Haldane fit (Table 4.3).

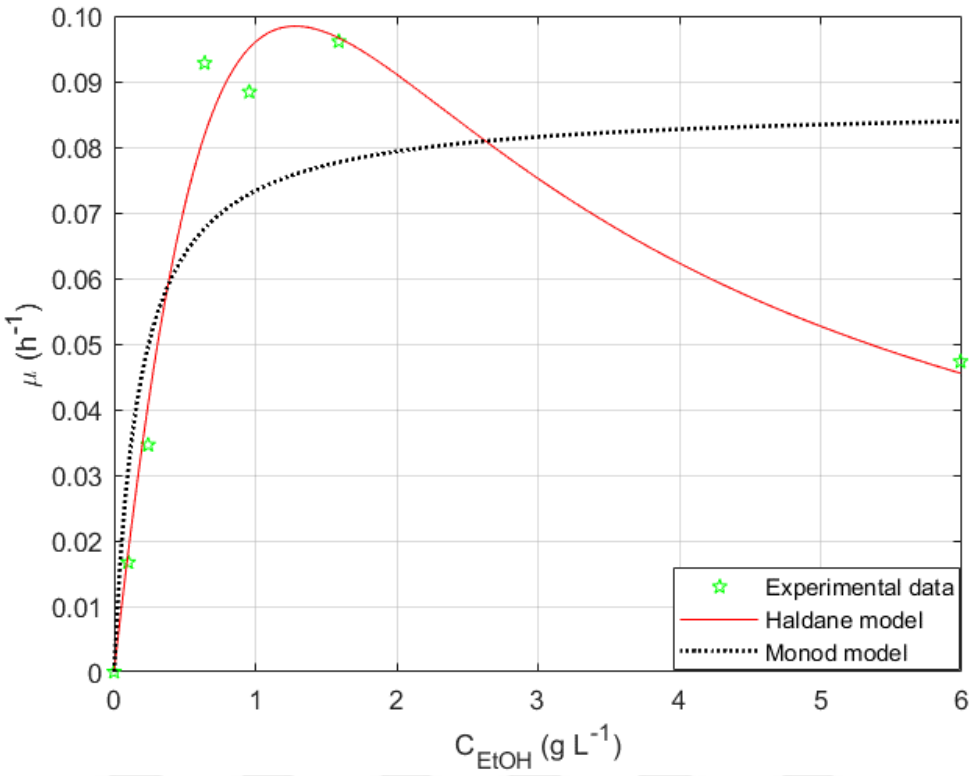

Figure 4.11. Haldane and Monod models for the relationship between specific growth rates versus ethanol concentrations.

Table 4.3. *Model Parameters for the correlation between specific growth rate and residual ethanol concentration.*

Parameter	Haldane Model	Monod Model
μ_{max} (h^{-1})	0.507	0.0864
K_s (g L^{-1})	2.66	0.178
K_i (g L^{-1})	0.618	----
$C_{EtOH,crit}$ (g L^{-1})	1.28	----
R^2	0.98	0.67

4.3.2. Specific Ethanol Uptake Rate Model

Similar to the effect of C_{EtOH} on the growth of *P. pastoris*, increasing C_{ETOH} lead to an increase in the mean specific ethanol uptake rate increased to reach a maximum of 0.12 g g^{-1} h^{-1} at C_{EtOH}= 1.6 g L^{-1}, followed by a 1.5-fold decrease with increasing C_{EtOH} (Figure 4.12), indicating that the Haldane model would be a better representation of

q_{EtOH} inhibition pattern than the Monod model. The high coefficient of determination ($R^2_{Haldane}$= 0.99) and low mean relative error (RE_{mean}= 0.027) supported the adequacy of the Haldane model (Table 4.4).

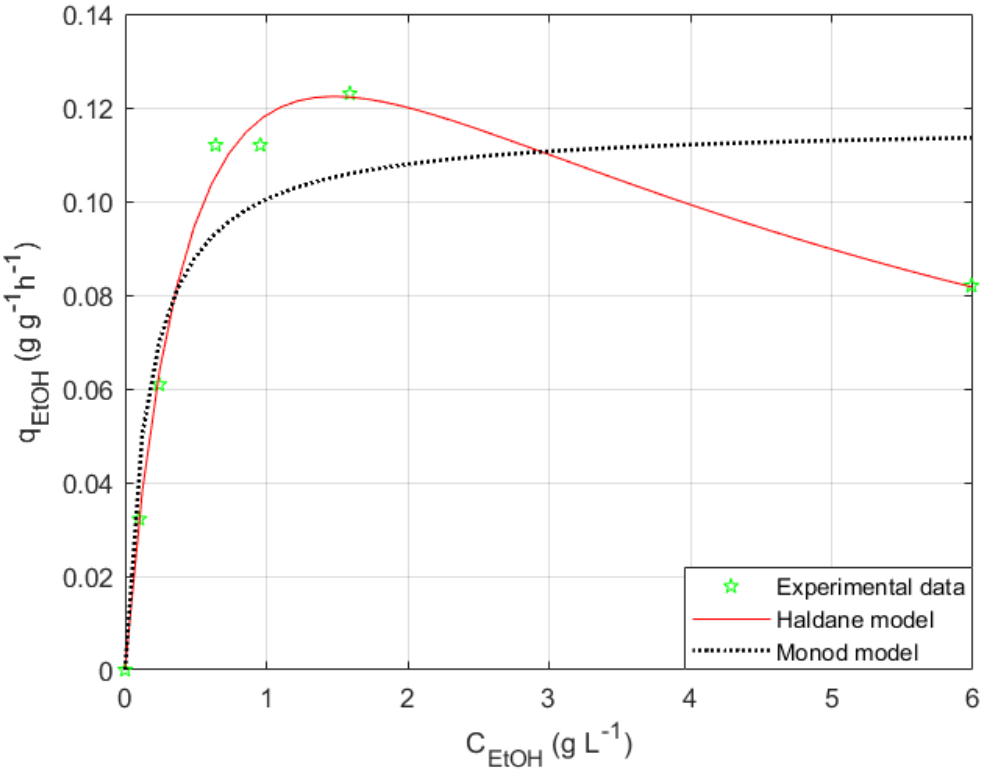

Figure 4.12. Haldane and Monod models for the relationship between specific ethanol uptake rates versus ethanol concentrations.

Table 4.4. *Model parameters for correlation between specific ethanol uptake rate and residual ethanol concentration.*

Parameter	Haldane model	Monod model
$q_{EtOH,max}$ (g g^{-1} h^{-1})	0.216	0.117
Ks,s (g L^{-1})	0.566	0.161
Ki,s (g L^{-1})	3.87	----
$C_{EtOH,crit}$ (g L^{-1})	1.48	----
R^2	0.99	0.84

4.3.3. Specific rhGH Production Rate Model

As C_{EtOH} increased, the mean specific rhGH production rate also increased to reach a maximum of 0.047 mg g^{-1} h^{-1} at C_{EtOH}= 0.96 g L^{-1}, followed by a 2.2-fold decrease with increasing C_{EtOH} (Figure 4.13), indicating that the Haldane model would be a better representation of q_p inhibition than the Monod model. This was supported by the high coefficient of determination ($R^2_{Haldane}$= 0.94) and low mean relative error (RE_{mean}= 0.11) of the Haldane fit (Table 4.5).

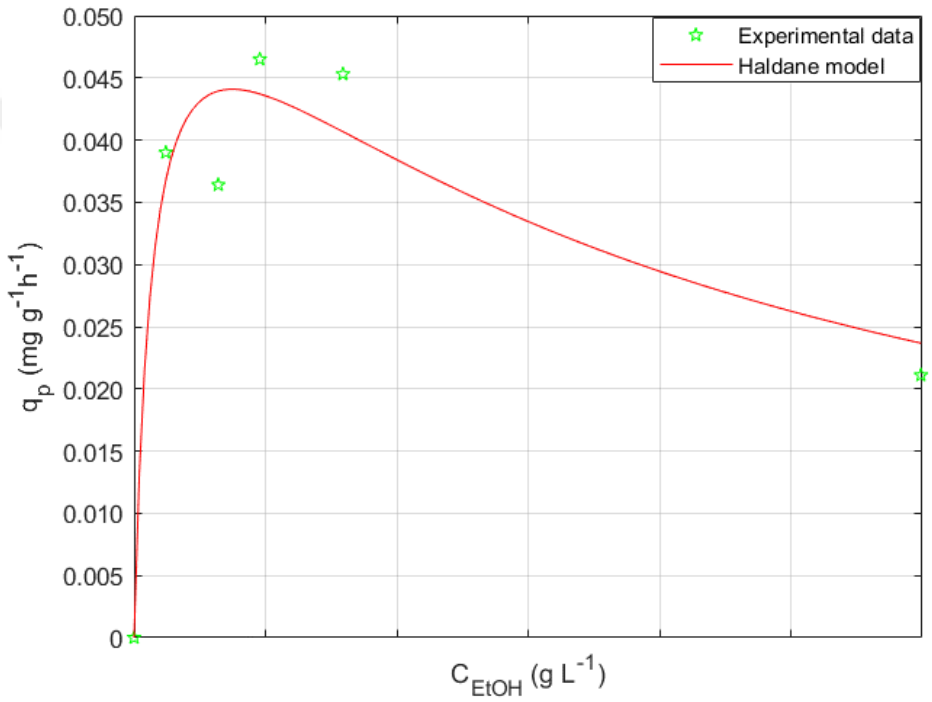

Figure 4.13. Haldane and Monod models for the relationship between specific rhGH production rates versus ethanol concentrations.

Table 4.5. *Model parameters for correlation between specific rhGH production rate and residual ethanol concentration.*

Parameter	Haldane model	Monod model
$q_{p,max}$ (mg g^{-1} h^{-1})	0.0613	0.0358
$K_{s,p}$ (g L^{-1})	0.146	-0.0311
$K_{i,p}$ (g L^{-1})	3.83	----
$C_{EtOH,crit}$ (g L^{-1})	0.75	----
R^2	0.94	0.75

Table 4.6. *Statistical data for the unstructured kinetic models relating μ, q_{EtOH} and q_p to C_{EtOH}.*

	Statistics			
Model	RE_{min}	RE_{max}	RE_{mean}	R^2
Haldane-μ	0.0057	0.18	0.085	0.98
Haldane-q_{EtOH}	0.0031	0.059	0.027	0.99
Haldane-q_p	0.058	0.21	0.11	0.94

Low mean relative errors (RE_{mean}) were obtained for all three Haldane models relating specific growth rates, specific ethanol uptake rates and specific rhGH production rates to the residual ethanol concentrations with values of 0.085, 0.027 and 0.11, respectively (Table 4.6). These low RE_{mean} combined with the high R^2 are strong indicators that the unstructured Haldane models can be used to predict the behavior of μ, q_{EtOH} and q_p at different residual ethanol concentrations.

4.3.4. Pirt and Luedeking-Piret Linear Models

The relationship between q_{EtOH} and μ followed the linear Pirt model with high coefficient of determination (R^2= 0.96) coupled with low mean relative error (RE_{mean}= 0.083), indicating that ethanol consumption was directly proportional to the specific growth rate of the cells in the culture (Figure 4.14 and Table 4.7). $Y_{EtOH/X}$ was 1.02 g g^{-1} and the maintenance energy demand was low at 0.023 g g^{-1} h^{-1} (Table 4.7), which is a necessity for *P. pastoris* to reach high cell densities (Jahic et al., 2002). However, the relationship between q_p and μ was not linear and hence did not follow the Luedeking-Piret model as was observed from Figure 4.15, which was further corroborated by a low coefficient of determination (R^2= 0.32) and higher relative errors with RE_{mean}= 0.22 and RE_{max}= 0.57 (Table 4.7).

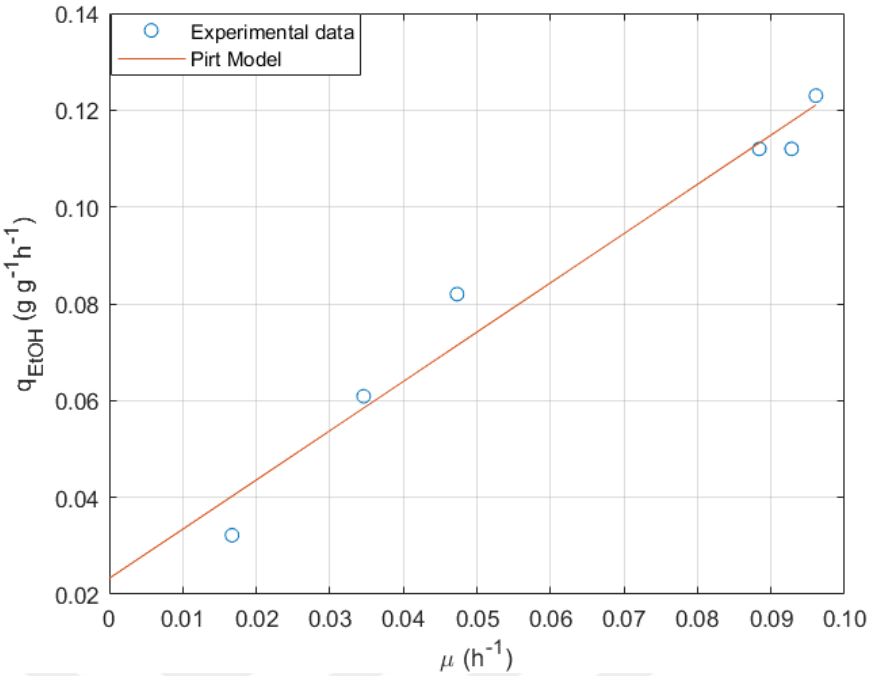

Figure 4.14. Pirt model for specific ethanol uptake rate versus specific growth rate.

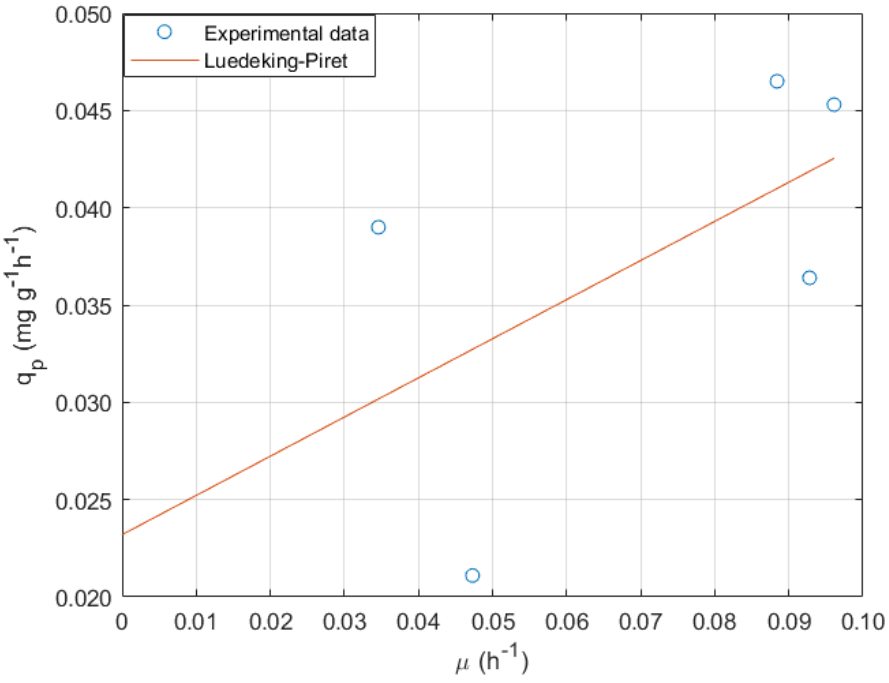

Figure 4.15. Luedeking-Piret model for specific rhGH production rate versus specific growth rate.

Table 4.7. *Kinetic parameters and statistical data of the linear models.*

Parameter	Pirt	Luedeking-Piret
$Y_{i/X}$ *	1.02 g g^{-1}	0.201 mg g^{-1}
m_i *	0.0233 g g^{-1} h^{-1}	0.0232 mg g^{-1} h^{-1}
RE_{min}	0.013	0.0078
RE_{max}	0.25	0.57
RE_{mean}	0.083	0.22
R^2	0.96	0.32

*"i" represents the subscripts s for Pirt model and p for Luedeking-Piret model

4.4. Model Simulation and Validation

In order to model and simulate the evolution of biomass over the cultivation time, the Haldane model, which relates the specific growth rate to the residual ethanol concentration, was chosen due to its high R^2 and low RE values to calculate the mean specific growth rates for the ethanol-stat bioreactors by inserting the residual ethanol concentrations in the equation. The mean specific growth rates were then inserted into the cell mass conservation equation (2.17) to determine C_xV.

In order to model and simulate the evolution of rhGH protein mass over the cultivation time, the Haldane model, which relates the specific rhGH production rate to the residual ethanol concentration, was chosen due to its high R^2 and low RE values to calculate the mean specific protein production rates for both the ethanol-stat bioreactors and the bioreactors designed with pre-determined μ. The mean specific rhGH production rates were then inserted into equation (3.23) to determine C_pV. It should be noted that the $\int_{t_i}^{t_f}(C_xV)dt$ term in equation (3.23) was calculated based on the equation (2.17) and not the experimental values.

The initial time was the same as the initial time chosen to calculate the mean specific rate values, i.e., the initial time for the bioreactors of μ_{set}=0.020, 0.035 and 0.050 h^{-1}, and $C_{EtOH,set}$= 1.0 and 1.5 g L^{-1} was chosen as t= 3 h whereas that of $C_{EtOH,set}$= 0.5 g L^{-1} was chosen as t=0 h so that all the C_xV values were within an average of 80 g, whereas the final time for each bioreactor was chosen based on the

proximity of the model results to the experimental results. The initial and final time principle also applied to the calculations of the C_pV values.

From Figure (4.16) and Table (4.8), it was observed that the biomass evolution throughout the cultivation time was well simulated with a low mean relative error of 0.065 and a maximum mean relative error of 0.13. The fed-batch bioreactors designed with low pre-determined μ values (μ_{set}= 0.020 and 0.035 h^{-1}) were two of the best simulated bioreactors with low mean relative errors of 0.017 and 0.014, respectively. The fed-batch bioreactor designed with high pre-determined μ (μ_{set}= 0.050 h^{-1}) had a higher mean relative error of 0.087 due to the sharp fluctuations in the specific growth rate values observed (Figure 4.8) resulting from the ethanol accumulation in the cultivation medium.

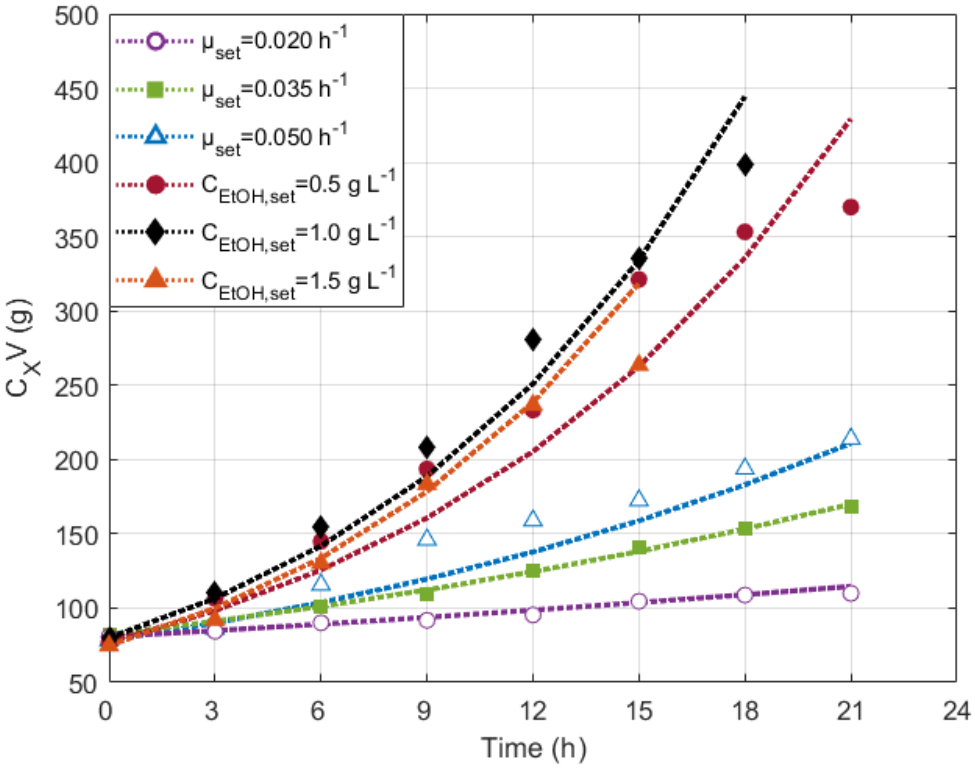

Figure 4.16. Evolution of cell generation, C_XV throughout the cultivation time for the CFS fed-batch bioreactors. Dashed lines represent the simulated data whereas point data represent the experimental data.

Table 4.8. *Performance of the proposed model for the simulation of the global state variable C_xV throughout the cultivation time.*

	Statistics for C_xV		
Bioreactor	RE_{min}	RE_{max}	RE_{mean}
μ_{set}=0.020 h^{-1}	0.002	0.041	0.017
μ_{set}=0.035 h^{-1}	0	0.03	0.014
μ_{set}=0.050 h^{-1}	0.014	0.18	0.087
$C_{EtOH,set}$=0.5 g L^{-1}	0.047	0.19	0.13
$C_{EtOH,set}$=1 g L^{-1}	0.007	0.11	0.074
$C_{EtOH,set}$=1.5 g L^{-1}	0.006	0.21	0.071
Overall Mean	0.014	0.13	0.065

Concerning the fed-batch bioreactors designed with ethanol-stat, the intermediate and high $C_{EtOH,set}$ designs, i.e., 1.0 and 1.5 g L^{-1} performed relatively better than the lowest $C_{EtOH,set}$ bioreactor of 0.5 g L^{-1} with mean relative errors of 0.074 and 0.071, respectively, compared to 0.13 for $C_{EtOH,set}$= 0.5 g L^{-1}. This resulted from the model predicting a mean μ value of 0.082 h^{-1} for $C_{EtOH,set}$= 0.5 g L^{-1} which was below the experimentally observed value of 0.093 h^{-1} which explains why the simulated C_xV curve remained below the experimental data points until t=21 h when the culture had been in the stationary phase for more than 3 hours. For the higher $C_{EtOH,set}$ ethanol-stat bioreactors, the predicted μ_{mean} values were 0.095 and 0.097 h^{-1} in comparison to their experimental mean values of 0.088 and 0.096 h^{-1} for $C_{EtOH,set}$ = 1.0 and 1.5 g L^{-1}, respectively. The simulated plot for $C_{EtOH,set}$ = 1.5 g L^{-1} passed through the experimental data points until the culture entered stationary phase after t=15 h (represented as t=12 h on the graph due to specific mean rates calculations explained previously). Also, the slopes of the simulated data for $C_{EtOH,set}$ = 1.0 and 1.5 g L^{-1} were close to each other due to the proximity of their predicted μ_{mean} values (0.095 and 0.097 h^{-1}).

From Figure (4.17) and Table (4.9), it was observed that the rhGH protein production throughout the cultivation time was better simulated for the ethanol-stat bioreactors. The best simulated C_pV values belonged to $C_{EtOH,set}$ of 0.5 and 1.5 g L^{-1} with RE_{mean} values of 0.025 and 0.065, respectively. The simulated C_pV values for the bioreactor

with $C_{EtOH,set}$=1.0 g L^{-1} showed a relatively high RE_{mean} value of 0.21 with the simulated data lying above the experimental data until t=9 h after which the simulated data approached the experimental ones. The simulated q_p values for $C_{EtOH,set}$= 0.5, 1.0 and 1.5 g L^{-1} were 0.0439, 0.0437 and 0.0407 mg g^{-1} h^{-1}, respectively, in comparison to their experimental values of 0.0364, 0.0465 and 0.0453 mg g^{-1} h^{-1}, respectively.

On the other hand, the C_pV values for the bioreactors designed with pre-determined μ exhibited high RE_{mean} values of 0.26 and 0.25 for μ_{set}= 0.035 and 0.050 h^{-1}, respectively, due to the sharp q_p peaks observed at t= 9 h (Figure 4.10) followed by a decrease to the values observed at the beginning of the cultivation time for both bioreactors. The proposed model does not consider time varying q_p values but rather the mean values, thus it cannot account for local changes in the q_p values and consequently sudden changes in C_pV values. This explains why the simulated model approached the experimental values of these bioreactors with pre-determined μ towards the end of the cultivation time. In addition, the predicted $q_{p,mean}$ values were 0.024 and 0.034 mg g^{-1} h^{-1}, approximately similar to their real experimental values of 0.021 and 0.039 mg g^{-1} h^{-1} for μ_{set}= 0.050 and 0.035 h^{-1}, respectively. Nevertheless, the C_pV simulated model had an acceptable RE_{mean} value of 0.16 and gives more reliable results with ethanol-stat bioreactors.

Table 4.9. *Performance of the proposed model for the simulation of the global state variable C_pV throughout the cultivation time*

	Statistics for C_pV		
Bioreactor	RE_{min}	RE_{max}	RE_{mean}
μ_{set}=0.035 h^{-1}	0.097	0.50	0.26
μ_{set}=0.050 h^{-1}	0.036	0.42	0.25
$C_{EtOH,set}$=0.5 g L^{-1}	0.005	0.058	0.025
$C_{EtOH,set}$=1 g L^{-1}	0.038	0.35	0.21
$C_{EtOH,set}$=1.5 g L^{-1}	0.013	0.099	0.065
Overall Mean	0.025	0.26	0.16

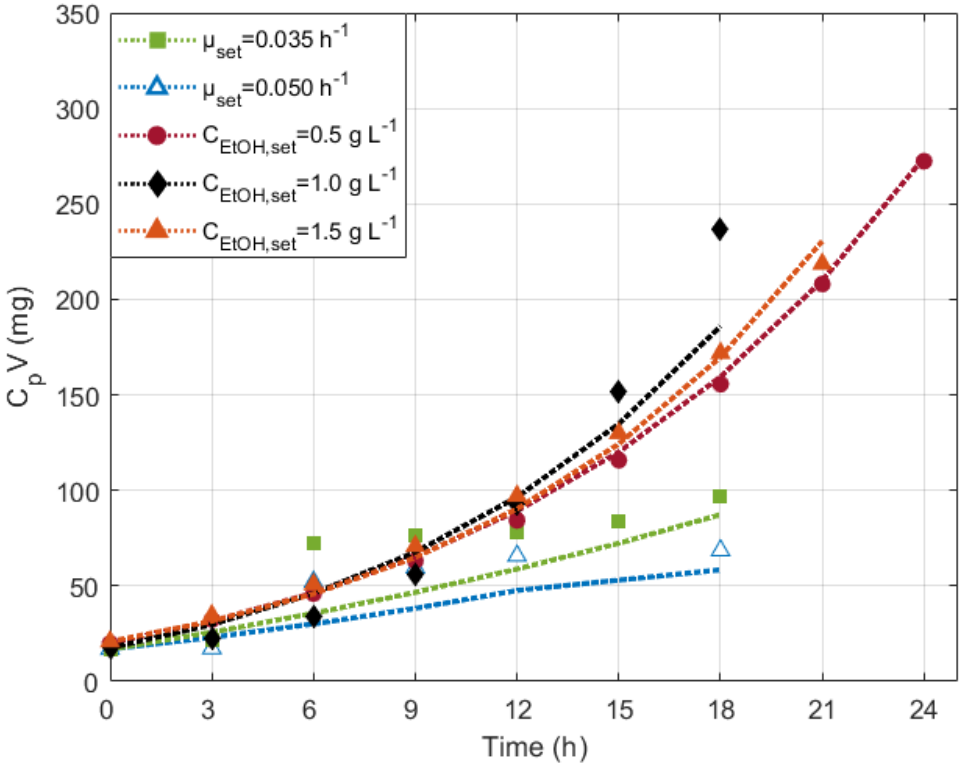

Figure 4.17. Evolution of rhGH production, C_pV throughout the cultivation time for the CFS fed-batch bioreactors. Dashed lines represent the simulated data whereas point data represent the experimental data.

CHAPTER 5

CONCLUSIONS

In this work, the effect of ethanol on the growth of a *P. pastoris* strain producing recombinant human growth hormone under the control of the engineered promoter $P_{ADH2\text{-}Cat8\text{-}L2}$ was first established by cultivating the cells in air-filtered shake flask bioreactors with varying concentrations of ethanol. Ethanol concentrations above 3 g L^{-1} inhibited the growth of the cells which was evident from the decrease of specific growth rates beyond that concentration. Also, the specific growth rate inhibition was mathematically modeled using Haldane and Monod equations. The Monod model failed to represent the ethanol inhibition on the specific growth rate whereas the Haldane model was successful at mathematically representing the inhibition pattern with a critical substrate value of 1.97 g L^{-1} and a maximum specific growth rate of 0.194 h^{-1}.

Also, the effects of two different continuous feed stream operational strategies on the specific growth rate, specific ethanol uptake rate and specific rhGH production rate were investigated as follows: three continuous feed stream fed-batch bioreactors designed with pre-determined specific growth rates of 0.020, 0.035 and 0.050 h^{-1}, and three continuous feed stream fed-batch bioreactors designed with constant residual ethanol concentrations (ethanol-stat) of 0.5, 1.0 and 1.5 g L^{-1}. The ethanol-stat bioreactors were able to reach higher final cell concentrations, approximately 1.6-fold that of the bioreactors designed with pre-determined μ values, and higher final rhGH protein titer, the highest being 91 mg L^{-1} for $C_{EtOH,set}$= 0.5 g L^{-1} which was 2.1-fold higher than the maximum rhGH concentration obtained by the bioreactors designed with pre-determined μ. Moreover, the ethanol-stat bioreactors generated 2-fold higher volumetric productivities and high protein on biomass yields, however, the highest $Y_{p/x}$ value belonged to the μ_{set}= 0.035 h^{-1} at 1.13 mg g^{-1} which was 1.2-fold higher

than the maximum obtained by the ethanol-stat bioreactors. In conclusion, the ethanol-stat strategy of $C_{EtOH,set}$= 0.5 g L^{-1} was the favorable operational strategy with the highest rhGH concentration produced, along with high volumetric productivity and protein on biomass yield.

Furthermore, unstructured, kinetic models were developed to relate the various kinetic rates and allow the simulation of the cultivation conditions without the need to use complex mathematical models. The specific growth rate, the specific ethanol uptake rate and the protein production rate against the residual ethanol concentration exhibited Haldane behavior with high R^2 values and low mean relative errors. From the Haldane model for specific growth rate, it was found that a critical ethanol concentration of 1.28 g L^{-1} was inhibitory, similar to the critical substrate concentration of the air-filtered shake flask bioreactor experiments of 1.97 g L^{-1}. The relationship between the specific ethanol uptake rate and specific growth rate was linear in nature and successfully described by the Pirt model, whereas the relationship between the specific protein production rate and the specific growth rate was not linear and thus could not be described by the Luedeking-Piret model.

Accordingly, the CFS bioreactors were simulated based on the Haldane models relating the specific growth rate and specific protein production rate to the residual ethanol concentration. The evolution of biomass throughout the cultivation time was well simulated with a mean relative error of 0.065, with the bioreactors designed with lower pre-determined μ values and higher ethanol-stat C_{EtOH} set values being better modeled. The evolution of rhGH mass throughout the cultivation time was better simulated for the bioreactors designed with ethanol-stat; the relative mean error of the C_pV simulations was 0.16 with the best simulated bioreactor being $C_{EtOH,set}$=0.5 g L^{-1} with a RE_{mean} of 0.025.

Future experiments involving co-substrate feeding (mannitol, sorbitol or glucose) coupled with ethanol-stat-based fed-batch bioreactor operations can be conducted, followed by DO-stat fed-batch bioreactor operations to determine the optimal

substrate feeding strategy and dissolved oxygen level required for maximum rhGH production efficiency.

REFERENCES

Aiba, S., Shoda, M., and Nagatani, M. (1968). Kinetics of product inhibition in alcohol fermentation. *Biotechnology and Bioengineering, 10*(6), 845-864.

Andrews, J. F. (1968). A mathematical model for the continuous culture of microorganisms utilizing inhibitory substrates. *Biotechnology and Bioengineering, 10*(6), 707-723.

Ata, Ö., Boy, E., Güneş, H., and Çalık, P. (2015). Codon optimization of xylA gene for recombinant *glucose isomerase* production in *Pichia pastoris* and fed-batch feeding strategies to fine-tune bioreactor performance. *Bioprocess and Biosystems Engineering, 38*(5), 889-903.

Barrigón, J. M., Montesinos, J. L., and Valero, F. (2013). Searching the best operational strategies for *Rhizopus oryzae lipase* production in *Pichia pastoris* Mut+ phenotype: Methanol limited or methanol non-limited fed-batch cultures? *Biochemical Engineering Journal, 75*, 47-54.

Barrigon, J. M., Valero, F., and Montesinos, J. L.(2015). A macrokinetic model-based comparative meta-analysis of recombinant pn prroteioduction by *Pichia pastoris* under AOX1 promoter. *Biotechnology and Bioengineering, 112*(6), 1132-1145.

Baumann, K., Maurer, M., Dragosits, M., Cos, O., Ferrer, P., and Mattanovich, D. (2008). Hypoxic fed-batch cultivation of *Pichia pastoris* increases specific and volumetric productivity of recombinant proteins. *Biotechnology and Bioengineering, 100*(1), 177-183.

Çalık, P., Bozkurt, B., Zerze, G. H., İnankur, B., Bayraktar, E., Boy, E., Orman, M.A., Açık, E. and Özdamar, T. H. (2013). Effect of co-substrate sorbitol different

feeding strategies on human growth hormone production by recombinant *Pichia pastoris. Journal of Chemical Technology and Biotechnology, 88*(9), 1631-1640.

Çalık, G., Kocabaş, P., Afşar, H., Çalık, P., and Özdamar, T. H. (2016). Parametric continuous feed stream design to fine-tune fed-batch bioreactor performance: recombinant human growth hormone production in *Bacillus subtilis. Journal of Chemical Technology and Biotechnology, 91*(11), 2740-2750.

Çalık, P., Hoxha, B., Çalık, G., and Özdamar, T. H. (2018). Hybrid fed-batch bioreactor operation design: control of substrate uptake enhances recombinant protein production in high-cell-density fermentations. *Journal of Chemical Technology and Biotechnology, 93*(11), 3326-3335.

Çelik, E., Çalık, P., and Oliver, S. G. (2009). Fed-batch methanol feeding strategy for recombinant protein production by *Pichia pastoris* in the presence of co-substrate sorbitol. *Yeast, 26*(9), 473-484.

Çelik, E., Çalık, P., and Oliver, S. G. (2009). A structured kinetic model for recombinant protein production by Mut+ strain of *Pichia pastoris. Chemical Engineering Science, 64*(23), 5028-5035.

Cereghino, G. P. L., Cereghino, J. L., Ilgen, C., and Cregg, J. M. (2002). Production of recombinant proteins in fermenter cultures of the yeast *Pichia pastoris. Current Opinion in Biotechnology, 13*(4), 329-332.

Charoenrat, T., Ketudat-Cairns, M., Stendahl-Andersen, H., Jahic, M., and Enfors, S. O. (2005). Oxygen-limited fed-batch process: an alternative control for *Pichia pastoris* recombinant protein processes. *Bioprocess and Biosystems Engineering, 27*(6), 399-406.

Chung, J. D. (2000). Design of metabolic feed controllers: Application to high-density fermentations of *Pichia pastoris. Biotechnology and Bioengineering, 68*(3), 298-307.

Cregg, JM, and Tolstorukov, II. (2012). *P. pastoris* ADH promoter and use thereof to direct expression of proteins. US 8222386 B2, United States Patent and Trademark Office.

Ergün, B. G., Gasser, B., Mattanovich, D., and Çalık, P. (2019). Engineering of *alcohol dehydrogenase 2* hybrid-promoter architectures in *Pichia pastoris* to enhance recombinant protein expression on ethanol. *Biotechnology and Bioengineering, 116*(10), 2674-2686.

Eskitoros, M. Ş., and Çalık, P. (2014). Co-substrate mannitol feeding strategy design in semi-batch production of recombinant human erythropoietin production by *Pichia pastoris. Journal of Chemical Technology and Biotechnology*, *89*(5), 644-651.

Feist, A. M., Henry, C. S., Reed, J. L., Krummenacker, M., Joyce, A. R., Karp, P. D., Broadbelt, L.J., Hatzimanikatis, V. and Palsson, B.Ø. (2007). A genome-scale metabolic reconstruction for *Escherichia coli K-12 MG1655 t*hat accounts for 1260 ORFs and thermodynamic information. *Molecular Systems Biology, 3*(1).

Garnier, A., and Gaillet, B. (2015). Analytical solution of Luedeking–Piret equation for a batch fermentation obeying Monod growth kinetics. *Biotechnology and Bioengineering, 112*(12), 2468-2474.

Glick, B. R., Pasternak, J. J., and Patten, C. L. (2010). *Molecular Biotechnology: Principles and Applications of Recombinant DNA.* Washington, DC: ASM Press,.

Graham, M. R., Evans, P., Davies, B., and Baker, J. S. (2008). Arterial pulse wave velocity, inflammatory markers, pathological GH and IGF states, cardiovascular and cerebrovascular disease. *Vascular Health and Risk Management, 4*(6), 1361.

Güneş, H., Boy, E., Ata, Ö., Zerze, G. H., Çalık, P., and Özdamar, T. H. (2016). Methanol feeding strategy design enhances recombinant human growth hormone production by *Pichia pastoris. Journal of Chemical Technology and Biotechnology, 91*(3), 664-671.

Güneş, H., and Çalık, P. (2016). Oxygen transfer as a tool for fine-tuning recombinant protein production by *Pichia pastoris under glyceraldehyde-3-phosphate dehydrogenase* promoter. *Bioprocess and Biosystems Engineering, 39*(7), 1061-1072.

Heyland, J., Fu, J., Blank, L. M., and Schmid, A. (2010). Quantitative physiology of *Pichia pastoris* during glucose-limited high-cell density fed-batch cultivation for recombinant protein production. *Biotechnology and Bioengineering, 107*(2), 357-368.

Hilt, W., and Wolf, D. H. (1992). Stress-induced proteolysis in yeast. *Molecular Microbiology, 6*(17), 2437-2442.

Inan, M., and Meagher, M. M. (2001). The effect of ethanol and acetate on protein expression in *Pichia pastoris. Journal of bioscience and bioengineering, 92*(4), 337-341.

Jahic, M., Rotticci-Mulder, J. C., Martinelle, M., Hult, K., and Enfors, S. O. (2002). Modeling of growth and energy metabolism of *Pichia pastoris* producing a fusion protein. *Bioprocess and Biosystems Engineering, 24*(6), 385-393.

Jahic, M., Veide, A., Charoenrat, T., Teeri, T., and Enfors, S. O. (2006). Process technology for production and recovery of heterologous proteins with *Pichia pastoris. Biotechnology Progress, 22*(6), 1465-1473.

Karaoğlan, M., Karaoğlan, F. E., and Inan, M. (2016). Comparison of ADH3 promoter with commonly used promoters for recombinant protein production in *Pichia pastoris. Protein Expression and Purification, 121*, 112-117.

Kobayashi, K., Kuwae, S., Ohya, T., Ohda, T., Ohyama, M., and Tomomitsu, K. (2000). High level secretion of recombinant human serum albumin by fed-batch fermentation of the methylotrophic yeast, *Pichia pastoris*, based on optimal methanol feeding strategy. *Journal of Bioscience and Bioengineering, 90*(3), 280-288.

Liu, W. C., Gong, T., Wang, Q. H., Liang, X., Chen, J. J., and Zhu, P. (2016). Scaling-up fermentation of *Pichia pastoris* to demonstration-scale using new methanol-feeding strategy and increased air pressure instead of pure oxygen supplement. *Scientific Reports, 6*, 18439.

Liu, W. C., Inwood, S., Gong, T., Sharma, A., Yu, L. Y., and Zhu, P. (2019). Fed-batch high-cell-density fermentation strategies for *Pichia pastoris* growth and production. *Critical Reviews in Biotechnology, 39*(2), 258-271.

Luedeking, R., and Piret, E. L. (1959). A kinetic study of the lactic acid fermentation. Batch process at controlled pH. *Journal of Biochemical and Microbiological Technology and Engineering, 1*(4), 393-412.

Macauley-Patrick, S., Fazenda, M. L., McNeil, B., and Harvey, L. M. (2005). Heterologous protein production using the *Pichia pastoris* expression system. *Yeast, 22*(4), 249-270.

Maurer, M., Kühleitner, M., Gasser, B., and Mattanovich, D. (2006). Versatile modeling and optimization of fed batch processes for the production of secreted heterologous proteins with *Pichia pastoris. Microbial cell factories, 5*(1), 37.

Møller, N., and Jørgensen, J. O. L. (2009). Effects of growth hormone on glucose, lipid, and protein metabolism in human subjects. *Endocrine Reviews, 30*(2), 152-177.

Monod, J. (1949). The growth of bacterial cultures. *Annual Review of Microbiology, 3*(1), 371-394.

Montesinos, J. L., Lafuente, J., Gordillo, M. A., Valero, F., Sola, C., Charbonnier, S., and Cheruy, A. (1995). Structured modeling and state estimation in a fermentation process: lipase production by *Candida rugosa. Biotechnology and Bioengineering*, *48*(6), 573-584.

Paalme, T., Elken, R., Vilu, R., and Korhola, M. (1997). Growth efficiency of *Saccharomyces cerevisiae* on glucose/ethanol media with a smooth change in the dilution rate (A-stat). *Enzyme and Microbial Technology*, *20*(3), 174-181.

Pirt, S. J. (1965). The maintenance energy of bacteria in growing cultures. *Proceedings of the Royal Society of London. Series B. Biological Sciences*, *163*(991), 224-231.

Potvin, G., Ahmad, A., and Zhang, Z. (2012). Bioprocess engineering aspects of heterologous protein production in *Pichia pastoris*: a review. *Biochemical Engineering Journal*, *64*, 91-105.

Ponte, X., Barrigón, J. M., Maurer, M., Mattanovich, D., Valero, F., and Montesinos-Seguí, J. L. (2018). Towards optimal substrate feeding for heterologous protein production in *Pichia pastoris (Komagataella spp)* fed-batch processes under P AOX1 control: a modeling aided approach. *Journal of Chemical Technology and Biotechnology*, *93*(11), 3208-3218.

Prabhu, A. A., and Venkata Dasu, V. (2017). Dual-substrate inhibition kinetic studies for recombinant human interferon gamma producing *Pichia pastoris. Preparative Biochemistry and Biotechnology*, *47*(10), 953-962.

Ren, H. T., Yuan, J. Q., and Bellgardt, K. H. (2003). Macrokinetic model for methylotrophic *Pichia pastoris* based on stoichiometric balance. *Journal of Biotechnology*, *106*(1), 53-68.

Romanos, M. (1995). Advances in the use of *Pichia pastoris* for high-level gene expression. *Current Opinion in biotechnology*, *6*(5), 527-533.

Shen, W., Xue, Y., Liu, Y., Kong, C., Wang, X., Huang, M., Cai, M., Zhou, X., Zhang, Y., and Zhou, M. (2016). A novel methanol-free *Pichia pastoris* system for recombinant protein expression. *Microbial Cell Factories, 15*(1), 178.

Sohn, S. B., Graf, A. B., Kim, T. Y., Gasser, B., Maurer, M., Ferrer, P., Mattanovich, D., and Lee, S. Y. (2010). Genome-scale metabolic model of methylotrophic yeast *Pichia pastoris* and its use for in silico analysis of heterologous protein production. *Biotechnology Journal, 5*(7), 705-715.

Theron, C. W., Berrios, J., Delvigne, F., and Fickers, P. (2018). Integrating metabolic modeling and population heterogeneity analysis into optimizing recombinant protein production by *Komagataella (Pichia) pastoris. Applied Microbiology and Biotechnology, 102*(1), 63-80.

Trinh, L. B., Phue, J. N., and Shiloach, J. (2003). Effect of methanol feeding strategies on production and yield of recombinant mouse endostatin from *Pichia pastoris. Biotechnology and Bioengineering*, *82*(4), 438-444.

Villadsen J, Nielsen J, Lidén G. (2011). *Bioreaction Engineering Principles* (3rd ed.). New York: Springer Science and Business Media.

Vogl, T., Hartner, F. S., and Glieder, A. (2013). New opportunities by synthetic biology for biopharmaceutical production in *Pichia pastoris. Current Opinion in Biotechnology, 24*(6), 1094-1101.

Waterham, H. R., Digan, M. E., Koutz, P. J., Lair, S. V., and Cregg, J. M. (1997). Isolation of the *Pichia pastoris glyceraldehyde-3-phosphate dehydrogenase* gene and regulation and use of its promoter. *Gene, 186*(1), 37-44.

Yamanè, T., and Shimizu, S. (1984). Fed-batch techniques in microbial processes. *Adv.Biochem. Eng. Biotech.* **30**:147–194

Young, J. D. (2015). Learning from the steersman: a natural history of cybernetic models. *Industrial and Engineering Chemistry Research, 54*(42), 10162-10169.

Yurimoto, H., Oku, M., and Sakai, Y. (2011). Yeast methylotrophy: metabolism, gene regulation and peroxisome homeostasis. *International Journal of Microbiology, 2011*.

Zhang, W., Bevins, M. A., Plantz, B. A., Smith, L. A., and Meagher, M. M. (2000). Modeling *Pichia pastoris* growth on methanol and optimizing the production of a recombinant protein, the heavy-chain fragment C of botulinum neurotoxin, serotype A. *Biotechnology and Bioengineering, 70*(1), 1-8.

Zhang, W., Potter, K. J. H., Plantz, B. A., Schlegel, V. L., Smith, L. A., and Meagher, M. M. (2003). *Pichia pastoris* fermentation with mixed-feeds of glycerol and methanol: growth kinetics and production improvement. *Journal of Industrial Microbiology and Biotechnology*, *30*(4), 210-215.

A. GC Calibration Curve for Ethanol Concentration

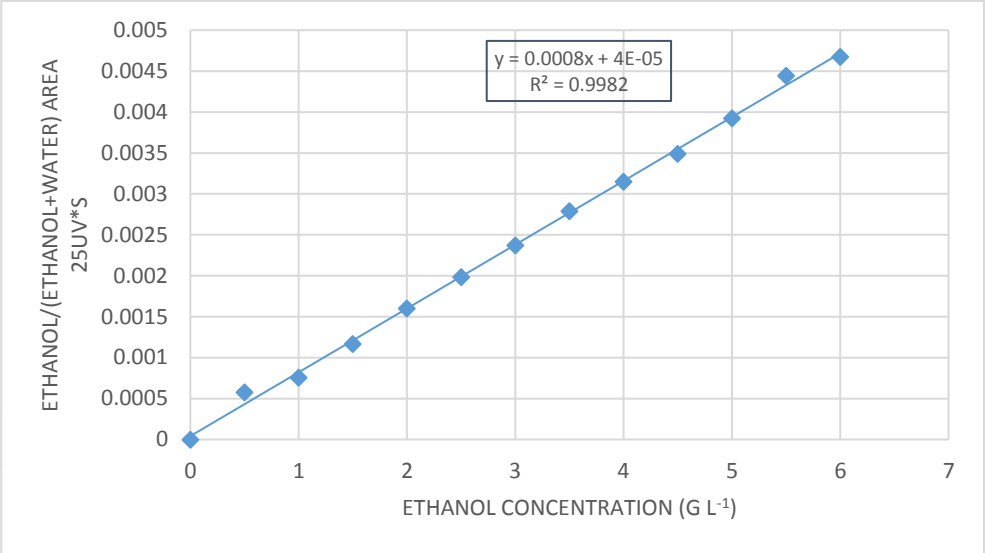

Figure A. Calibration curve of ethanol concentration in GC.

B. ELISA Calibration Curve

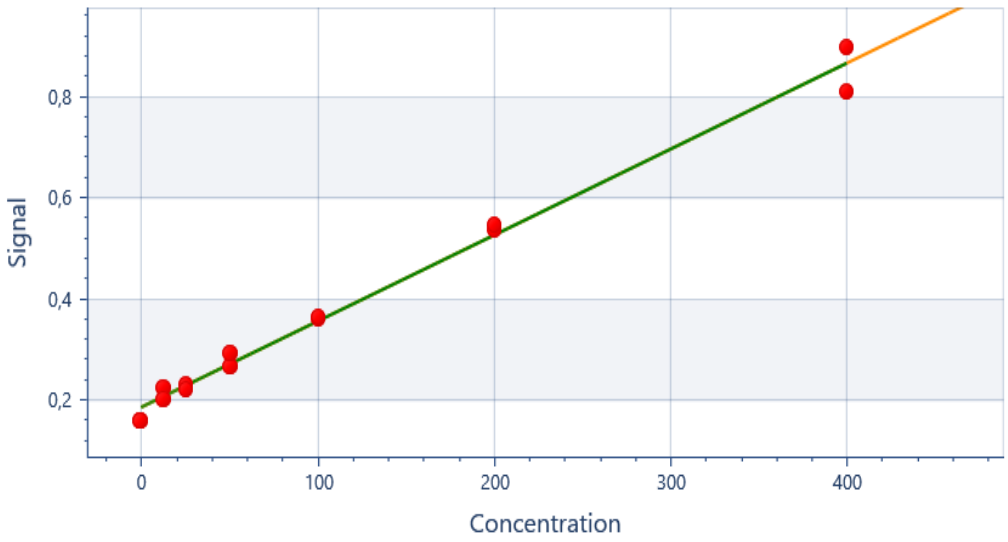

Figure B. Calibration curve using hGH standards for ELISA readings.

y = 0,00169983x + 0,187326
R^2: 0,997

C. Gas Chromatography Negative Control Experiment

Table C. *Change of ethanol concentrations after t=8 h of incubation without cells.*

	C_{EtOH} (g L^{-1})							
Initial C_{EtOH} (g L^{-1})	1	2	3	4	5	7	8	16
t=0 h	1.35	2.10	3.02	3.99	5.02	7.12	8.03	15.75
t=8 h	1.31	2.12	3.03	3.79	4.74	6.94	7.93	14.86

D. Haldane and Monod MATLAB® Code for Air-Filtered Shake Flask Bioreactor Experiments

```
% Parameters: mumax = b(1),  Ks = b(2),  Ki = b(3)
HaldaneInhMdl = @(b,S) b(1).*S ./ (b(2) + S + S.^2./b(3));
MonodInhMdl = @(b,S) b(1).*S ./ (b(2) + S);
mu = [0 0.129 0.133 0.140 0.131 0.114 0.110 0.101 0.0734];
S = [0 1 2 3 4 5 7 8 16];
SSECF = @(b) sum((mu - HaldaneInhMdl(b,S)).^2);
SSECF_monod = @(b) sum((mu - MonodInhMdl(b,S)).^2);
B0 = [0.1; 0.1; 1];
[B, SSE] = fminsearch(SSECF, B0)
[B_monod, SSE_monod] = fminsearch(SSECF_monod, B0)
Sp = linspace(min(S), max(S), 150);
fitmu = HaldaneInhMdl(B,Sp);
fitmu_monod = MonodInhMdl(B_monod,Sp);
plot(S, mu, 'pg')
hold on
plot(Sp, fitmu, '-r')
hold off
set(gca, 'YLim', [0, 0.150],'YTick', 0:0.015:0.150,'YTickLabel',
0:0.015:0.150);
set(gca, 'XLim', [0, 17]);
grid
xlabel('C_{s} (g L^{-1})')
ylabel('\mu (h^{-1})')
legend('Data', 'Fit-haldane', 'Location', 'NE')
txtlbl = sprintf('\\mu = %.3f \\times S / (%6.0f + S + s^2/%.1f)',
B);
text(1500, 0.0006, txtlbl)
```

E. Specific Growth Rate, Ethanol Uptake Rate and Protein Production Rate Calculations Using MATLAB®

%μ_{set}=0.050 h^{-1}

```
t_BR1=[0 3 6 9 12 15 18 21 24];
Cx_BR1=[31.6 36.5 39.8 52.6 65.2 69.7 73.7 81.1 87.0];
V_BR1=[2.05 2.14 2.16 2.20 2.24 2.28 2.34 2.39 2.46];
Qt_BR1=[0.00838 0.00973 0.01131 0.01314 0.01526 0.01774 0.02061
0.02394 0.02781];
Cs_BR1=[3.62 5.52 8.07 1.66 1.39 4.76 9.76 15.18 15.06];
Cp_BR1=[7.1 7.9 8.0 23.7 26.6 28.1 28.7];
t_BR1_Cp=[0 3 6 9 12 18 21];
V_BR1_Cp=[2.05 2.14 2.16 2.20 2.24 2.34 2.39];
Cx_BR1_Cp=[31.6 36.5 39.8 52.6 65.2 73.7 81.1];
Biomass_BR1_Cp=Cx_BR1_Cp.*V_BR1_Cp;
Qt_BR1_Cp=[0.00838 0.00973 0.01131 0.01314 0.01526 0.02061 0.02394];
Cs0=790;
Biomass_BR1=Cx_BR1.*V_BR1
Protein_BR1_Cp=Cp_BR1.*V_BR1_Cp
myu_new_BR1=(1./Cx_BR1(2:end)).*(diff(Cx_BR1)./diff(t_BR1))+Qt_BR1(2
:end)./V_BR1(2:end)
myu_mean_BR1=((Biomass_BR1(8)-
Biomass_BR1(2)))/trapz(t_BR1(2:8),Biomass_BR1(2:8))
qs_new_BR1=-
(1./Cx_BR1(2:end)).*(diff(Cs_BR1)./diff(t_BR1)+((Cs_BR1(2:end).*Qt_B
R1(2:end))./V_BR1(2:end))-(Qt_BR1(2:end).*Cs0)./V_BR1(2:end))
qs_mean_BR1=(Cs0*trapz(t_BR1(2:8),Qt_BR1(2:8))-(Cs_BR1(8)*V_BR1(8)-
Cs_BR1(2)*V_BR1(2)))/trapz(t_BR1(2:8),Biomass_BR1(2:8))
qp_new_BR1=(1./Cx_BR1_Cp(2:end)).*(diff(Cp_BR1)./diff(t_BR1_Cp)+(Cp_
BR1(2:end).*Qt_BR1_Cp(2:end))./V_BR1_Cp(2:end))
qp_mean_BR1=(Protein_BR1_Cp(7)-
Protein_BR1_Cp(2))/trapz(t_BR1_Cp(2:7),Biomass_BR1_Cp(2:7))
Cs_mean_BR1=trapz(t_BR1(2:8),Cs_BR1(2:8)/(t_BR1(8)-t_BR1(2)))
```

%μ_{set}=0.035 h^{-1}

```
t_BR2=[0 3 6 9 12 15 18 21 24];
Cx_BR2=[34 38.60 41.60 47.30 50.70 57.80 64.40 69.00 75.30];
V_BR2=[2.11 2.13 2.13 2.14 2.15 2.17 2.19 2.22 2.23];
Qt_BR2=[0.00550 0.00611 0.00679 0.00754 0.00837 0.00930 0.01033
0.01147 0.01274];
Cs_BR2=[4.70 1.73 0.00 0.00 0.00 0.00 0.58 0.00 0.39];
Cp_BR2=[7 7.9 10.0 33.7 35.7 35.9 38.4 43.6 34.8];
Cs0=790;
Biomass_BR2=Cx_BR2.*V_BR2
Protein_BR2=Cp_BR2.*V_BR2
myu_new_BR2=(1./Cx_BR2(2:end)).*(diff(Cx_BR2)./diff(t_BR2))+Qt_BR2(2
:end)./V_BR2(2:end)
myu_mean_BR2=((Biomass_BR2(8)-
Biomass_BR2(2)))/trapz(t_BR2(2:8),Biomass_BR2(2:8))
```

```
qs_new_BR2=-
(1./Cx_BR2(2:end)).*(diff(Cs_BR2)./diff(t_BR2)+((Cs_BR2(2:end).*Qt_B
R2(2:end))./V_BR2(2:end))-(Qt_BR2(2:end).*Cs0)./V_BR2(2:end))
qs_mean_BR2=(Cs0*trapz(t_BR2(2:8),Qt_BR2(2:8))-(Cs_BR2(8)*V_BR2(8)-
Cs_BR2(2)*V_BR2(2)))/trapz(t_BR2(2:8),Biomass_BR2(2:8))
qp_new_BR2=(1./Cx_BR2(2:end)).*(diff(Cp_BR2)./diff(t_BR2)+(Cp_BR2(2:
end).*Qt_BR2(2:end))./V_BR2(2:end))
qp_mean_BR2=(Protein_BR2(8)-
Protein_BR2(2))/trapz(t_BR2(2:8),Biomass_BR2(2:8))
Cs_mean_BR2=trapz(t_BR2(2:8),Cs_BR2(2:8))/(t_BR2(8)-t_BR2(2))
```

$\%\mu_{set}=0.020\ h^{-1}$

```
t_BR3=[0 3 6 9 12 15 19 21 24];
Cx_BR3=[33.17 37.90 39.80 42.50 43.50 45.00 49.10 51.30 52.10];
V_BR3=[2.12 2.13 2.12 2.12 2.11 2.12 2.13 2.12 2.11];
Qt_BR3=[0.00298 0.00317 0.00336 0.00357 0.00379 0.00403 0.00428
0.00454 0.00482];
Cs_BR3=[4 0.00 0.00 0.00 0.00 0.00 0.00 0.00 0.00];
Cs0=790;
Biomass_BR3=Cx_BR3.*V_BR3
myu_new_BR3=(1./Cx_BR3(2:end)).*(diff(Cx_BR3)./diff(t_BR3))+Qt_BR3(2
:end)./V_BR3(2:end)
myu_mean_BR3=((Biomass_BR3(8)-
Biomass_BR3(2)))/trapz(t_BR3(2:8),Biomass_BR3(2:8))
qs_new_BR3=-
(1./Cx_BR3(2:end)).*(diff(Cs_BR3)./diff(t_BR3)+((Cs_BR3(2:end).*Qt_B
R3(2:end))./V_BR3(2:end))-(Qt_BR3(2:end).*Cs0)./V_BR3(2:end))
qs_mean_BR3=(Cs0*trapz(t_BR3(2:8),Qt_BR3(2:8))-(Cs_BR3(8)*V_BR3(8)-
Cs_BR3(2)*V_BR3(2)))/trapz(t_BR3(2:8),Biomass_BR3(2:8))
Cs_mean_BR3=trapz(t_BR3(2:8),Cs_BR3(2:8))/(t_BR3(8)-t_BR3(2))
```

$\%C_{s,set}=0.5\ g\ L^{-1}$

```
t_BR7=[0 3 6 9 12 15 18 21 24];
Cx_BR7=[37.5 50.9 66.5 83.83 96 122.6 128 128 128];
V_BR7=[2.05 2.09 2.18 2.31 2.43 2.62 2.76 2.89 2.97];
Qt_BR7=[0.00725 0.01122 0.02291 0.02873 0.03338 0.04662 0.03105
0.03287 0.02253];
Cs_BR7=[2.49 0.51 0.98 0.00 0.26 0.42 0.44 1.11 1.54];
Cp_BR7=[8.3 19.2 19.3 25.8 33.3 49.8 51.2 74.7 91];
Cp_BR7_poly=[9.75 15.5 21.1 27.3 34.7 44.2 56.4 72 91.7];
Cs0=790;
Biomass_BR7=Cx_BR7.*V_BR7
Protein_BR7=Cp_BR7.*V_BR7;
Protein_BR7_poly=Cp_BR7_poly.*V_BR7
myu_new_BR7=(1./Cx_BR7(2:end)).*(diff(Cx_BR7)./diff(t_BR7))+Qt_BR7(2
:end)./V_BR7(2:end)
myu_mean_BR7=((Biomass_BR7(6)-
Biomass_BR7(1)))/trapz(t_BR7(1:6),Biomass_BR7(1:6))
qs_new_BR7=-
(1./Cx_BR7(2:end)).*(diff(Cs_BR7)./diff(t_BR7)+((Cs_BR7(2:end).*Qt_B
R7(2:end))./V_BR7(2:end))-(Qt_BR7(2:end).*Cs0)./V_BR7(2:end))
```

```
qs_mean_BR7=(Cs0*trapz(t_BR7(1:6),Qt_BR7(1:6))-(Cs_BR7(6)*V_BR7(6)-
Cs_BR7(1)*V_BR7(1)))/trapz(t_BR7(1:6),Biomass_BR7(1:6))
qp_new_BR7=(1./Cx_BR7(2:end)).*(diff(Cp_BR7)./diff(t_BR7)+(Cp_BR7(2:
end).*Qt_BR7(2:end))./V_BR7(2:end))
qp_mean_BR7=(Protein_BR7_poly(6)-
Protein_BR7_poly(1))/trapz(t_BR7(1:6),Biomass_BR7(1:6))
Cs_mean_BR7=trapz(t_BR7(1:6),Cs_BR7(1:6))/(t_BR7(6)-t_BR7(1))
```

$\%C_{s,set}$=1 g L^{-1}

```
t_BR4=[0 3 6 9 12 15 18 21 24];
Cx_BR4=[29.6 37.6 50.6 67.6 86 108 119.3 133 135];
V_BR4=[2.08 2.13 2.19 2.29 2.42 2.60 2.81 3.00 3.14];
Qt_BR4=[0.00717 0.01236 0.01662 0.02346 0.03034 0.03781 0.04278
0.04059 0.03329];
Cs_BR4=[0 1.39 1.21 0.96 0.62 1.00 0.60 1.10 0.95];
Cp_BR4=[7.3 9.3 9.5 12.9 25.5 37.3 50.9 80.1 60.9];
Cp_BR4_poly=[7.52 8.22 10.3 14.9 23 35.7 54 79 60.9];
Cs0=790;
Biomass_BR4=Cx_BR4.*V_BR4
Protein_BR4=Cp_BR4.*V_BR4;
Protein_BR4_poly=Cp_BR4_poly.*V_BR4
myu_new_BR4=(1./Cx_BR4(2:end)).*(diff(Cx_BR4)./diff(t_BR4))+Qt_BR4(2
:end)./V_BR4(2:end)
myu_mean_BR4=((Biomass_BR4(7)-
Biomass_BR4(2)))/trapz(t_BR4(2:7),Biomass_BR4(2:7))
qs_new_BR4=-
(1./Cx_BR4(2:end)).*(diff(Cs_BR4)./diff(t_BR4)+((Cs_BR4(2:end).*Qt_B
R4(2:end))./V_BR4(2:end))-(Qt_BR4(2:end).*Cs0)./V_BR4(2:end))
qs_mean_BR4=(Cs0*trapz(t_BR4(2:7),Qt_BR4(2:7))-(Cs_BR4(7)*V_BR4(7)-
Cs_BR4(2)*V_BR4(2)))/trapz(t_BR4(2:7),Biomass_BR4(2:7))
qp_new_BR4=(1./Cx_BR4(2:end)).*(diff(Cp_BR4)./diff(t_BR4)+(Cp_BR4(2:
end).*Qt_BR4(2:end))./V_BR4(2:end))
qp_mean_BR4=(Protein_BR4_poly(7)-
Protein_BR4_poly(2))/trapz(t_BR4(2:7),Biomass_BR4(2:7))
Cs_mean_BR4=trapz(t_BR4(2:7),Cs_BR4(2:7))/(t_BR4(7)-t_BR4(2))
```

$\%C_{s,set}$=1.5 g L^{-1}

```
t_BR6=[0 3 6 9 12 15 18 21 24];
Cx_BR6=[31 35.8 43.4 59.5 80.13 97 101 101 101];
V_BR6=[2.10 2.09 2.12 2.19 2.29 2.44 2.61 2.80 2.93];
Qt_BR6=[0.00725 0.01232 0.01114 0.02080 0.02608 0.03895 0.04236
0.04662 0.03578];
Cs_BR6=[0.59 4.14 2.06 1.62 0.55 0.12 0.34 0.30 1.20];
Cp_BR6=[7 8.1 9.8 23.7 36.3 49.7 39.7 57.0 78.8];
Cp_BR6_poly=[4.17 9.99 16.3 23.2 30.9 39.8 49.8 61.4 74.6];
Cs0=790;
Biomass_BR6=Cx_BR6.*V_BR6
Protein_BR6=Cp_BR6.*V_BR6;
Protein_BR6_poly=Cp_BR6_poly.*V_BR6
myu_new_BR6=(1./Cx_BR6(2:end)).*(diff(Cx_BR6)./diff(t_BR6))+Qt_BR6(2
:end)./V_BR6(2:end)
```

```
myu_mean_BR6=((Biomass_BR6(6)-
Biomass_BR6(2)))/trapz(t_BR6(2:6),Biomass_BR6(2:6))
qs_new_BR6=-
(1./Cx_BR6(2:end)).*(diff(Cs_BR6)./diff(t_BR6)+((Cs_BR6(2:end).*Qt_B
R6(2:end))./V_BR6(2:end))-(Qt_BR6(2:end).*Cs0)./V_BR6(2:end))
qs_mean_BR6=(Cs0*trapz(t_BR6(2:6),Qt_BR6(2:6))-(Cs_BR6(6)*V_BR6(6)-
Cs_BR6(2)*V_BR6(2)))/trapz(t_BR6(2:6),Biomass_BR6(2:6))
qp_new_BR6=(1./Cx_BR6(2:end)).*(diff(Cp_BR6)./diff(t_BR6)+(Cp_BR6(2:
end).*Qt_BR6(2:end))./V_BR6(2:end))
qp_mean_BR6=(Protein_BR6_poly(6)-
Protein_BR6_poly(2))/trapz(t_BR6(2:6),Biomass_BR6(2:6))
Cs_mean_BR6=trapz(t_BR6(2:6),Cs_BR6(2:6))/(t_BR6(6)-t_BR6(2))
```

F. Haldane and Monod Codes for CFS Bioreactor Experiments Using MATLAB®

%Specific growth rate:

```
figure (1)
% Parameters: mumax = b(1),  Ks = b(2),  Ki = b(3)
HaldaneInhMdl = @(b,S) b(1).*S ./ (b(2) + S + S.^2./b(3));
MonodInhMdl = @(b,S) b(1).*S ./ (b(2) + S);
mu = [0 0.0167 0.0346 0.0928 0.0884 0.0961 0.0473];
S = [0 0.1 0.241 0.641 0.957 1.59 5.99];
SSECF = @(b) sum((mu - HaldaneInhMdl(b,S)).^2);
SSECF_monod = @(b) sum((mu - MonodInhMdl(b,S)).^2);
B0 = [0.1; 0.1; 1];
[B, SSE] = fminsearch(SSECF, B0)
[B_monod, SSE_monod] = fminsearch(SSECF_monod, B0)
Sp = linspace(min(S), max(S), 150);
fitmu = HaldaneInhMdl(B,Sp);
fitmu_monod = MonodInhMdl(B_monod,Sp);
plot(S, mu, 'pg')
hold on
plot(Sp, fitmu, '-r')
plot(Sp, fitmu_monod, ':k')
hold off
grid
xlabel('C_{s} (g L^{-1})')
ylabel('\mu (h^{-1})')
legend('Data', 'Fit-haldane','Fit-monod', 'Location', 'NE')
txtlbl = sprintf('\\mu = %.3f \\times S / (%6.0f + S + s^2/%.1f)',
B);
text(1500, 0.0006, txtlbl)
```

%Specific ethanol uptake rate:

```
figure (2)
% Parameters: mumax = b(1),  Ks = b(2),  Ki = b(3)
HaldaneInhMdl = @(b,S) b(1).*S ./ (b(2) + S + S.^2./b(3));
MonodInhMdl = @(b,S) b(1).*S ./ (b(2) + S);
qs = [0 0.0322 0.0609 0.112 0.112 0.123 0.082];
S = [0 0.1 0.241 0.641 0.957 1.59 5.99];
SSECF = @(b) sum((qs - HaldaneInhMdl(b,S)).^2);
SSECF_monod = @(b) sum((qs - MonodInhMdl(b,S)).^2);
B0 = [0.1; 0.1; 10];
[B, SSE] = fminsearch(SSECF, B0)
[B_monod, SSE_monod] = fminsearch(SSECF_monod, B0)
Sp = linspace(min(S), max(S), 50);
fitqs = HaldaneInhMdl(B,Sp);
fitqs_monod = MonodInhMdl(B_monod,Sp);
plot(S, qs, 'pg')
hold on
plot(Sp, fitqs, '-r')
plot(Sp, fitqs_monod, ':k','LineWidth',1)
```

```
hold off
grid
xlabel('C_{s} (g L^{-1})')
ylabel('q_{s} (g EtOH g^{-1}DCW h^{-1})')
legend('Data', 'Fit-haldane','Fit-monod', 'Location', 'NE')
txtlbl = sprintf('\\mu = %.3f \\times S / (%6.0f + S + s^2/%.1f)',
B);
text(1500, 0.0006, txtlbl)
```

%Specific protein production rate:

```
figure (3)
% Parameters: mumax = b(1),  Ks = b(2),  Ki = b(3)
HaldaneInhMdl = @(b,S) b(1).*S ./ (b(2) + S + S.^2./b(3));
MonodInhMdl = @(b,S) b(1).*S ./ (b(2) + S);
qp = [0 0.039 0.0364 0.0465 0.0453 0.0211];
S = [0 0.241 0.641 0.957 1.59 5.99];
SSECF = @(b) sum((qp - HaldaneInhMdl(b,S)).^2);
SSECF_monod = @(b) sum((qp - MonodInhMdl(b,S)).^2);
B0 = [0.1; 0.1; 1];
[B, SSE] = fminsearch(SSECF, B0)
[B_monod, SSE_monod] = fminsearch(SSECF_monod, B0)
Sp = linspace(min(S), max(S), 50);
fitqp = HaldaneInhMdl(B,Sp);
fitqp_monod = MonodInhMdl(B_monod,Sp);
plot(S, qp, 'pg')
hold on
plot(Sp, fitqp, '-r')
plot(Sp, fitqp_monod, ':k')
hold off
grid
xlabel('C_{s} (g L^{-1})')
ylabel('q_{p} (mg hGH g^{-1}DCW h^{-1})')
legend('Data', 'Fit-haldane','Fit-monod', 'Location', 'NE')
txtlbl = sprintf('\\mu = %.3f \\times S / (%6.0f + S + s^2/%.1f)',
B);
text(1500, 0.0006, txtlbl)
```

G. Pirt and Luedeking-Piret Models for CFS Bioreactor Experiments Using MATLAB®

%Pirt Model:

```
figure (1)
mu = [0.0167 0.0346 0.0928 0.0884 0.0961 0.0473];
qs = [0.0322 0.0609 0.112 0.112 0.123 0.082];
p = polyfit(mu,qs,1)
f = polyval(p,mu);
freg= [0.0233 f];
xreg= [0 mu];
plot(mu,qs,'o',xreg,freg,'-')
legend('Experimental data','Pirt Model')
Rsq2 = 1 - sum((qs - f).^2)/sum((qs - mean(qs)).^2)
grid
xlabel('\mu (h^{-1})')
ylabel('q_{s} (g EtOH g^{-1}DCW h^{-1})')
```

%Luedeking-Piret Model:

```
figure (2)
mu = [0.0346 0.0928 0.0884 0.0961 0.0473];
qp = [0.039 0.0364 0.0465 0.0453 0.0211];
p = polyfit(mu,qp,1)
f = polyval(p,mu);
freg= [0.0232 f];
xreg= [0 mu];
plot(mu,qp,'o',xreg,freg,'-')
legend('Experimental data','Luedeking-Piret')
Rsq2 = 1 - sum((qp - f).^2)/sum((qp - mean(qp)).^2)
grid
xlabel('\mu (h^{-1})')
ylabel('q_{p} (mg hGH g^{-1}DCW h^{-1})')
```

H. Codes of C_xV and C_pV Simulations for CFS Bioreactor Experiments Using MATLAB®

%μ_{set}=0.050 h^{-1}

```
S = 5.72;
mu_set = 0.0473;
qp = 0.0243;
XV_BR1 = zeros(7,1);
PV_BR1 = zeros(6,1);
Time = [0.00 3.00 6.00 9.00 12.00 15.00 18.00 21.00];
Time_PV=[0.00 3.00 6.00 9.00 12.00 18.00];
XV_EXP_BR1 = [78.11 85.97 115.72 146.05 158.92 172.46 193.83
214.02];
PV_EXP_BR1 = [16.91 17.28 52.14 59.58 65.75 68.59];
XV_BR1(1) = XV_EXP_BR1(1);
PV_BR1(1) = PV_EXP_BR1(1);

for i=1:7
    XV_BR1(i+1) = XV_BR1(i)*exp((Time(i+1)-Time(i))*mu_set);
end

for i=1:6
    PV_BR1(i+1) = PV_BR1(i)+qp*(1.5*XV_BR1(i)+1.5*XV_BR1(i+1));
end
```

%μ_{set}=0.035 h^{-1}

```
S = 0.199;
mu_set = 0.0346;
qp = 0.0343;
XV_BR2 = zeros(7,1);
PV_BR2 = zeros(7,1);
Time = [0.00 3.00 6.00 9.00 12.00 15.00 18.00 21.00];
XV_EXP_BR2 = [82.22 88.61 101.22 109.01 125.43 141.04 153.18
167.92];
PV_EXP_BR2 = [16.83 21.30 72.12 76.76 77.90 84.10 96.79 77.60];
XV_BR2(1) = XV_EXP_BR2(1);
PV_BR2(1) = PV_EXP_BR2(1);

for i=1:7
    XV_BR2(i+1) = XV_BR2(i)*exp((Time(i+1)-Time(i))*mu_set);
    PV_BR2(i+1) = PV_BR2(i)+qp*(1.5*XV_BR2(i)+1.5*XV_BR2(i+1));
end
```

%μ_{set}=0.020 h^{-1}

```
mu_set = 0.0167;
XV_BR3 = zeros(7,1);
PV_BR3 = zeros(7,1);
Time = [0.00 3.00 6.00 9.00 12.00 15.00 18.00 21.00];
```

```
XV_EXP_BR3 = [80.73 84.38 90.10 91.79 95.40 104.58 108.76 109.93];
XV_BR3(1) = XV_EXP_BR3(1);

for i=1:7
    XV_BR3(i+1) = XV_BR3(i)*exp((Time(i+1)-Time(i))*mu_set);
end
```

%$C_{s,set}$=1.5 g L^{-1}

```
S_set = 1.59;
mu = 0.0966;
qp = 0.0407;
XV_BR6 = zeros(7,1);
PV_BR6 = zeros(7,1);
Time = [0.00 3.00 6.00 9.00 12.00 15.00 18.00 21.00];
XV_EXP_BR6 = [74.82 92.01 130.31 183.50 236.68 263.61 282.80
295.93];
PV_EXP_BR6 = [20.88 34.56 50.81 70.76 97.11 129.98 171.92 218.58];
XV_BR6(1) = XV_EXP_BR6(1);
PV_BR6(1) = PV_EXP_BR6(1);

for i=1:7
    XV_BR6(i+1) = XV_BR6(i)*exp((Time(i+1)-Time(i))*mu);
    PV_BR6(i+1) = PV_BR6(i)+qp*(1.5*XV_BR6(i)+1.5*XV_BR6(i+1));
end
```

%$C_{s,set}$=1 g L^{-1}

```
S_set = 0.957;
mu = 0.0952;
qp = 0.0437;
XV_BR4 = zeros(7,1);
PV_BR4 = zeros(7,1);
Time = [0.00 3.00 6.00 9.00 12.00 15.00 18.00 21.00];
XV_EXP_BR4 = [80.09 110.81 154.80 208.12 280.80 335.23 399 423.90];
PV_EXP_BR4 = [17.51 22.56 34.12 55.66 92.82 151.74 237.00 191.23];
XV_BR4(1) = XV_EXP_BR4(1);
PV_BR4(1) = PV_EXP_BR4(1);

for i=1:7
    XV_BR4(i+1) = XV_BR4(i)*exp((Time(i+1)-Time(i))*mu);
     PV_BR4(i+1) = PV_BR4(i)+qp*(1.5*XV_BR4(i)+1.5*XV_BR4(i+1));
end
```

%$C_{s,set}$=0.5 g L^{-1}

```
S_set = 0.641;
mu = 0.0819;
qp = 0.0439;
XV_BR7 = zeros(8,1);
PV_BR7 = zeros(8,1);
Time_BR7 = [0.00 3.00 6.00 9.00 12.00 15.00 18.00 21.00 24.00];
```

```
XV_EXP_BR7 = [76.88 106.38 144.97 193.65 233.28 321.21 353.28 369.92
380.16];
PV_EXP_BR7 = [19.99 32.40 46.00 63.06 84.32 115.80 155.66 208.08
272.35];
XV_BR7(1) = XV_EXP_BR7(1);
PV_BR7(1) = PV_EXP_BR7(1);

for i=1:8
    XV_BR7(i+1) = XV_BR7(i)*exp((Time_BR7(i+1)-Time_BR7(i))*mu);
    PV_BR7(i+1) = PV_BR7(i)+qp*(1.5*XV_BR7(i)+1.5*XV_BR7(i+1));
end
```

%Simulation Plots

```
figure(1)
hold on
B1= plot(Time(1:8),XV_BR1(1:8),':b','LineWidth',1.5)
plot(Time(1:8),XV_EXP_BR1(1:8),'b+')
B2= plot(Time(1:8),XV_BR2(1:8),':g','LineWidth',1.5)
plot(Time(1:8),XV_EXP_BR2(1:8),'g*')
B3= plot(Time(1:8),XV_BR3(1:8),':r','LineWidth',1.5)
plot(Time(1:8),XV_EXP_BR3(1:8),'rs')
B7= plot(Time_BR7(1:8),XV_BR7(1:8),':m','LineWidth',1.5)
plot(Time_BR7(1:8),XV_EXP_BR7(1:8),'mo')
B4= plot(Time(1:7),XV_BR4(1:7),':k','LineWidth',1.5)
plot(Time(1:7),XV_EXP_BR4(1:7),'kd')
B6= plot(Time(1:6),XV_BR6(1:6),':c','LineWidth',1.5)
plot(Time(1:6),XV_EXP_BR6(1:6),'c^')
set(gca, 'XLim', [0, 24], 'XTick', 0:3:24,'XTickLabel',
0:3:24);
set(gca,'ylim',[50,500])
xlabel('Time (h)')
ylabel('C_{X}V (g)')
Bio3 = plot(nan, nan,
':o','color','#7E2F8E','markerfacecolor','white','linewidth',1
.5);
Bio2 = plot(nan, nan,
':s','color','#77AC30','markerfacecolor','#77AC30','markeredge
color','#77AC30','linewidth',1.5);
Bio1 = plot(nan, nan,
':^','color','#0072BD','markerfacecolor','white','linewidth',1
.5);
Bio7 = plot(nan, nan,
':o','color','#A2142F','MarkerFaceColor','#A2142F','markeredge
color','#A2142F','linewidth',1.5);
Bio4 = plot(nan, nan,
':kd','color','k','MarkerFaceColor','k','linewidth',1.5);
Bio6 = plot(nan, nan,
':^','color','#D95319','MarkerFaceColor','#D95319','markeredge
color','#D95319','linewidth',1.5);
```

```
legend([Bio3 Bio2 Bio1 Bio7 Bio4 Bio6],'μ_{set}=0.020 h^{-
1}','μ_{set}=0.035 h^{-1}','μ_{set}=0.050 h^{-
1}','C_{EtOH,}_{set}=0.5 g L^{-1}','C_{EtOH,}_{set}=1.0 g L^{-
1}','C_{EtOH,}_{set}=1.5 g L^{-1}','Location','northwest')
grid
figure(2)
hold on
set(gca, 'XLim', [0, 25], 'XTick', 0:3:24,'XTickLabel',
0:3:24);
set(gca,'ylim',[0,350])
BP1= plot (Time_PV(1:6),
PV_BR1(1:6),':','color','#0072BD','linewidth',2)
plot(Time_PV(1:6),PV_EXP_BR1(1:6),'^','color','#0072BD','marke
rfacecolor','white')
BP2= plot (Time(1:7),
PV_BR2(1:7),':','color','#77AC30','linewidth',2)
plot(Time(1:7),PV_EXP_BR2(1:7),'s','markerfacecolor','#77AC30'
,'markeredgecolor','#77AC30')
BP7= plot (Time_BR7(1:9),
PV_BR7(1:9),':','color','#A2142F','linewidth',2)
plot(Time_BR7(1:9),PV_EXP_BR7(1:9),'o','MarkerFaceColor','#A21
42F','markeredgecolor','#A2142F')
BP4= plot (Time(1:7), PV_BR4(1:7),':k','linewidth',2)
plot(Time(1:7),PV_EXP_BR4(1:7),'kd','MarkerFaceColor','k')
BP6= plot (Time(1:8),
PV_BR6(1:8),':','color','#D95319','linewidth',2)
plot(Time(1:8),PV_EXP_BR6(1:8),'^','MarkerFaceColor','#D95319'
,'markeredgecolor','#D95319')

grid on
xlabel('Time (h)')
ylabel('C_{p}V (mg)')
Bio2 = plot(nan, nan,
':s','color','#77AC30','markerfacecolor','#77AC30','markeredge
color','#77AC30','linewidth',1.5);
Bio1 = plot(nan, nan,
':^','color','#0072BD','markerfacecolor','white','linewidth',1
.5);
Bio7 = plot(nan, nan,
':o','color','#A2142F','MarkerFaceColor','#A2142F','markeredge
color','#A2142F','linewidth',1.5);
Bio4 = plot(nan, nan,
':kd','color','k','MarkerFaceColor','k','linewidth',1.5);
Bio6 = plot(nan, nan,
':^','color','#D95319','MarkerFaceColor','#D95319','markeredge
color','#D95319','linewidth',1.5);
legend([Bio2 Bio1 Bio7 Bio4 Bio6],'μ_{set}=0.035 h^{-
1}','μ_{set}=0.050 h^{-1}','C_{EtOH,}_{set}=0.5 g L^{-
```

```
1}','C_{EtOH,}_{set}=1.0 g L^{-1}','C_{EtOH,}_{set}=1.5 g L^{-
1}','Location','northwest')
hold off
```